Effects of Oxygenated Fuels on DI Diesel Combustion and Emissions

by

Brian E. Hallgren

Bachelor of Science in Mechanical Engineering
Binghamton University
(1998)

Submitted to the Department of Mechanical Engineering
in Partial Fulfillment of the Requirements for the Degree of
Master of Science in Mechanical Engineering

at the

Massachusetts Institute of Technology

June 2000

Signature of Author _____
Department of Mechanical Engineering
June 2000

Certified by _____
John B. Heywood
Sun Jae Professor of Mechanical Engineering
Thesis Supervisor

Accepted by _____
Ain A. Sonin
Chairman, Department Committee on Graduate Students

Effects of Oxygenate Fuels on DI Diesel Combustion and Emissions

by

Brian E. Hallgren

Submitted to the Department of Mechanical Engineering
June 2000 in Partial Fulfillment of the Requirements
for the Degree of Master of Science in Mechanical Engineering

ABSTRACT

Emissions from compression ignition (CI) engines are being placed under stricter regulations. The use of oxygenated fuels has been proposed as a means of complying with future emission levels. Previous research on oxygenates has suggested the presence of molecular oxygen within the fuel significantly reduces the formation of particulate matter (PM). The PM reduction is logarithmic and correlates with the weight percent of oxygen in the fuel and not with other properties such as chemical structure and volatility. However, many studies fail to correctly decouple the effects of oxygenates from other fuel properties that impact emission levels; such as cetane number, density, aromatic content, and volatility.

Mechanisms responsible for changes in the combustion process and emissions were investigated with a matrix containing 14 fuels, addressing oxygenate proportionality, structure, volatility, equivalent structure without oxygen, and changes in the base diesel fuel. A scanning mobility particle sizer (SMPS) was used to evaluate changes in particle size distributions, in addition to gravimetric filter and oxides of nitrogen (NO_x) measurements.

Engine emissions tests were conducted using a Ricardo Hydra MK IV direct injection (DI) diesel engine. The sensitivity of engine operation parameters to intake temperature, load, injection timing, and ignition delay (ID) were evaluated with the baseline fuel. All fuels in the matrix were matched for total released energy and combustion phasing, using a cetane improving additive. The changes in emission have been quantified with agreement between the relative trends observed with the integrated SMPS volume concentrations and filter measurements. In order to evaluate changes among fuels and measurements taken with the SMPS, various fuels were subjected to physical and chemical characterization in order to determine morphological and compositional changes.

Thesis Advisor: Professor John B. Heywood
Title: Sun Jae Professor of Mechanical Engineering

ACKNOWLEDGMENTS

It has been a pleasure to have Professor John Heywood as my thesis supervisor. His dedication and insightful knowledge into the area of internal combustion engines made this work possible. The guidance and patience I received, was appreciated and had a profound impact on my research.

Thanks to all of the members of the MIT Engine and Fuels Consortium (DaimlerChrysler, Ford, General Motors, ExxonMobil, Shell Oil, and Volvo Car) for their valuable feedback and financial support. Special thanks to Dr. Michael Noorman of ExxonMobil, for the fuel analysis and diesel fuel, and to Dr. Richard Chase of Ford Motor Company, who provided advice in conducting the particulate sampling during the project's early stages. Additionally, the effort made by Lenore Rainy of MIT in taking the TEM photomicrographs was greatly appreciated. It was a pleasure to work with all of the above, and I hope to continue our working relationship in the future.

Thanks to the all the members of the Sloan Automotive Laboratory, past and present. Professor Wai Cheng and Professor James Keck provided useful suggestions and insights, sending me in new directions. During the first six months of my research, Cornelius O'Sullivan assisted me in conducting engine experiments.

A special thanks to my officemate for the past two years, Gary Landsberg, for his contributions within and outside of the Sloan Lab. He aided not only in my research (holding wrenches, cutting locks, and editing this thesis), but also was instrumental in getting me through the stressful times (with his great sense of humor and grueling mountain bike rides). He is a good friend and I wish him the best of luck in the future.

Thanks to my fiancée, Meredith, for allowing me to follow a dream. Without her love, encouragement, and understanding for the past four and a half years, none of this would be a reality. She is my best friend and truly the greatest part of my life.

Thanks to my entire family for the love and support during my time at the Sloan Lab. MIT is strenuous without life's other obstacles, but through it all, my parents have always provided encouragement. I owe them so much; thank you mom and dad.

Brian Hallgren
May 2000

TABLE OF CONTENTS

LIST OF TABLES

LIST OF FIGURES

NOMENCLATURE

ACRONYMS/SYMBOLS

$\eta_{f,i}$	indicated fuel conversion efficiency (gross)
ϕ	fuel/air equivalence ratio
μm	micron
^{85}Kr	Krypton isotope
A/F	air-fuel ratio mass basis
ABDC	after bottom-dead-center
ATDC	after top-dead-center
BBDC	before bottom-dead-center
BTDC	before top-dead-center
CA	crank angle
CI	compression ignition
CN	cetane number
CPC	condensation particle counter
DI	direction injection
DMA	differential mobility analyzer
D_p	particle diameter based on electrical mobility
EBP	end boiling point
EGR	exhaust gas recycling
EI	emission index
EOI	end of injection
EVC	exhaust valve close
EVO	exhaust valve open
FID	flame ionization detector
GC	gas chromatography
HC	hydrocarbons
IBP	initial boiling point
ID	ignition delay
IDI	indirection injection
imep	indicated mean effective pressure
isfc	indicated specific fuel consumption
ISOF	insoluble organic fraction
isPart	indicated specific particulates
IVC	intake valve close
IVO	intake valve open
m/e	mass-to-charge ratio
MBT	maximum break torque
MS	mass spectrometer
NDIR	non-disperse infrared
nm	nanometer
NO_x	oxides of nitrogen
NVH	noise, vibration, harshness
PAH	poly-aromatic hydrocarbon
PFI	port fuel injected
PM	particulate matter
ppm	parts per million
$ppmC_1$	parts of carbon per million
ppmv	parts per million-volume basis
psig	pounds per square inch gauge
Q_{hv}	heating value (lower)

R_d	dilution ratio
ROHR	rate of heat release
RPM	revolutions per minute
SI	spark ignition
slpm	standard liters per minute
SMPS	scanning mobility particle sizer
SOC	start of combustion
SOF	soluble organic fraction
SOHC	single overhead cam
SOI	start of injection
T10	front-end volatility
T50	mid-volatility
T90	back-end volatility
TEM	transmission electronic microscopy

FUEL/ADDITIVE ABBREVIATIONS

2-EHN	2-ethylhexyl nitrate (cetane improver)
BP10+	1-bromopropane 10 vol-%, blended with D-377 and 2-EHN (alkyl halide)
D-377	Phillips 66 low-sulfur diesel fuel
D-377+	Cetane improved Phillips 66 low-sulfur diesel fuel
DG10	Diglyme 10 vol-%, blended with D-377 (4 wt-% oxygen)
DG20	Diglyme 10 vol-%, blended with D-377 (8 wt-% oxygen)
DG30	Diglyme 10 vol-%, blended with D-377 (12 wt-% oxygen)
DM17+	diethyl maleate 17 vol-%, blended with D-377 and 2-EHN (8 wt-% oxygen)
DT17+	diethylene triamine 17 vol-%, blended with D-377 and 2-EHN (amine)
DTBP	di-tert-butyl peroxide (cetane improver)
FT	Mobil diesel fuel from the Fischer-Tropsch process
FTDG19	Diglyme 19 vol-%, blended with FT (8 wt-% oxygen)
MG21	Monoglyme 21 vol-%, blended with D-377 (8 wt-% oxygen)
ND20+	n-decane 20 vol-%, blended with D-377 (alkane)
PG19+	propylene glycol monomethyl ether acetate 19 vol-%, blended with D-377 and 2-EHN (8 wt-% oxygen)
TG19	Tetraglyme 19 vol-%, blended with D-377 (8 wt-% oxygen)

CHAPTER 1

INTRODUCTION

1.1 MOTIVATION

Emission standards for compression ignition (CI) engines are becoming stricter, increasing the challenge on the engine and petroleum industry to comply with future legislation. New stringent emission standards for light-duty diesels, outlined in the Tier 2 and Low Emission Vehicle II (LEV II) standards, will be phased-in beginning in 2004 [1]. The United States Environmental Protection Agency (USEPA) and California Air Resources Board (CARB) have also proposed new heavy-duty diesel regulations cutting current particulate matter (PM) and the oxides of nitrogen (NO_x) levels by approximately 80% and limiting the maximum sulfur level for on-highway usage from 500 ppm to 30 ppm.

With increasing emission standards for CI engines, research has not only focused on new engine technologies and after-treatments, but also on modifying diesel fuel. The use of oxygenates to produce cleaner burning diesel fuel has been recognized as a way of complying with new stringent emission levels. A small amount of molecular oxygen blended with diesel fuel has been shown to reduce particulate matter (PM) [2-10]. Studies indicate the PM reduction is a function of the oxygen content, independent of an oxygenate's physical and chemical properties such as volatility and structure [3,11].

However, many studies have failed to correctly decouple the effects splash blending has on other fuel properties that impact emissions. Changes in sulfur content, density, cetane number, aromatic content, or distillation temperatures can alter emission levels in diesel engines. The focus of this study is to correctly decouple and appraise the effects changes in fuel properties, particularly the addition of oxygenates, have on NO_x and PM emissions.

1.2 BACKGROUND

In 1892, Rudolf Diesel invented the engine design that bears his name [12]. This new engine design utilized higher expansion ratios than other internal combustion engine designs, greatly improving its thermal efficiency. In a direct injection (DI) diesel engine, fuel is directly injected into the cylinder, where it ignites by compression ignition. The limitations of low compression ratio, crevice volume hydrocarbon losses, throttling loss, lean flame speed limits, and cyclical variability inherent to SI engines were avoided [12]. The diesel engine operates lean of stoichiometric at a high compression ratio, resulting in higher thermal efficiencies compared to spark ignition (SI) engines. The increase in efficiency results in lower fuel consumption reducing the amount of the greenhouse gas, carbon dioxide (CO_2), per kilowatt generated. At the same normalized torque value, unburned hydrocarbons (HC) and carbon monoxide (CO) levels for DI diesel engines are lower that those of port fuel injected (PFI) SI engines. However, the high temperature close to stoichiometric environment and locally fuel-rich regions inside the combustion chamber contribute to two major air pollutants that hinder all CI engines; the oxides of nitrogen (NO_x) and particulate matter (PM).

Today, diesel PM is a major contributor to air pollution and is the subject of increasingly tighter regulations. Diesel engines emit 0.2 - 0.5 percent of the fuel's mass as PM. The PM consists of organic and inorganic compounds, 90% by mass are less than 1 μm in diameter, making them readily respirable [12]. Recent epidemiological evidence suggests that diesel exhaust is responsible for the increase occurrences in cancer as well as pulmonary and cardiovascular diseases. Supporting data has shown a correlation between environmental particulate air pollution and a range of respiratory complications [28].

As engine technologies and fuel properties evolve to meet new emission standards, increasing attention has been placed not only on the mass of particles, but also on the number and sizes of the particles emitted. A decrease in mass can be misleading, as the total number of particles can increase, and the size distribution can shift to smaller diameter particles. As a result, there are growing concerns about the ultrafine-particles (less than 100 nm in diameter) and nano-particles (less than 50 nm) emitted from internal

combustion engines [14]. Ultrafine-particles are smaller than cell structures. Therefore, it is unclear what physical characteristics impact the toxicity of these small particles; mass, surface area, and/or particle number. Driscoll showed that toxicity correlates well with surface area, not particle mass [13]. Additional supporting evidence has shown that the rate of lung injury and pathology increases when exposed to ultrafine particles, compared to fine-particles with the identical mass and material deposited.

The chemical composition and its impact on toxicity is another poorly understood variable. PM is carbonaceous soot, un/partially burned fuel/lubricant and water as well as fuel derived sulfate [15]. Below an in-cylinder temperature of 500^{o} C, the particulate's carbon core provides a site for the adsorption and condensation of oxygen and nitrogen derived hydrocarbon chemicals, including poly-aromatic hydrocarbons (PAHs). PAHs are known mutagens and carcinogens [14]. Nevertheless, Heinrich and others have discovered that the occurrences of tumor overload rates were approximately equal with the following compounds; TiO_2, carbon black, and diesel exhaust. Even though, the diesel exhaust contained approximately 40% by weight of extractable organic compounds, including the highly toxic PAHs [28]. Others have suggested that large quantities of ultrafine-particles provide an increase in frequency of surface chemistry reactions caused by the presence of hydroxyl radicals ($OH^{\bullet}$) [13].

The other major pollutant, NOx, plays an active role in the formation of low level ozone and acid rain. These gaseous pollutants are primarily composed of nitric oxide (NO) and small amounts of nitrogen dioxide (NO_2). The oxides of nitrogen lead to the formation of various primary and secondary compounds through photochemical reactions within the atmosphere. NO_2 can react with the hydroxyl radical ($OH^{\bullet}$), to form nitric acid (HNO_3). The primary step in the formation of ozone results from the photolysis of NO_2 during the day resulting in the nitrate ion (NO_3^{-}), an ozone precursor. PAHs react with hydroxyl radicals in the presence of the oxides of nitrogen to form secondary nitro-PAHs and oxygenated nitro-PAHs. These nitro-PAHs are even more soluble than PAHs, thus increasing their bioavailability. Hence, these nitro-PAHs are more mutagenic and carcinogenic than PAHs [14].

1.3 DIESEL POLLUTANT FORMATION

A recent publication of Flynn *et al* [16] has given detailed insight into the formation and oxidation of soot during the diesel combustion process. Upon exiting the injector nozzle, a liquid fuel spray undergoes Rayleigh breakup, forming droplets that penetrate the combustion chamber and entrain hot cylinder air. The entertainment promotes fuel-air mixing and aids in vaporizing the droplets. This results in a fuel rich mixture, a fuel-air equivalence ratio between 2 and 4, around the jet's periphery. Within this fuel rich region, pyrosis causes the formation of fuel fragments; acetylene (C_2H_2), ethylene (C_2H_4), propargyl radical ($C_3H_3^{\bullet}$), CO, and H_2O. The fragmented hydrocarbon molecules are unstable and lead to the formation of stable multi-ringed aromatic compounds, PAHs. The PAH species collide into other PAHs, forming an initial soot particle nuclei in the fuel rich reaction zone [17]. As the entertainment of air continues, the fuel fragments release energy, increasing the reaction region's temperature to approximately 1700 K. Around the jets outer edges, a thin diffusion flame begins to form around the partial oxidized products. The particulates coagulate, forming larger particles as the mixture progresses downstream inside of the spray plume. As the fuel fragments are transported through the interior of the plume, their temperature increases through radiative and convective heat transfer from the flame sheath. As they reach the thin diffusion flame sheath, the fragments are oxidized in a thin reaction zone where release the rest of their chemical energy and approach temperatures of 2500 – 2800 K (Figure 1.1). It is widely believed that it is the premature quenching of the final oxidation process that results in the high PM emitted by diesel engines [16].

The diffusion flame also presents the ideal conditions for the formation of the oxides of nitrogen (NO_x). The high temperature region where oxygen is readily available with the presence of nitrogen is dominated by the thermal reactions (Figure 1.1). These are generally called the Zeldovich mechanism. The rates of formation strongly dependent upon the local burned gas temperature. Nitric oxide (NO) forms in the high-temperature, close to stoichiometric gas regions on the lean side of the diffusion flame. Nitrogen dioxides make up approximately 10 to 30 percent of the NO_x emissions in diesel engines. A fraction of the total NO production can also come from the fixed nitrogen, HCN, in the

fuel rich regions during the premixed and mixing controlled burn of the heat release. Nitrogen is present in heavy distillates and can exist as amines and ring compounds. During combustion these compounds undergo thermal decomposition forming NH_3, HCN, or CN. The fixed nitrogen fraction to the total NO formation is believed to be small, except of fuels containing significant amounts of nitrogen.

1.4 SOOT FORMATION

Fuel structure influences the tendency to form particulates. The formation of soot is observed in both diffusion and premixed combustion, indicating similarities in the chemical and physical mechanisms governing soot formation. The formation of PAHs occurs regardless of the fuel type and is a critical step in the nucleation of a soot particle. For non-aromatic fuels, the precursors undergo cyclization forming an aromatic ring. The rates at which first and second ring structures are formed govern the rate at which incipient soot particles are created. The first aromatic ring structures are presumably formed by reaction with two propynyl ($C_3H_3^{\bullet}$) radials. It is hypothesized that the ring structure adds alkyl groups, developing into a PAH structure that grows in the presence of acetylene (C_2H_2) and other soot precursors. At higher temperatures, the aromatic structure grows until reaching a critical size, developing into a particle nuclei. The particles then dehydrogenate, due to the high temperature environment, and absorb gaseous hydrocarbon species, increasing its mass. The individual particles agglomerate and conglomerate, forming larger secondary particles. The absorbed hydrocarbon species undergo chemical reformation, resulting in a carbonaceous soot structure. These steps appear to be independent of the fuel used [18].

According to Glassman [18], experiments conducted with a laminar diffusion flame, showed an increase in sooting tendencies in the following order; alkanes, alkenes, alkynes, and aromatics having the highest sooting tendency. Supporting evidence has been observed in diesel engines. Branched alkanes and cycloalkanes (naphthenes) in diesel fuels have been shown to increase PM emissions, especially in the case of a low aromatic diesel fuel [19]. The carbon to hydrogen (C/H) ratio is another critical

parameter in the formation of soot. An increase in the concentration of H atoms increases the soot pyrolysis rate and hydroxyl radicals ($OH^{\bullet}$) that attack soot precursors. The presence of halogen additives, acting as a homogeneous catalyst, substantially increases the tendency of all fuels to soot under diffusion flame conditions [18].

Other factors, such as combustion flame temperatures, also impact the soot formation process. As the flame temperatures are reduced with EGR, the formation of soot decreased [7]. Fuel properties such as cetane number and volatility also influence PM emission. The concentration of pyrolysis products in the fuel spray was noted to increase as fuel volatility and cetane number were increased. The addition of molecular oxygen to the fuel was observed to reduce the pyrolysis products, resulting in lower PM levels [7].

1.5 OXYGENATED FUELS

Recent publications indicate that modest amounts of molecular oxygen in the fuel substantially reduce particulates [2-10]. Some oxygenates also offer secondary benefits as well, such as increasing the cetane number (CN) and reducing sulfur content [49]. A compilation of several literature sources, shown in Figure 1.2, indicate that the PM mass reduction is logarithmic with increasing weight percent oxygen in the fuel. Many authors have commented that the decline in PM appears to be a function of only the weight percent of oxygen in the fuel and independent of the organic functional group [3,10]. The data presented in Figure 1.2 is from a variety of different direct injection engines, testing conditions, oxygenates, and base fuels [3-6, 11, 41]. The variation is more clearly defined in Figure 1.3, which depicts one specific type of oxygenate, Diglyme, blended with diesel fuel to yield a mixture containing 4% oxygen by weight. In Figure 1.3 the PM reduction is a function of engine load and engine technology. Different engine test cycles lead to different results. For instance, low molecular weight oxygenates greatly reduce PM during the cold-start testing phase. Additional factors such as the engine's loading (or fuel/air equivalence ratio) also impacts the observed PM reductions with oxygenates [4,9]. As the engine's load is increased, the lean environment inside the combustion

chamber becomes increasingly richer. Thus, the additional oxygen contained in the fuel plays an increasingly important function in reducing PM. Similar results have been observed by enriching the intake air with a higher molar concentration of oxygen [10, 42, 43]. Likewise, as engine designers continue to lower PM emissions by, incorporating better fuel-air mixing, reduced oil consumption, exhaust gas recirculation (EGR), intercooling, and oxidation catalysis, the impact of oxygenates in the fuel diminishes.

1.6 OBJECTIVES

Splash blending fuels modifies fuel properties that can alter engine operating parameters, the combustion process, and emission levels. The addition of an oxygenate to diesel fuel changes the aromatic hydrocarbon content, sulfur content, cetane number, density, and distillation temperatures, all of which are known to influence emission levels. Changes in cetane number and energy density, impact ignition delay and rate of heat release (ROHR), thus changing the combustion process and emissions. A reduction in PM level was observed as the following was decreased; aromatics, cetane, sulfur, temperature of the T90 distillation, and density. The oxides of nitrogen are also impacted by fuel modifications, see Table 1.1 [5, 44, 45].

The focus of this research was to measure the effects of oxygenates on diesel emissions. A fuel matrix was developed to decouple fuel property interactions and isolate possible mechanisms responsible for changes in the combustion process and emission levels. The fuel matrix addressed how emissions scale with: 1) increasing weight percent oxygen in the blended fuel mixture, 2) oxygenate volatility, 3) oxygenate structure, 4) a similar non-oxygen containing hydrocarbon. All fuels were approximately matched for combustion phasing, using a cetane additive, and emphasis has been place upon particle size distributions, using a scanning mobility particle sizer (SMPS).

Fuel Modification	PM[1] ⇓	NOx[1] ⇓
Aromatics	↓	↓
Cetane	↓	↑
Sulfur	↓	-
Distillation T90	↓	-
Density	↓	↓

Table 1.1 Impact of fuel modifications on PM and NO_x emissions [5, 44, 45].

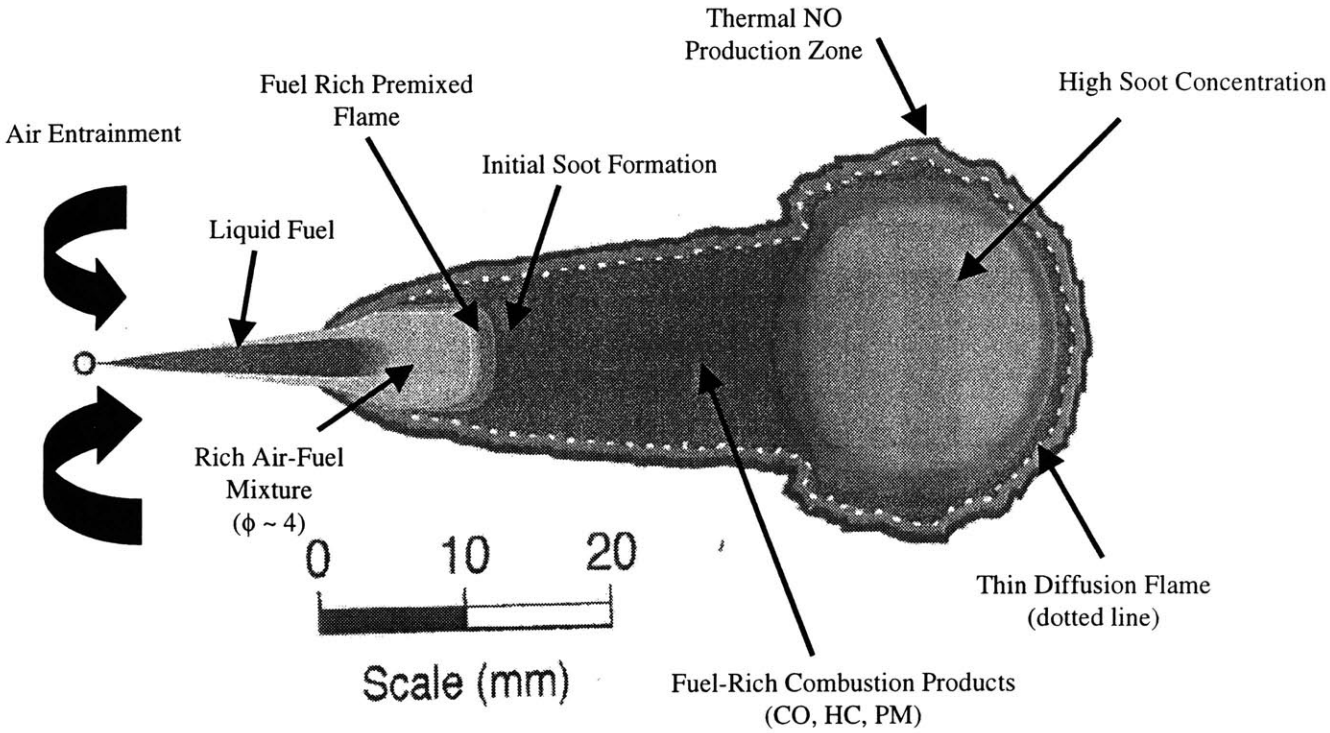

Figure 1.1 Schematic of quasi-steady burning spray plume [4].

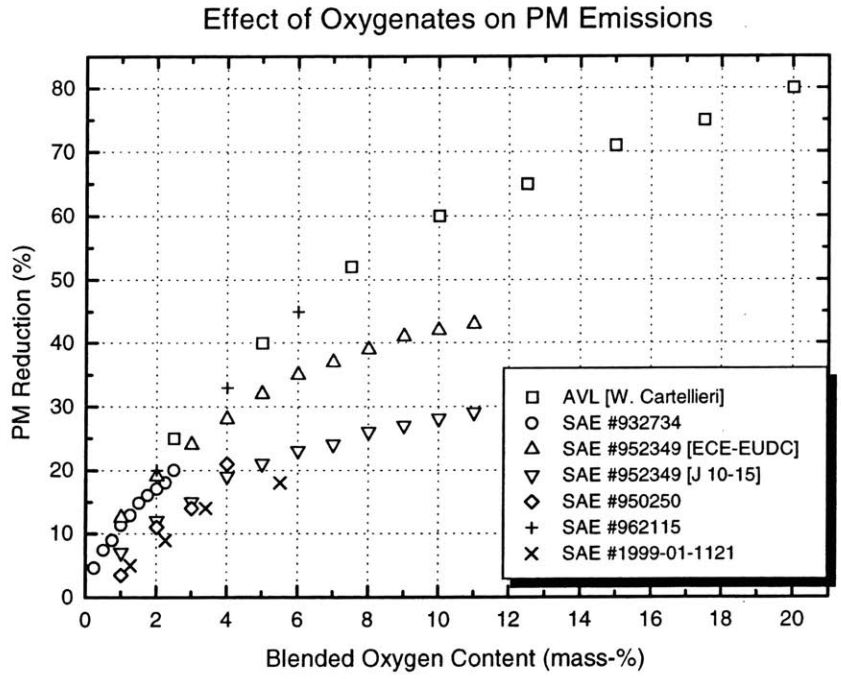

Figure 1.2 PM mass reductions versus blended oxygen content for various oxygenates and testing cycles [3-6, 11, 41].

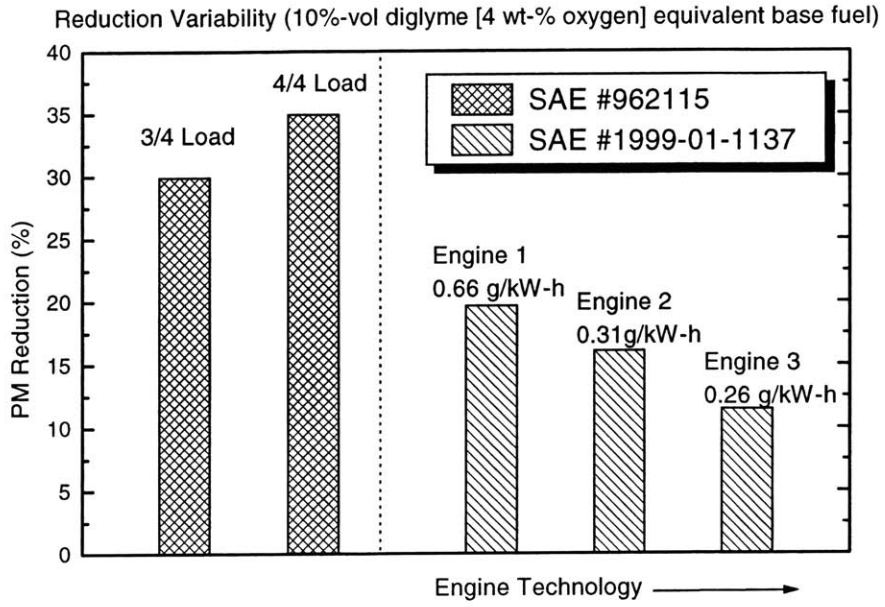

Figure 1.3 PM mass reduction versus loading and engine technology for a specific oxygenate and common base fuel [4, 9].

CHAPTER 2

IMPACT OF FUEL EFFECTS ON EMISSIONS

2.1 DIESEL FUEL OVERVIEW

Diesel fuel is a mixture of hydrocarbon molecules distilled from crude oil. The organic material is primarily composed of alkanes (paraffins), cycloalkanes (naphthenes), and aromatics, each with a range of physical properties and chemical compositions. Petroleum fuels also contain alkenes (olefins), which are formed during the formation of lighter molecular weight hydrocarbons, cracking, part of the refining process. Diesel fuel contains various additives for improved stability, cold starting, corrosion inhibitors, biocides, etc... [20, 21]. Crude oil and refineries throughout the world differ in composition and processes, therefore the resulting diesel fuel compositions are also quite different region to region. Past research has focused on a better fundamental understanding of fuel property and engine technology interactions and their combined impact on emissions. The following paragraphs outline important fuel properties, from an emissions standpoint, they include; cetane number, density, aromatic content, back end volatility (T90), sulfur content, and oxygenates [15]. Results suggest that lowering sulfur, density, distillation temperatures and multi-ringed aromatics reduce PM emissions. Other studies indicate that fuel effects depend upon the engine systems utilized for the test.

2.2 CETANE NUMBER

Diesel engines operate without an external ignition source, the fuel is injected directly into the hot compressed air charge several crank angles (°CA) before-top-dead center (BTDC) of the compression stroke. As the fuel is injected, there is a brief period of time before the fuel spontaneously ignites. This delay, physically and chemically

governed, between the start of injection (SOI) and start of combustion (SOC) is typically referred to as the ignition delay. The delay is a function of the ignition quality of the fuel that is characterized by the cetane number. The higher the cetane number, the easier it is for the fuel to ignite and the shorter the ignition delay. The chemical compound Cetane, also known as n-hexadecane ($C_{16}H_{34}$), has excellent ignition qualities and is assigned a reference value of 100. Heptamethylnonane ($C_{16}H_{34}$) has poor ignition qualities and is assigned a cetane number of 15 [20]. Paraffinic components in the fuel have high cetane numbers where as the cracked components, such as aromatics and olefins, impair the ignition quality. The higher the cetane number, the reduced premixed combustion phase. The premixed combustion phase results in a rapid rise in pressure at all engine loadings. Reducing the rate of pressure rise reduces the engine's noise, vibration, and harshness (NVH). Studies have also indicated that increasing the cetane number, slightly increases the PM emissions due to poor fuel-air mixing prior to ignition and reduces the HC emissions; others indicate a modest benefit in PM emissions. For engines with little premixed combustion, the impact of cetane on NO_x is small [15]. Thus, there is no general trend for cetane number, the impact is specific to the engine technology utilized. Many of the other fuel properties are difficult to generalize their impact on emissions and must be investigated for each engine and operating condition.

2.3 Aromatic Content

Evidence indicates that reducing the percentage of hydrocarbons that contain both poly and mono-aromatics, lowers the peak flame temperature during combustion. The reduction of high flame temperatures leads to a lower formation rate of NO_x. Additionally, reducing the high carbon to hydrogen (C/H) ratio of aromatics will lead to a smaller amount of CO_2 and an increase in H_2O. Water has a lower tendency to dissociated and will lead to a lower concentrations of oxygen, also decreasing NO_x production. The studies also indicate that lessening poly-aromatics increases the cetane number, thus aiding in the reduction of gaseous HC emissions [15].

The literature is unclear whether lowering aromatics reduces PM emissions. Some studies indicate that di and tri-aromatics affected PM emissions more than mono-aromatics. Reducing poly-aromatics reduces PM in older higher emitting engines, but for modern engines, reducing poly-aromatics has little impact [15]. The expected reduction is based on experiments conducted on a low temperature diffusion flame. However, the high temperatures of diesel engines, 2800 K, produces products that break down the carbon ring structure before oxidation and soot formation. Therefore, a more critical indication might be the fuels overall C/H ratio. Studies have indicated that decreasing this ratio, decreases the amount of soot. Likewise, a recent study has concluded that the tendency of fuel to soot is as follows; paraffins, olefins, naphthenes, and aromatics, with aromatics have the highest sooting tendency [19].

2.4 Sulfur Content

Sulfur is present in the crude oil's cracked components. During combustion, sulfur forms acidic by-products such as sulfur dioxide (SO_2), sulfur trioxide (SO_3), and gases and solid sulfate (SO_4) compounds. These solid sulfate particles contribute to the mass of the particulate matter emitted and interfere with the effectiveness of the catalytic surfaces. Previous studies have indicated that the amount of fuel sulfur, converted to sulfate via SO_2 and eventually into PM, is 1% - 2% of the fuel's weight percent sulfur, regardless of the fuel sulfur level or engine technology [15]. These sulfate particles are approximately 50 nm or less in diameter [36]. In addition to increasing PM, sulfur is also responsible for the unpleasant exhaust odor and acid rain (H_2SO_4). New regulations are requiring lower sulfur fuel content [1]. However, as the sulfur content decreases, the cost is increased and the side effect of the refinery process results in poor fuel lubricity [22, 49].

2.5 Fuel Density

A reduction in fuel density has been found to provide an emissions benefit in older technology engines. Fuel density impacts both injection spray dispersion angle and penetration. Injection spray dispersion angle depends on the ratio of the in-cylinder air density to the fuel and early injection spray penetration (liquid phase) and is proportional to $\rho^{-1/2}$. Decreasing fuel density will tend to increase both spray dispersion angle and spray penetration. Both of these effects are desirable, because they enhance the fuel-air mixing process. The actual impact on emissions will depend on the overall factors such as injection pressure and combustion chamber geometry, swirl rate, and charge temperature [46].

A change in fuel density also impacts the energy density of the fuel. Mechanical injection systems utilize a fixed volume delivery per crank angle, thus a decrease in density, will cause an increase in the injection duration. The end of injection (EOI) will occur at a later crank angle, changing the rate heat release (ROHR).

2.6 Fuel Volatility

Typically diesel fuel has a boiling point between 150° C and 380° C. The low boiling components are referred to as the front-end volatility (T10). This temperature range plays a critical role in cold starting, warm up, and the flash point (which is specified by law). The mid-volatility (T50) of diesel fuel has been shown to impact the fuel's sooting tendency and influence the fuel-air mixing upon injection. Sandia National Laboratories indicates that there is a strong correlation between the fuel volatility (T50) and maximum liquid fuel spray jet penetration and no observable correlation with ignition delay. A high volatility fuel will produce a shorter liquid-phase penetration length [15]. The high-end boiling points (T90) may not be completely oxidized and lead to the formation of engine deposits and increased PM levels. Research has shown that within the 350° C to 400° C range, high-end volatility has little impact on PM emissions [47]. A small decrease has been observed in NO_x as the back-end volatility has been decreased,

no effect on PM was noted [15]. In general, as the fuel's volatility is increased, the rate of premixed burning will also increase.

2.7 OXYGENATES

The effect of adding oxygenates to the fuel is not well understood. However, it is strongly believed that oxygenates impact the fuel spray's local equivalence ratio. As the amount of molecular oxygen is increased, there is a reduction in the formation of fuel fragments, a larger portion of carbon leaves the rich premixed zone as CO. It is has been suggested that oxygenates have a lower flame temperature, thus changing the rate of vaporization and the local air-fuel equivalence ratio [47]. Similar results have been found by utilizing oxygen enrichment of the intake air [42, 43]

The addition of oxygenates to diesel fuel could be used to comply with future emissions requirements. Prior studies have utilized chemicals such as: methylal also known as dimethoxymethane (DMM), Diglyme (DGM), dimethoxy ethane (DME), dimethyl carbonate (DMC), diethyl ether (DEE), various other acetates, maleates, and alcohols. These chemicals have been tested in neat and blended forms and have been shown to substantially reduce PM. The reduction in PM is occasionally accompanied by a small increase in NO_x emissions, when modest amounts of an oxygenate is utilized. Although oxygenates reduce the total particulate emissions, the relative composition of the particulate generally remains unchanged. The ratio of soluble organic fraction (SOF) to the insoluble organic fraction (ISOF) remains approximately equal to the PM derived from non-oxygenated fuel. Oxygenated diesel fuels have significantly lower unregulated emissions of aldehyde, keytone, and formaldehyde emissions [2-4, 23]. The changes in PM emissions were strongly affected by the blended oxygen content, rather than its molecular structure, cetane number, or boiling point [5]. Oxygenates increase the cetane number, reduce CO emissions, and increase HC emissions [24]. However, there are few studies that have attempted and correctly decoupled the modified fuel properties [15].

CHAPTER 3

EXPERIMENTAL FUEL MATRIX

3.1 FUEL MATRIX OVERVIEW

Previous studies have failed to decouple fuel effects brought about by "splash" blending of diesel fuel with oxygenates [15]. As outlined in the previous chapter, changes in other fuel properties such as, aromatic content, density, cetane, and volatility, can effect emissions. If several fuel properties are changed simultaneously, by "splash" blending an oxygenate with a base diesel fuel, it is difficult to ascribe emissions changes to the addition of molecular oxygen. Therefore, a carefully designed fuel matrix was utilized in order to isolate the fundamental mechanism(s) responsible for the changes in PM and NO_x emissions. The experimental fuel matrix attempts to systematically match specific fuel properties and quantify the relative impact on emissions.

3.2 BASE DIESEL FUEL

Phillips 66 low-sulfur type 2 diesel was selected as the base fuel. The low-sulfur content, 0.4 ppm, eliminated the sulfur-derived particulates, simplifying the fuel and emission analysis. Fuels containing modest levels of sulfur results in the formation of sulfate particles. These particles are 20 nm to 40 nm in diameter and are sensitive to dilution conditions. Adding 1,000 ppmv of Stanadyne Lubricity Additive enhanced the poor lubricity properties and the final mixture was given the abbreviation D-377. A cetane improved base fuel was formulated in order to match the higher cetane numbers of other fuels in the test matrix. The cetane matched fuel was given the abbreviation D-377+ and contained 10,000 ppm of 2-ethyl hexyl nitrate (2-EHN). Refer to Table 3.1 and Figure 3.1 for the base diesel fuel properties and distillation curve, respectively.

3.3 Oxygenate Proportionality

Initially, diethylene glycol dimethyl ether, commonly known by its trade name Diglyme, was added to the low-sulfur base fuel. This oxygenate was chosen due to its high solubility in diesel fuel and extensive use in previous studies [25, 26]. The blended mixture contains 20 vol-% Diglyme (abbreviated by DG20), resulting in 8 wt-% of the blended fuel's overall oxygen content. Previous studies indicate a 20% – 50% reduction in PM emission [3, 5]. In order to investigate the effects of different amount of molecular oxygen have on PM and NO_x emissions, 10 and 30 vol-% of Diglyme (DG10 and DG30) were also blended with the base fuel. The resulting test fuels contained 4, 8, and 12 wt-% oxygen of the oxygenate Diglyme. The densities of these compounds

3.4 Oxygenate Volatility

Diglyme is a member of the Glymes family of chemicals. The boiling point of these saturated polyethers is dependent upon the number of CH_2CH_2O groups. The volatility can be varied from 85 °C, 162 °C, and 276 °C, by utilizing three members of the Glyme family; Monoglyme, Diglyme, and Tetraglyme. Chemical structures and fuel properties are given in Table 3.2 and Figure 3.2. The weight percent of oxygen in the blend fuel was held constant at 8 wt-%, as the volatility of the oxygenate added to the base fuel was varied. The test fuels containing Monoglyme and Diglyme changed the front-end volatility (T10) of the test fuel, from the base fuel (D-377) temperature of 220° C to 100° C and 180° C for the Monoglyme (MG20) and Diglyme (DG20) blends containing 8 wt-% oxygen. Likewise, Tetraglyme (TG19) extended the mid-volatility (T50) of the fuel without a noticeable deviation from the base fuel's distillation curve, see Figure 3.3.

3.5 Oxygenate Structure

Holding the weight percent of oxygen constant at 8%, different oxygen containing function groups were blended with the diesel base fuel. Propylene glycol monomethyl ether acetate was added 19 vol-% with the base fuel and given the abbreviation PG19+. Another oxygenate containing, diethyl maleate, was added 17 vol-% with the base fuel (DM17+). Both of these compounds were selected due to their similar properties to Diglyme (DG20), see Table 3.3. However, 5,000 ppmv of 2-EHN was added to the maleate and acetate in order to match the cetane rating of the fuels containing Diglyme. All of these compounds have approximately equivalent boiling points, weight percent oxygen, and density. However, the acetate (PG19+) contains a double bonded carbon-oxygen molecule and chain branching. The ether (DG20) is a straight chained, fully saturated hydrocarbon compound, whereas the ester (maleate) contains a carbon-carbon double bond and an carbon-oxygen double bond. Refer to Figure 3.4 for a more detailed chemical and physical property information.

3.6 Oxygen Effect

The splash blending of oxygenates varies several fuel properties, such as density, volatility, sulfur content, aromatic content, and cetane number. Special attention has been placed upon matching the cetane numbers of all fuels in the test matrix. Emission sensitivity to oxygenate volatility has been addressed with three chemicals from the Glyme family of ethers. In order ascribe emission changes to the molecular oxygen, non-oxygen containing hydrocarbons, with similar fuel properties to the oxygen containing chemicals were utilized. These additives have similar chemical structures and physical properties to Diglyme, but lack the presence of oxygen. Two chemicals, n-decane, a straight chained hydrocarbon, and diethylene triamine, a nitrogen containing hydrocarbon, were added 20 vol-% and 17 vol-%, respectively, to the base fuel. A third chemical, 1-bromopropane, was added 10 vol-% to the base fuel in order to determine the impact an alkyl halide compound had on emissions. All of these non-oxygen containing fuels

required the addition 2-EHN to achieve cetane numbers comparable to the oxygenated fuels.

3.7 FISCHER-TROPSCH/OXYGENATE COMPARISION

In addition to the low-sulfur base fuel (D-377), a Mobil diesel fuel produced by the Fischer-Tropsch (FT) process was also tested. Fuels from the FT process, used extensively during the Second World War by Germany and in Africa where sanctions limited the amount of crud oil into the country, has recently experienced renewed interest. The fuel is made from natural gas or coal, which supplies the synthesis gas (CO and H_2) through partial oxidation, steam reforming, or a combination of both (autothermal reforming). Reactions with cobalt catalysts, hydrate the carbon atoms producing hydrocarbons and water. Currently natural gas discovered in crude oil fields is usually flared. It is speculated that the global reserves of natural gas are larger than that of crud oil.

Diesel fuel produced from the Fischer-Tropsch process, are fully paraffinic, contain zero sulfur, and have a distillation curve similar to that from crude oil, refer to Table 3.5 and Figure 3.6. The low soot forming and high cetane rating makes the FT a possibility of satisfying future emissions requirements. As a result, a fuel from this Fischer-Tropsch process was used in the fuel matrix to evaluate the effect of an inherently "cleaner" fuel has on emissions. In addition, Diglyme was also added 20% by volume to the FT fuel to determine the impact oxygenates have on a low sooting fuel.

Phillips 66 (D-377)	
Specific Gravity (16 °C)	0.830
Sulfur (wppm)	0.4
Flash Point (°C)	78
Pour Point (°C)	-18
Cloud Point (°C)	-20
Viscosity, cs 40c	2.6
Carbon (wt-%)	86.24
Hydrogen (wt-%)	13.76
Net Heat Combustion (MJ/kg)	43.08
Cetane Number	42
Aromatics (vol-%)	28.9
Olefins (vol-%)	4.7
Saturates (vol-%)	66.4

Table 3.1 Fuel properties for Phillips 66 low-sulfur diesel base fuel (D-377).

Fuel	Monoglyme	Diglyme	Tetraglyme
Chemical Formula	$C_4H_{10}O_2$	$C_6H_{14}O_3$	$C_{10}H_{22}O_5$
Specific Gravity	0.867	0.943	1.009
Boiling Point (°C)	85	162	276
Qhv (MJ/kg)	31.6	30.3	27.91
wt-% Oxygen	36.6	35.8	36

Table 3.2 Properties of the Glyme family of oxygenates.

Fuel	Diglyme	Propylene Glycol Monomethyl Ether Acetate	Diethyl Maleate
Chemical Formula	$C_6H_{14}O_3$	$C_6H_{12}O_3$	$C_8H_{12}O_4$
Specific Gravity	0.943	0.969	1.064
Boiling Point (°C)	162	146	225
Qhv (MJ/kg)	30.3	30.2	30.3
wt-% Oxygen	35.8	36.4	37.2

Table 3.3 Properties of different functional groups containing oxygen.

Fuel	n-Decane	Diethylenetriamine	1-Bromopropane
Chemical Formula	$C_{10}H_{22}$	$C_4H_{13}N_3$	C_3H_7Br
Specific Gravity	0.73	0.951	1.354
Boiling Point (°C)	174	207	71
Qhv (MJ/kg)	44.6	36.4	35.4

Table 3.4 Properties of different non-oxygen containing hydrocarbon compounds.

Mobil Fischer-Tropsch (FT)	
Specific Gravity (16 °C)	0.781
Sulfur (wppm)	0.0
Flash Point (°C)	96
Pour Point (°C)	-
Cloud Point (°C)	-1
Viscosity, cs 40c	3.2
Carbon (wt-%)	84.75
Hydrogen (wt-%)	15.23
Net Heat Combustion (MJ/kg)	43.81
Cetane Number	85
Aromatics (vol-%)	0.6
Olefins (vol-%)	1.1
Saturates (vol-%)	98.4

Table 3.5 Fuel properties for the Mobil Fischer-Tropsch process (FT).

Fuel Properties I												
Chemical Additive	Phillips 66		n-Decane	Monoglyme	Diglyme			Tetraglyme	Propylene Glycol Monomethyl Ether Acetate	Diethyl Maleate	Diethylene triamine	1-Bromopropane
Chemical Formula	-	-	$C_{10}H_{22}$	$C_4H_{10}O_2$	$C_6H_{14}O_3$			$C_{10}H_{22}O_5$	$C_6H_{12}O_3$	$C_8H_{12}O_4$	$C_4H_{13}N_3$	C_3H_7Br
Volume (%)	-	-	20	21	10	20	30	19	19	17	17	10
Specific Gravity (16 °C)	0.830	0.830	0.810	0.838	0.841	0.852	0.864	0.864	0.856	0.870	0.850	0.882
Sulfur (ppm)	0.40	0.40	0.32	0.32	0.36	0.32	0.28	0.32	0.32	0.33	0.33	0.36
Qhv (MJ/kg)	43.08	43.08	43.35	40.58	41.65	40.25	38.89	39.71	40.30	40.42	41.62	41.90
Cetane Number	42	58	58	47	51	54	57	59	60	60	60	60
Aromatics (vol-%)	28.9	28.9	23.1	22.8	26.0	23.1	20.2	23.4	23.4	24.0	24.0	26.0
Olefins (vol-%)	4.7	4.7	3.8	3.7	4.2	3.8	3.3	3.8	3.8	3.9	3.9	4.2
Saturates (vol-%)	66.4	66.4	73.1	73.5	69.8	73.1	76.5	72.8	72.8	72.1	72.1	69.8
Carbon (wt-%)	86.24	86.24	85.93	79.08	82.59	79.05	75.59	79.11	79.41	79.90	78.69	77.50
Hydrogen (wt-%)	13.76	13.76	14.07	12.96	13.39	13.03	12.68	12.90	12.75	12.35	13.54	12.52
Oxygen (wt-%)	0	0	0	7.96	4.01	7.92	11.73	7.99	7.84	7.75	7.77 (N)	9.98 (Br)
Stoich [A/F]	14.7	14.7	14.8	13.2	14.0	13.3	12.6	13.2	13.2	13.1	14.1	13.2
C/O Ratio	-	-	-	13.3	27.4	13.3	8.6	13.2	13.5	13.7	11.8 (C/N)	51.7 (C/Br)
H/C Ratio	1.91	1.91	1.97	1.97	1.95	1.98	2.01	1.96	1.93	1.85	2.06	1.94
Lubricity Additive (ppmv)	1,000	1,000	1,000	1,000	1,000	1,000	1,000	1,000	1,000	1,000	1,000	1,000
Cetane Improver (ppmv)	-	10,000	5,000	-	-	-	-	-	15,000	10,000	15,000	15,000
Fuel Code	D-377	D-377+	ND20+	MG21	DG10	DG20	DG30	TG19	PG19+	DM17+	DT17+	BP10+

Table 3.6 Properties for the fuels in the test matrix. All chemical additives are blended with the Phillips 66 low-sulfur diesel fuel (D-377).

Fuel Properties II		
Chemical Additive	Mobil Fischer-Tropsch	Diglyme
Chemical Formula	-	$C_6H_{14}O_3$
Volume (%)	-	19
Specific Gravity (16 °C)	0.781	0.812
Sulfur (ppm)	0	0
Qhv (MJ/kg)	43.81	40.83
Cetane Number	>74	
Aromatics (vol-%)	0.6	0.5
Olefins (vol-%)	1.1	0.9
Saturates (vol-%)	98.4	98.7
Carbon (wt-%)	84.8	77.90
Hydrogen (wt-%)	15.2	14.18
Oxygen (wt-%)	0	7.90
Stoich [A/F]	15.0	13.5
C/O Ratio	-	13.1
H/C Ratio	2.16	2.18
Lubricity Additive (ppmv)	1,500	1,500
Cetane Improver (ppmv)	-	-
Fuel Code	FT	FT-DG19

Table 3.7 Properties for the fuels in the test matrix. All chemical additives are blended with diesel fuel from the Mobil Fischer-Tropsch process (FT).

Chemical	Abbreviation	Comment
Phillips 66	D-377	Base fuel unless otherwise noted
Oxygenates		
Monoglyme	MG	Ether
Diglyme	DG	Ether
Tetraglyme	TG	Ether
Propylene glycol monomethyl ether acetate	PG	Acetate
Diethyl Maleate	DM	Ester
Non-oxygen containing compounds		
n-Decane	ND	Paraffin, Alkane
Diethylenetriamine	DT	Amine (Nitrogen)
1-Bromopropane	BP	Alkyl Halide (Halogen)
Alternative base fuel		
Mobil FT	FT	Fischer Tropsch
Cetane additives		
2-EHN	+	Nitrate
DTBP	#	Peroxide

Table 3.8 Summary of fuels and chemical additives utilized in the fuel test matrix.

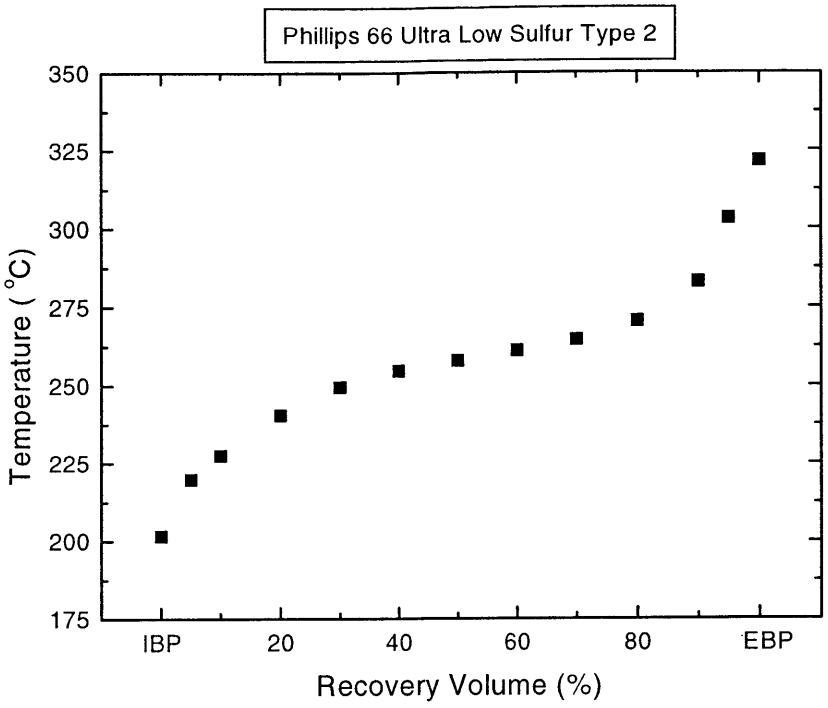

Figure 3.1 Fuel distillation curve for Phillips 66 low-sulfur diesel base fuel (D-377).

Monoglyme 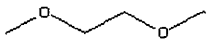 [110-71-4]

Diglyme 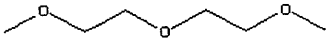 [111-96-6]

Tetraglyme 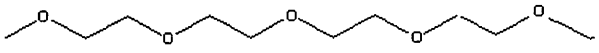 [143-24-8]

Figure 3.2 Chemical structures for the Glyme family of oxygenates.

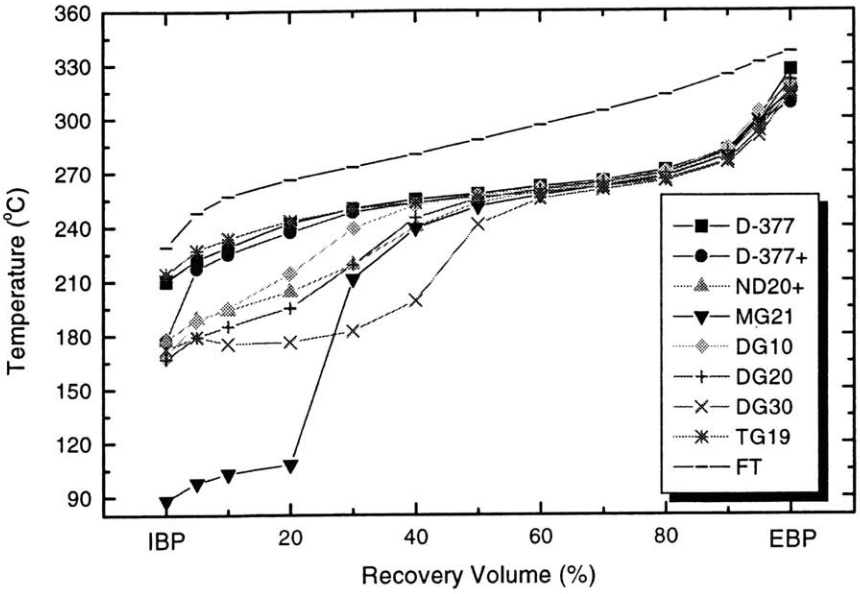

Figure 3.3 Fuel distillation curve for various fuels in the test matrix.

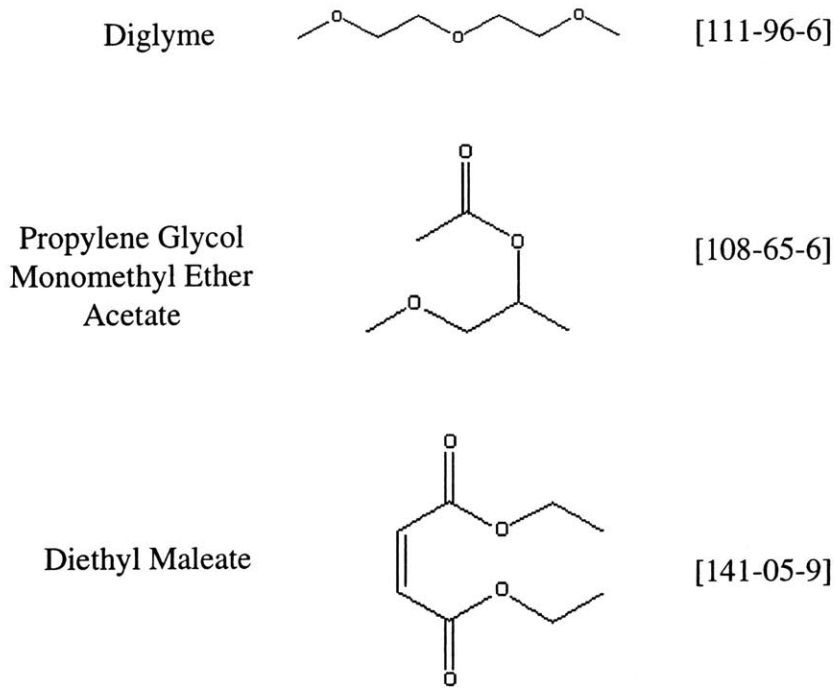

Figure 3.4 Chemical structures for the different functional groups containing oxygen.

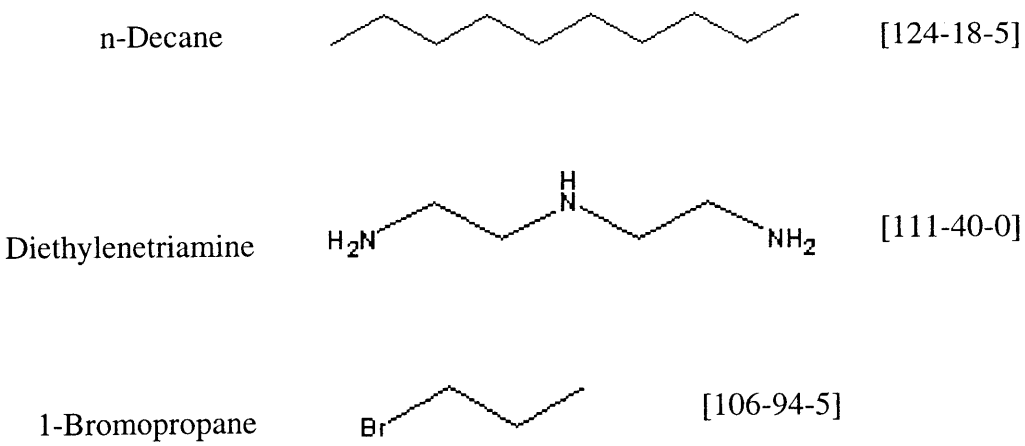

Figure 3.5 Chemical structures for the different non-oxygen containing hydrocarbon compounds.

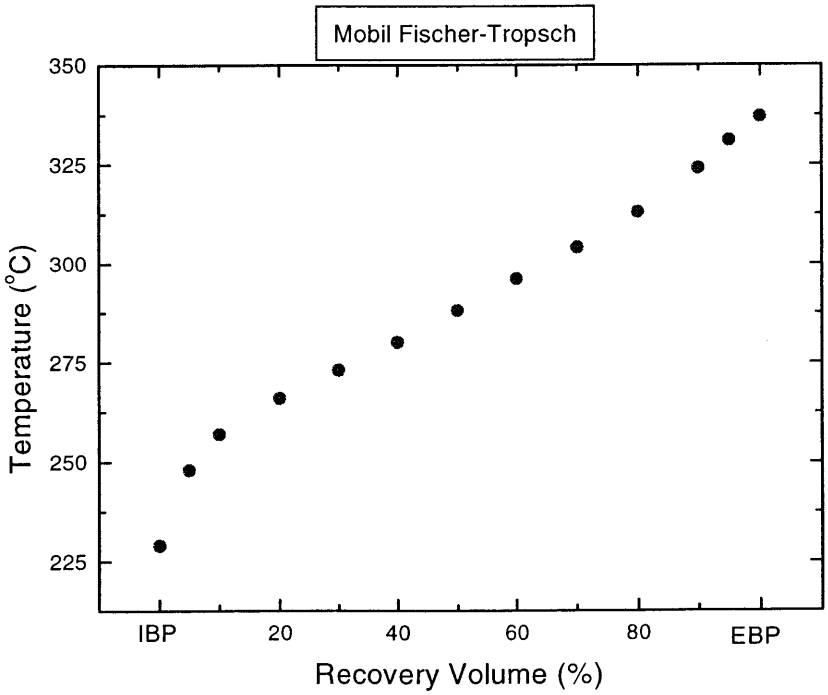

Figure 3.6 Fuel distillation curve for Mobil Fischer-Tropsch diesel fuel (FT).

CHAPTER 4

EXPERIMENTAL SETUP

4.1 ENGINE

A direct injection single cylinder Ricardo MK IV Hydra was used to conduct the engine experiments. The naturally aspirated engine utilizes a toroidal bowl-in piston design and directed ports to achieve rapid fuel-air mixing necessary for high-speed operation. The fuel is delivered via a Bosch type-A in-line, plunger-and-barrel, pump with a maximum rated pressure of 600 bar. The hole-nozzle type injector is located off axis, between the intake and exhaust valves, and has an opening pressure of 250 bar. Refer to Figures 4.1 and 4.2, and Table 4.1 for additional details. An electric actuator that varies the position of the pump relative to the crankshaft controls injection timing. Fuel metering was adjusted by varying the engagement of the plunger's helical groove relative to the spill port in the barrel, thus changing the end-of-delivery point [27]. The engine test setup is equipped with pre-heaters for the intake air, coolant, and oil. The engine is coupled to a Dynamatic Model 20 AC dynamometer with a Digalog controller.

4.2 IN-CYLINDER PRESSURE AND NEEDLE LIFT MEASUREMENTS

Cylinder pressure was measured using a flush-mounted Kistler 6125 piezo-electric transducer located directly opposite of the off-axis injector. The transducer's current output is converted to a voltage amplifier using a Kistler, model 504, charge amplifier. A hall-effect proximity sensor, designed and machined by Wolff Controls Corporation, is outfitted in fuel injector. The sensor outputs a voltage proportional to the needle lift in order to determine the start and end of injection.

A data acquisition system, running Global Lab software, was used to capture both in-cylinder pressure and needle lift measurements. A 360-degree optical shaft encoder

located on the crank shaft provided the external clock signal with a superimposed 2 volt spike on the pressure trace to mark the start of the compression stroke. External post-processing code was used to determine the gross indicated mean effective pressure (imep) and start of injection (SOI). The pressure transducer was periodically checked with log-pressure versus log-volume plots ensuring linearity of the compression and expansion strokes. The in-cylinder transducer was also periodically cleaned and re-calibrated as specified by the manufacture.

4.3 Fuel and Air Measurements

The engine test setup uses two fuel systems that allow switching between multiple fuels while still firing the engine. Both systems utilized heat exchangers to maintain the fuel at a constant temperature of 25° C after the fuel circulates through the pump and injector. Due to the strong solvent properties of the oxygenates and the other chemical additives, sections of the fuel system were replaced with flexible chemical resistant PTFE tubing when the rigid stainless steel tubing could not be utilized. Each fuel system contains two stain steel 7 μm mesh filters used to eliminate any damaging debris from entering the fuel system or returning from the pump. The primary fuel system uses a M.A.X. Rotary Flowmeter while the secondary system uses an A.N.D., model 50010, electronic balance for gravimetric fuel measuring (Figure 4.3). A Kurz Instruments, model 505-9A-02, laminar airflow element located in the engine's intake, enables accurate measurements of the air mass flow inducted.

4.4 Heat Release Analysis

The heat release procedure used was initially adapted by Shihadeh [28] for diesel combustion analysis from an SI code developed by Cheung [29]. The program utilizes a First Law, single-zone treatment of the combustion chamber contents, assuming perfect gas relations. The model uses thermodynamic properties that are a function of the temperature, pressure, and equivalence ratio. The energy release per crank angle degree

can be found in the appendix. Output from the code has a frequency of oscillation corresponds to the 4k Hz natural frequency of the combustion chamber. A spline fit was used to better interpolate the heat release rates between crank angles.

The energy release occurs in two-stages, the premixed combustion phase and mixing-controlled combustion phase. The premixed combustion is fuel-rich ($\phi \sim 4$) and characterized by a rapid energy release as the fuel is broken down into fuel fragments, eventually leading the formation of PM. At the maximum of the premixed spike, the diffusion flame forms around the rich products. The fuel spray is characterized by both a fuel rich region and a diffusion flame region. The diffusion flame is approximately stoichiometric and leads to high formation of NO. The PM formed by the fuel-rich zone, undergoes oxidation and agglomeration as it passes through the diffusion flame. Retarding the SOI or SOC from the maximum break torque (MBT) timing lowers the formation of NO_x, but increases particulates. Likewise, the opposite condition occurs as the timing is advanced, and referred to as the PM-NO_x trade off. The rate of combustion is determined by the fuel-air mixing rate, and the engine load is selected by the amount of fuel injected [12].

4.5 Dilution Tunnel

The particulates were sampled from a mini-dilution tunnel. The United States Environmental Protection Agency (USEPA) defined diesel particulate matter as all solid and/or liquid matter that collects on a filer in a diluted exhaust stream at a temperature less than 52 °C [30]. The dilution tunnel simulates the dilution process that occurs as the engine's exhaust enters the atmosphere. Particles undergo a number of processes such as coagulation, deposition, and growth via condensation, adsorption, or absorption of vapors as they are diluted. The tunnel's air source is supplied by an oil-free 100-psig compressor. The compressed air temperature averaged 25° C and 10% relative humidity throughout the engine experiments. The air from the compressor passed through a 2" Balson (A15/80-DX) filter, rated at 93% efficiency at 0.01 μm. The tunnel has a 2-inch diameter, with a venturi contraction where a fraction of the raw exhaust is introduced.

The pressure drop across the venturi, draws a continuous sample into the tunnel for dilution. Sampling ports on the dilution tunnel were located approximately 33 inches (greater than 10 pipe diameters) from the introduction of the exhaust gases. Stainless steel probes, located at the pipe's center, sampled the diluted exhaust for both the particulate and gas sampling. All sampling was approximately iso-kinetic.

4.6 Carbon Dioxide and NO_x Measurements

In order to calculate the dilution ratio, R_d, for the dilution system, a Rosemount Analytical, model 880A, non-disperse infrared (NDIR) analyzer was used to determine the volume percent of CO_2 on a dry basis. Two ranges were used for the monitoring the tunnel and raw exhaust, 1% and 10% respectively. As a result, four different concentrations of CO_2 were used to generate a fourth order polynomial calibration curve for each range. Sampling the concentrations of CO_2 in the dilution air, raw exhaust, and dilution tunnel, was used to determine the dilution ratio in the tunnel. Since the NDIR requires the removal of water vapor, the mass concentration are determined on a dry basis and must be corrected by the concentration of the water vapor in the original gas (See Appendix for calculation). Injecting a known flow rate and concentration of CO2 into the tunnel and monitoring the CO2 levels in the tunnel approximated the tunnels flow rate.

The oxides of nitrogen (NO_x) were monitored in the raw exhaust stream (dry basis) with a Thermo Environmental Instruments Inc., model 10A, chemiluminescence analyzer. The detector's linear scale requires two calibration gases, a zero gas (nitrogen) and 990 ppm NO span gas. All concentration of NO and NOx were recorded and converted to reflect the mass of NO_x per indicated per mass of fuel injected, using the emissions index (EI).

4.7 Unburned Hydrocarbons

Unburned hydrocarbons (HC) in the raw exhaust stream were measured using a Rosemount Analytical Hydrocarbon Analyzer (model 402). The flame ionization detector

(FID) utilizes a heated (275° C) inlet sample line and PM filter for diesel measurements. The analyzer's linear scale was calibrated using a zero gas (nitrogen) and 4,536-ppmC1 gas (propane). All measurements reflect C_1 hydrocarbons on a "wet" exhaust basis.

4.8 Particulate Size Distribution

A Scanning Mobility Particle Sizer (SMPS) manufactured by TSI, model 3934, was utilized to investigate the size distribution of the particulates. The instrument approximates diameters based on the behavior of the particles to transverse a flow fluid balanced against its electrical mobility. The SMPS consists of a neutralizer, electrical mobility section, and a particle detection stage (Figure 4.5). The sampled dilute polydisperese aerosol initially flows through a single stage inertia impactor, limiting the particle size into the detector to less than 1 μm in diameter. The smaller particles follow the streamlines and enter the classifier where they pass through a ^{85}Kr bipolar beta-emitting source. The aerosol is subjected to a Boltzmann bipolar charge distribution, symmetrical around zero, with a fraction of positive charged particles equal to that of the negative charged fraction. The SMPS software is equipped with a charge correction algorithm that is used to correct for deviations in the Boltzmann distribution caused by multiple charges on large particles. The aerosol is then sent through an annulus, in the center is an electrostatically charged rod with a small slit at its far end. Particles with a positive charge are drawn toward this tube through a concentric flow of highly filtered air, called sheath air, located between the rod and aerosol. Particles with too little aerodynamic drag (too small a diameter) are drawn toward the charged tube early in the process. As a result, they impact the wall before reaching the hole. Particles with too high a drag (large diameter) are not drawn in sufficiently far toward the tube to enter the slit (Figure 4.6). Therefore, only a certain size range of particles passes through the slit and on to the Condensation Particle Counter (CPC).

The CPC consist of a saturator, condenser, particle optical sensor, flow control orifice, and pump. The aerosol entering the CPC is saturated with butanol alcohol and cooled in a condenser tube. The particle undergoes heterogeneous condensation,

increasing allowing for the PM to be optically counted interrupting a laser beam (Figure 4.8). These pulses are counted by the CPC, which has a 50% detection efficiency at 10-nm diameter. It operates in single count mode and up to 10,000 counts per cm^3. The CPC software corrects of the probability of coincidence errors, having more than one particle in the view volume upon a single pulse.

The CPC was set up to operate in an underpressure mode. However, the dilution tunnel is slightly above pressure, as a result, the sample line from the tunnel's sampling port to the SMPS is vented to reduce pressure to atmospheric. The flow rates for the monodisperse, excess, and sheath air were set by valves until the corresponding voltages, listed in the Classifier manual, were obtained. An A.P. Buck bubble flow meter was used to confirm these flow rates. The SMPS is capable of measuring concentration from 1 to 10^7 particles per cubic centimeter within any given size range from a diameter of 20 nm to 1000 nm. The flow rates used for the this study used were 0.2 standard liters per minute (slpm) of particle-laden gas and 2.0 slpm of sheath air, giving a scanning range diameter between 21-865 nm. The scanning rates were set at 120 seconds for the up-scan and 60 seconds for the down-scan. The SMPS software corrects for flow rates, multiply charged particles, and negatively charged particles. The final outputs are the particle count size distribution per channel. Both the number and volume distribution are normalized by the bin width of 32 channels per decade. The results can be integrated to reflect the total number and volume of particles per sample volume [31].

4.9 Filter Sampling, Conditioning, and Weighing

Pallflex 47 mm diameter filters, model TX40H120-WW, were utilized for all gravimetric mass measurements. The Teflon bonded borosilicate micro-glass fiber filters reduce moisture uptake and chemical transformation, making them suitable for chemical analysis. The filters were stored in glass petri dishes to minimize losses due to static charge. The USEPA guidelines for conditioning, handling, and weighing require the temperature in the filter conditioning room to be maintained within 10° F (6° C) of a set point between 68 and 86° F (20 - 30° C) during filter conditioning and weighing.

Likewise, the USEPA specifies that the humidity should be held within 10 percent of a point between 30 to 70%, with an 8 to 56 hour conditioning time [32]. During filter testing, the temperature was within the USEPA specifications. However, without an environmental controlled room, the humidity varied outside of the USEPA's guidelines and was measured with a Cole-Palmer model 37950-00 thermohygrometer. It was thought that the low moisture uptake Teflon filters and low-sulfur content, minimized the effects of varying levels of humidity. An Ohaus Explorer E11140 microbalance, accurate to 0.1 mg, was used for filter weighing.

A dilution ratio between 15:1 to 20:1 was utilized for filter measurements with a critical flow orifice allowing 38 slpm. Filter testing was done with a BGI stainless steel 47-mm filter holder, up stream of an O'Keefe Controls #86 precision metal orifice. A vacuum pump was used to sustain choked flow through the critical flow orifice. The pressure ratio was monitored to ensure the pressure ratio was less than 0.528 necessary for choked flow. As the filter's face collects PM, the down stream of the filter, upstream of the orifice, begins to decrease. The volume flow rate through the orifice is held constant, however, the mass flow rate decreases. The sampling was terminated before the upstream pressure dropped too low and choked flow was no longer sustained. The upstream pressure was recorded at regular intervals and an average mass flow was calculated for each filter sample.

Model	Ricardo Hydra MK IV
Number of Cylinders	1
Combustion System	Direct Injection
Bore (mm)	80.3
Stroke (mm)	88.9
Displacement (liters)	0.45
Compression Ratio	19.8 : 1
Aspiration	Naturally Aspirated
Valve System	2 Valves (SOHC)
Valve Timing	IVO: 10° BTDC | IVC: 41° ABDC
	EVO: 58° BBDC | EVC: 11° ATDC
Fuel Injection Pump	Bosch Type A
Peak Pump Pressure (bar)	600
Injection Nozzle	4 X Φ 0.21mm X 155° Cone
Nozzle Opening Pressure (bar)	250
Maximum Speed (rpm)	4500
Maximum Power (kW)	8
Oil Temperature (°C)	85
Coolant Temperature (°C)	85

Table 4.1 Test engine specifications.

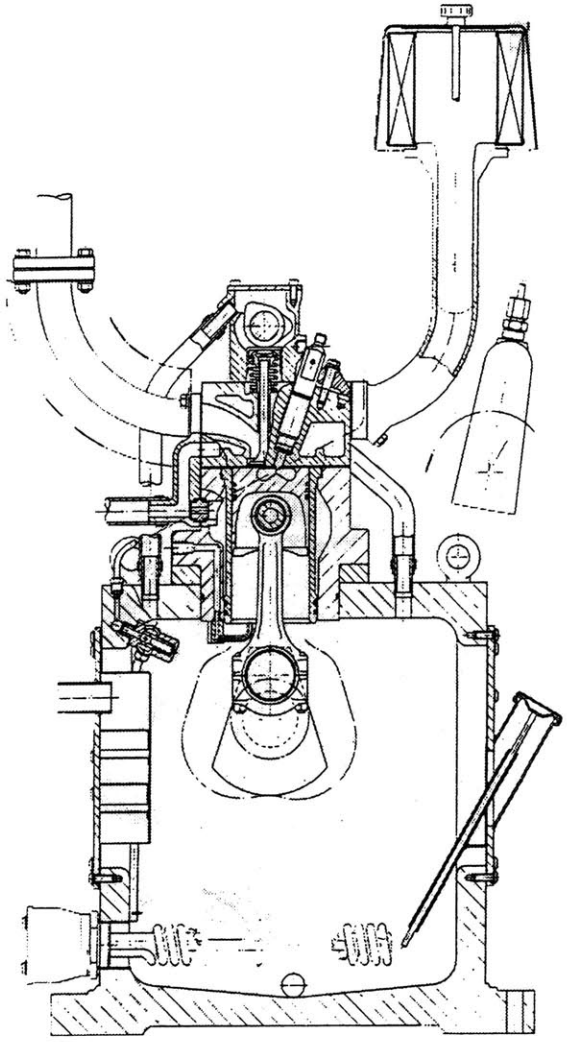

Figure 4.1 Ricardo Hydra MK IV cross section view

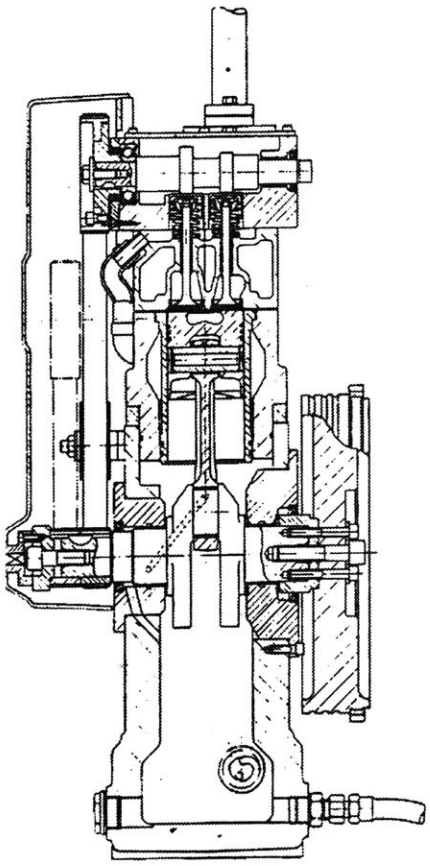

Figure 4.2 Ricardo Hydra MK IV longitudinal section view

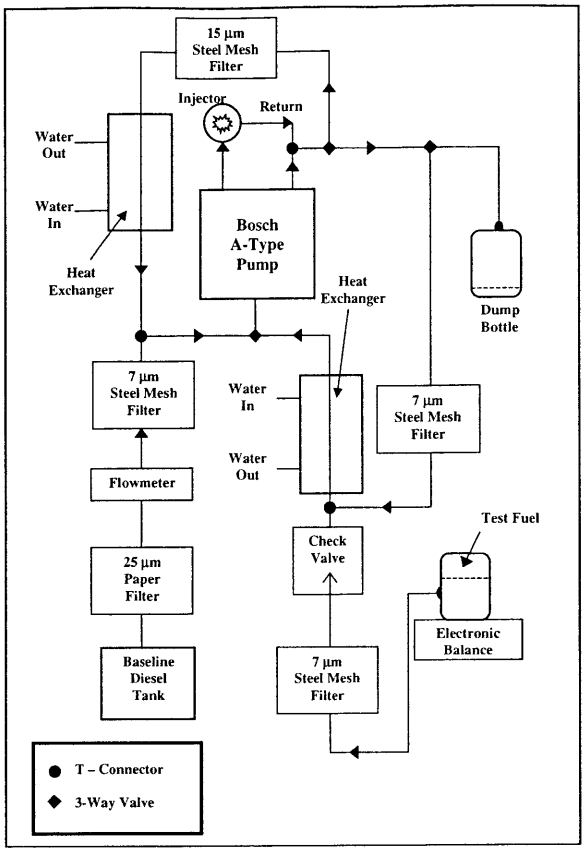

Figure 4.3 Fuel system schematic.

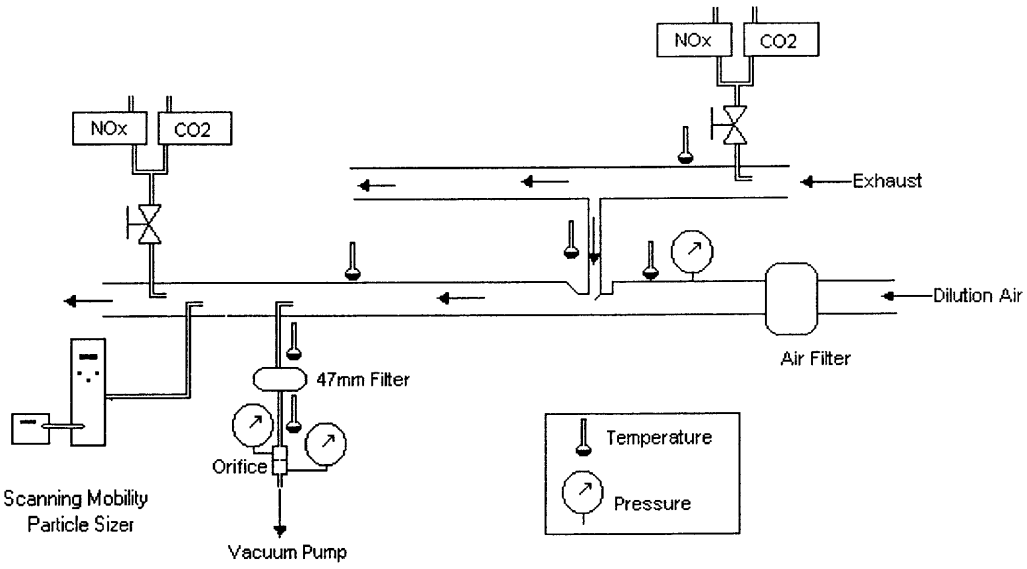

Figure 4.4 Dilution tunnel schematic (not to scale). Location of gaseous sampling in exhaust and diluted exhaust. Filter and SMPS measurements taken <52 °C in diluted exhaust stream.

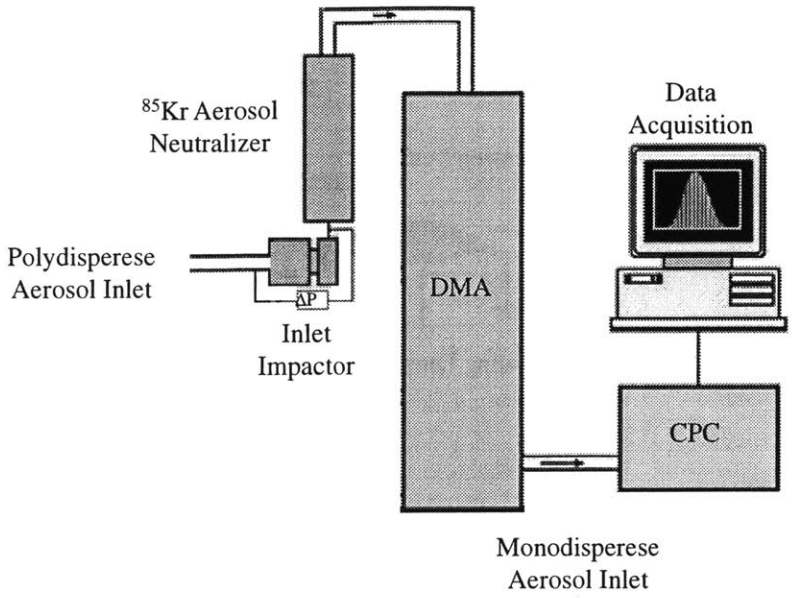

Figure 4.5 SMPS measurement system schematic, TSI model 3934.

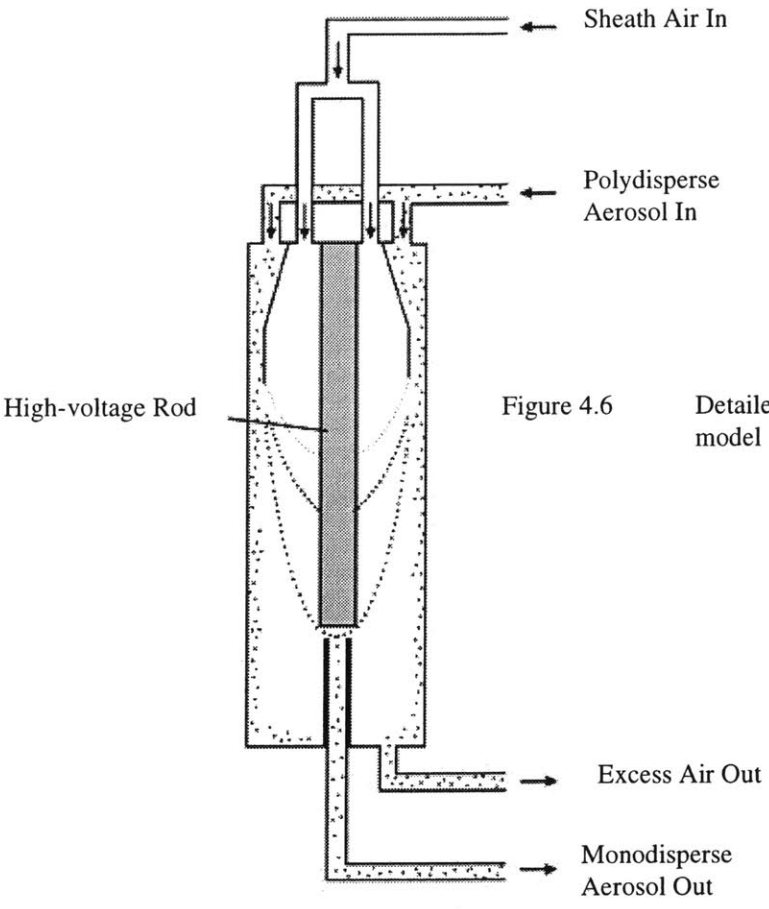

Figure 4.6 Detailed schematic of SMPS DMA classifier, TSI model 3071.

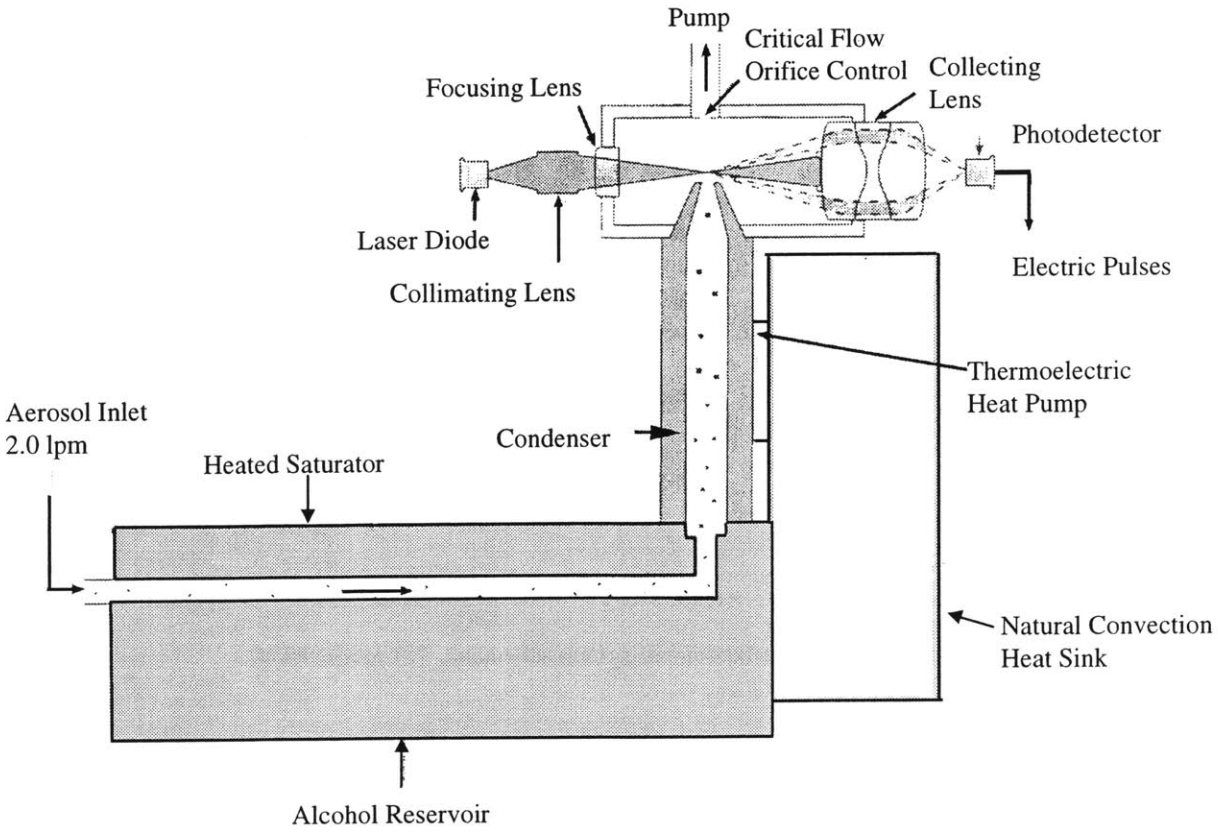

Figure 4.7 Detailed schematic of condensation particle counter (CPC), TSI model 3010.

CHAPTER 5

EXPERIMENTAL PROCEDURE

5.1 FUELING STRATEGY

The fuels outlined in the experimental matrix vary in cetane number, density, energy density, and chemical composition. Attention has been give to approximately match the combustion phasing for all of the test fuels. By using a cetane improper, to obtained cetane numbers in the mid-fifties, and fixed SOI timing, the start of combustion has been equally phased for all of the fuels. The injection duration varies slightly with each fuel (within 2° CA), which is a reflection of the different energy densities. The current fuel injection system on the Ricardo engine utilizes a fixed volume fuel delivery per crank angle. Fuels with the lowest energy densities (MG21, DT17+, and DM17+) experienced an increase in injection duration from 11.5° CA with the base fuel to 13.5° CA. Likewise, there are some differences in the combustion process itself. The maximum premixed burn heat release rate also varies among the fuels due to both chemical and physical differences. The indicated fuel conversion efficiency and specific fuel consumption is given in Figure 5.1. The indicated fuel conversion efficiencies for all of the fuels are approximately equivalent, with variations in specific fuel consumption due to energy density differences.

The engine's sensitivity to operating parameters, with base fuel (D-377), was investigated for different intake temperatures, start of injections, ignition delays, and load. Subsequent testing of the fuel matrix was conducted with an equivalent injected energy and combustion phasing. Differences in emission levels were quantified by matching imep, SOI, and SOC by use of a cetane improver. Later tests were conducted at equal fuel/air equivalence ratios and a lower normalized torque in order to further evaluate emission changes due to oxygenates.

5.2 ENGINE OPERATION

All engine tests were conducted under steady state conditions. An engine speed of 2400 RPM was utilized for all engine experiments. Before beginning each engine test, the gas analyzers, SMPS, and dilution tunnel air system, were given adequate time to reach their operating temperatures and then calibrated. The lubrication oil and engine coolant were preheated to their set point temperatures of 85° C. Before engaging the dynamometer, the torque offset was recorded. Once engaged, a motoring pressure trace was captured, processed to reflect an imep value from 100 engine cycles, and compared to previous runs (See Figures 5.2 and 5.3). The engine was then fired on the standard base fuel (D-377) for a period of thirty minutes at an imep of 5.6 bar and SOI timing of 6° BTDC. During this period of time, the lubrication oil, engine coolant, intake, and exhaust, temperatures reached steady state values. At the end of the thirty minutes, emission levels and engine operating parameters were recorded. Then a fraction of the exhaust was directed through the dilution tunnel.

5.3 DILUTION TUNNEL OPERATING CONDITIONS

After the engine and exhaust system reached steady state temperatures, the transfer valve connecting the dilution tunnel and engine exhaust system was opened. The temperature and CO_2 concentration within the tunnel and raw engine exhaust were continuously monitored. Particulate measurements began once a stabilized dilution ratio and diluted air temperatures were obtained.

Background PM levels in the dilution tunnel and ambient air were measured during engine testing. Ambient air and dilution tunnel background SMPS measurements are shown in Figures 5.5 and 5.6. Integrated SMPS and filter results are located in Table 5.1. The dilution air was found to contain an order of magnitude fewer number of particles than the surrounding ambient air within the test cell area. When compared to the engine exhaust levels, the dilution air was two orders of magnitude lower in the number of particles and more than an order of magnitude lower in the volume of particles. In

addition to the SMPS measurements, filter background tests were also conducted with the dilution air. Filter samples from the dilution air were taken for a period of 6 hours and weighed. The mass collected on the filters was outside the range of the balance and determined to be negligible.

Particle size distributions have been found to be highly dependent upon the dilution conditions [33]. Ultrafine particles are sensitive to dilution ratio and dilution air temperature. Maricq *et al* [34] observed artifacts from the tunnel and sampling lines that substantially altered particle size distribution. Currently, the USEPA does not stipulate any regulations on PM sampling other than the specified maximum temperature (52° C) at the point of sampling. Recent publications have indicated that particle size distributions are sensitive to the dilution conditions [34, 35, 48]. Variables such as dilution air temperature, humidity, and PM residence time in the dilution tunnel can impact the measured size distribution.

The sampling probes were orientated parallel to the direction of the flow stream. The compressed oil-free dilution air utilized a drier system, averaged an air temperature of 25° C and a relative humidity of 10%. Likewise the dilution ratio was adjusted to 180:1, 350:1, 600:1 with no notable changes in particulate behavior during the SMPS scans (Figures 5.7 and 5.8). Given the range of CO_2 analyzer and inaccuracy of the NO_x meter at low concentrations, a dilution ratio of 600:1 proved to be a compromise between accuracy and prevention of saturation of the CPC (less than 10,000 particles/cm^3) which occurred at the 180:1 dilution setting.

The flow rate of 1,600 slpm was utilized for the dilution tunnel, with turbulent pipe flow to ensure mixing over the length of 10 pipe diameters (Reynolds number approximately 45,800). The test point with SMPS with the standard fuel (D-377) was taken during every test to compare the baseline emission levels to previous experiments. Figure 5.9 and 5.10 show the day to day variability of 30 SMPS measurements, the error bars reflecting a 95% confidence interval. Standard filter measurements were taken at a dilution ratio of 25:1, for 10 minutes.

Sample	Total No. ($\#/cm^3$)	Peak No. ($\#/cm^3$)	Peak No. D_p (nm)	Total Vol. (nm^3/cm^3)	Peak Vol. (nm^3/cm^3)	Peak Vol. D_p (nm)	Filter Mass Measurement (g)
Ambient	8.64E+03	4.38E+02	45	2.96E+10	3.53E+09	865	Not Detectable
Dilution Tunnel Air	7.44E+02	3.13E+01	45	1.51E+10	1.88E+09	850	Not Detectable

Table 5.1 Integrated SMPS and gravimetric filter results from ambient and dilution tunnel background PM.

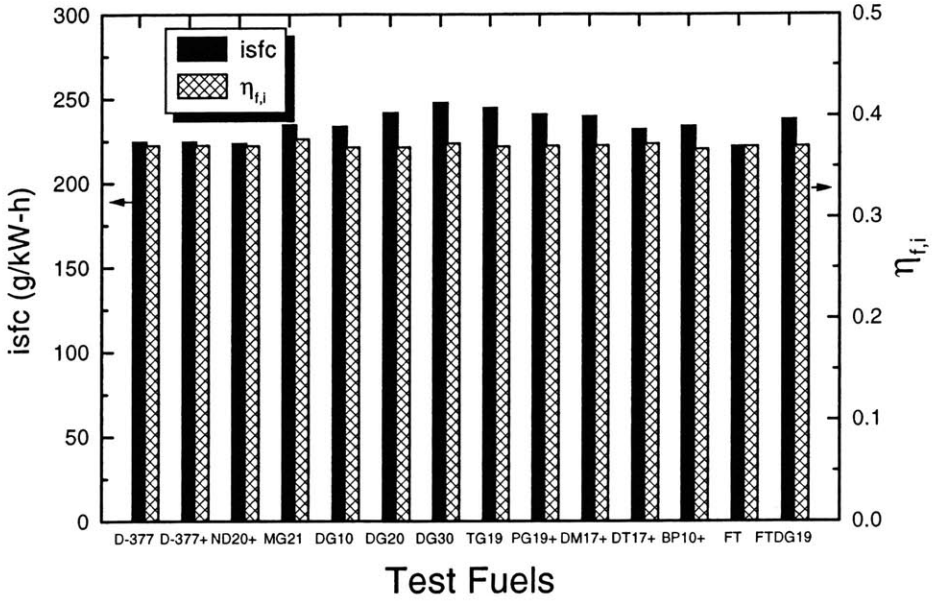

Figure 5.1 Indicated specific fuel consumption (isfc) and indicated fuel conversion efficiency ($\eta_{f,i}$) for various test fuels.

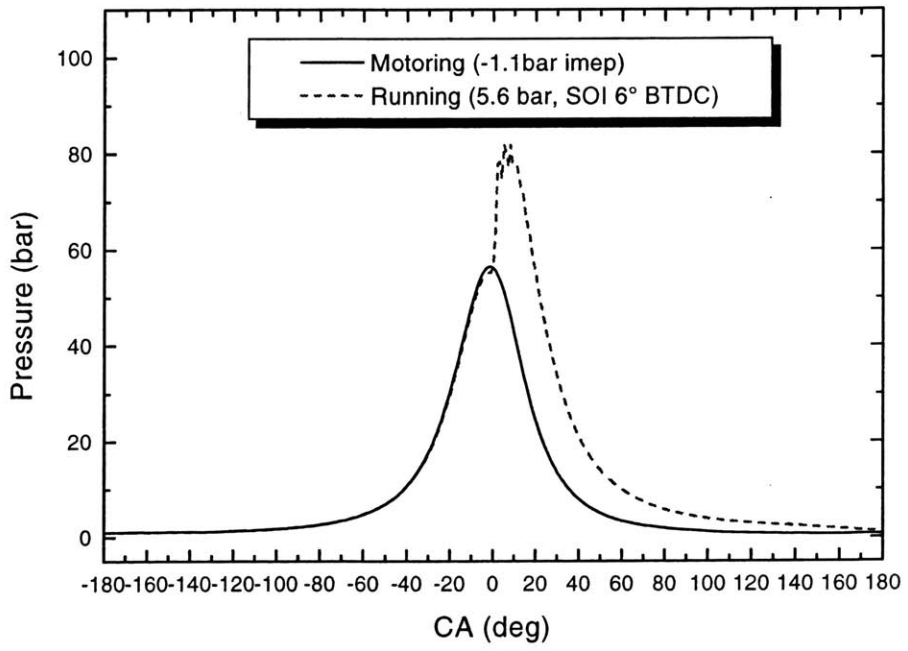

Figure 5.2 Motoring and running pressure trace versus crank angle for the compression and expansion strokes. Operating at 2400 RPM, the motoring trace has a negative imep value, due to heat transfer losses.

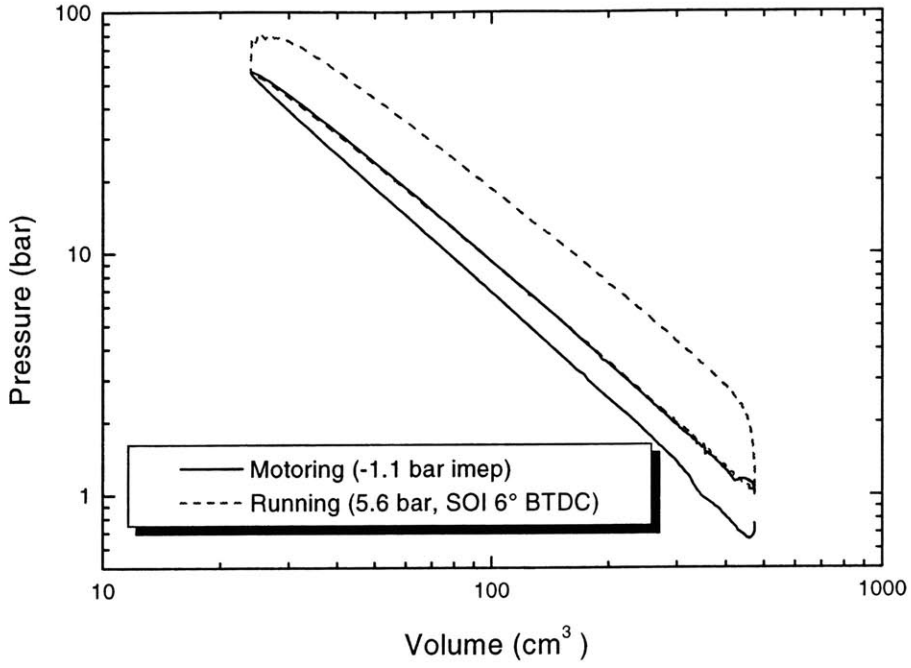

Figure 5.3 Log P versus log V diagram for the motoring and running condition. Operating at 2400 RPM.

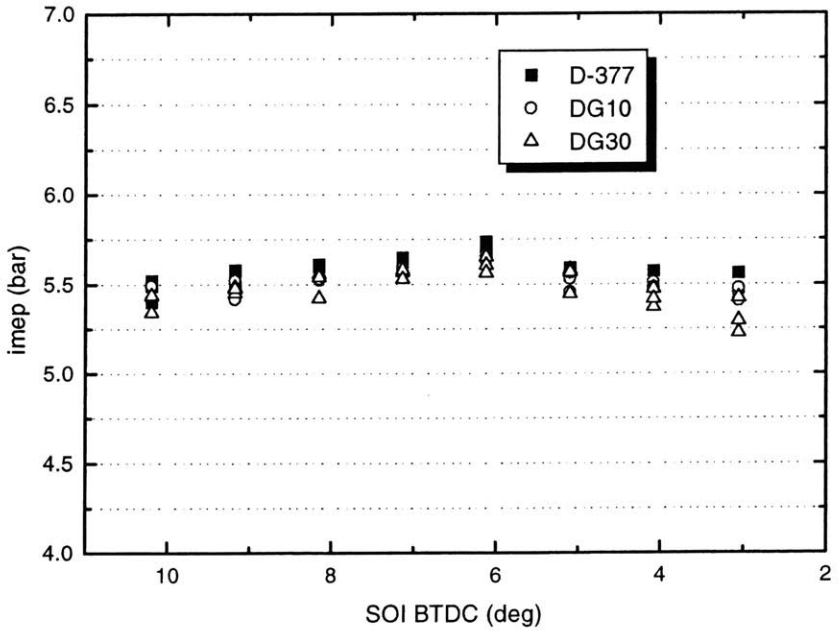

Figure 5.4 Indicated mean effective pressure versus start of injection timing. Optimum timing corresponds to 6° BTDC.

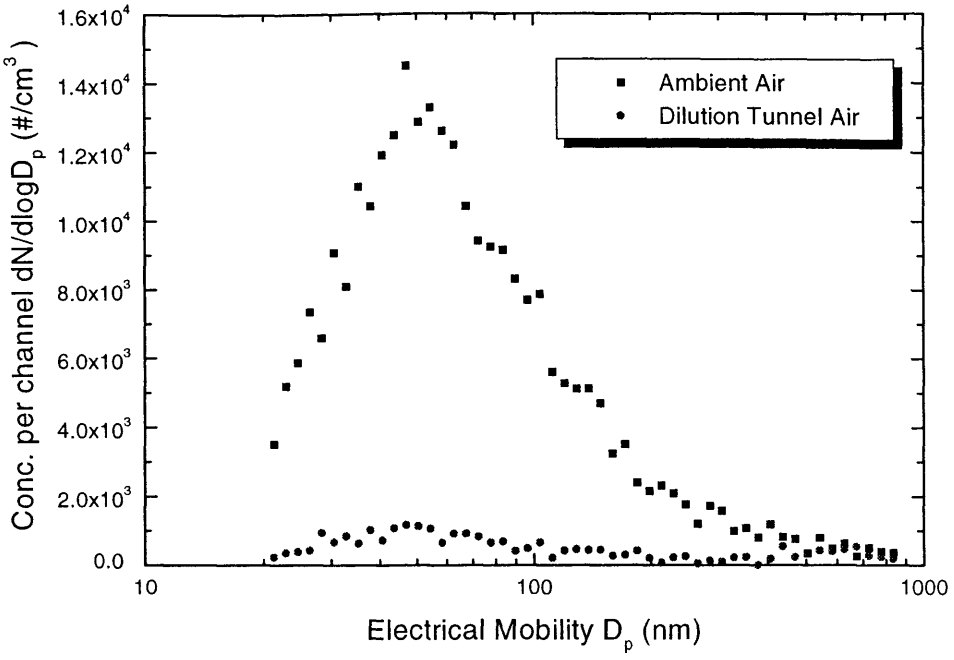

Figure 5.5 SMPS number concentration per channel versus electrical mobility diameter for ambient and dilution tunnel background PM.

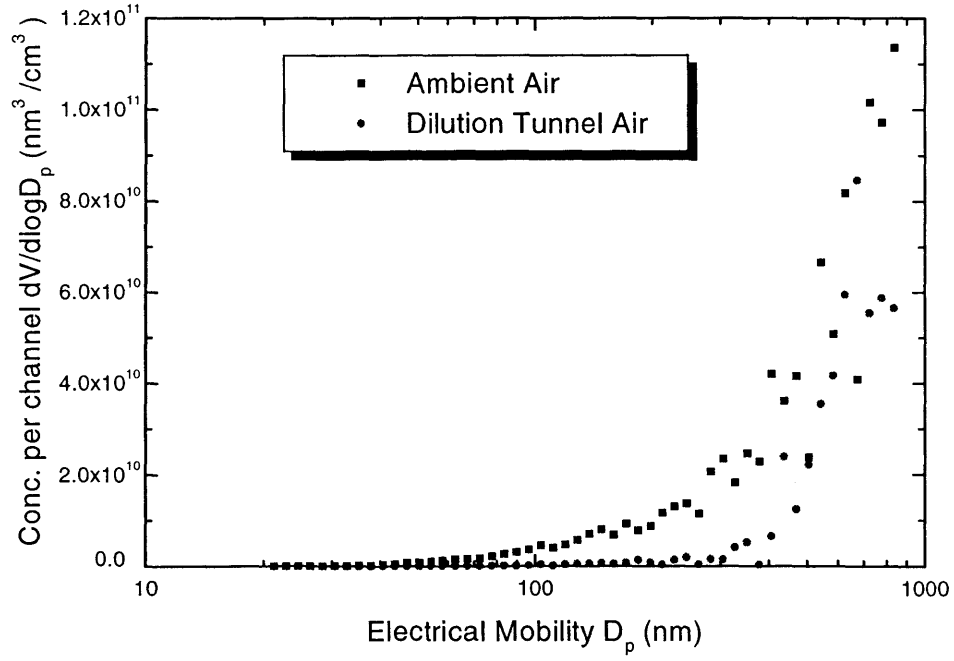

Figure 5.6 SMPS volume concentration per channel versus electrical mobility diameter for ambient and dilution tunnel background PM.

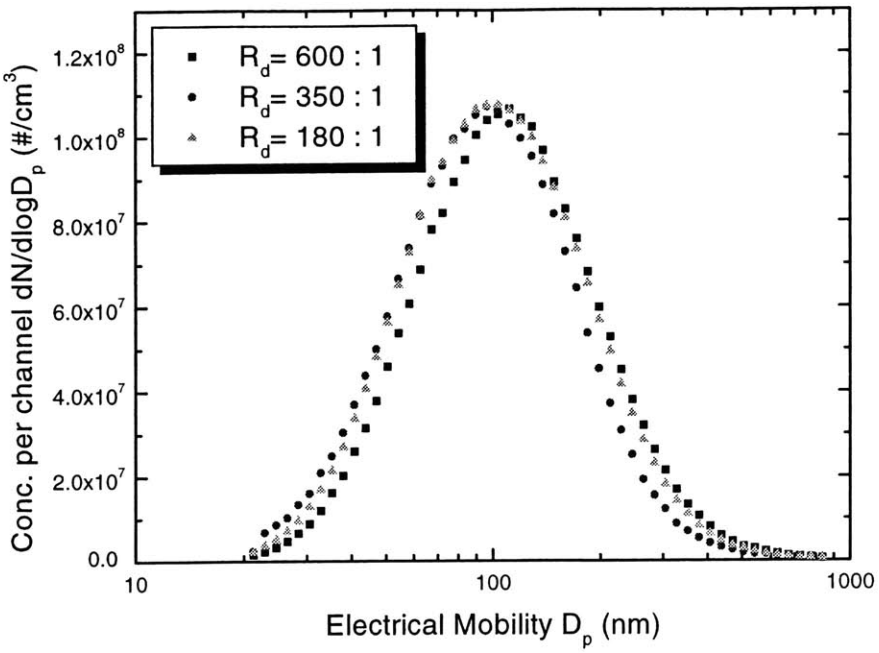

Figure 5.7 SMPS number concentration per channel versus electrical mobility diameter for different dilution ratios (R_d).

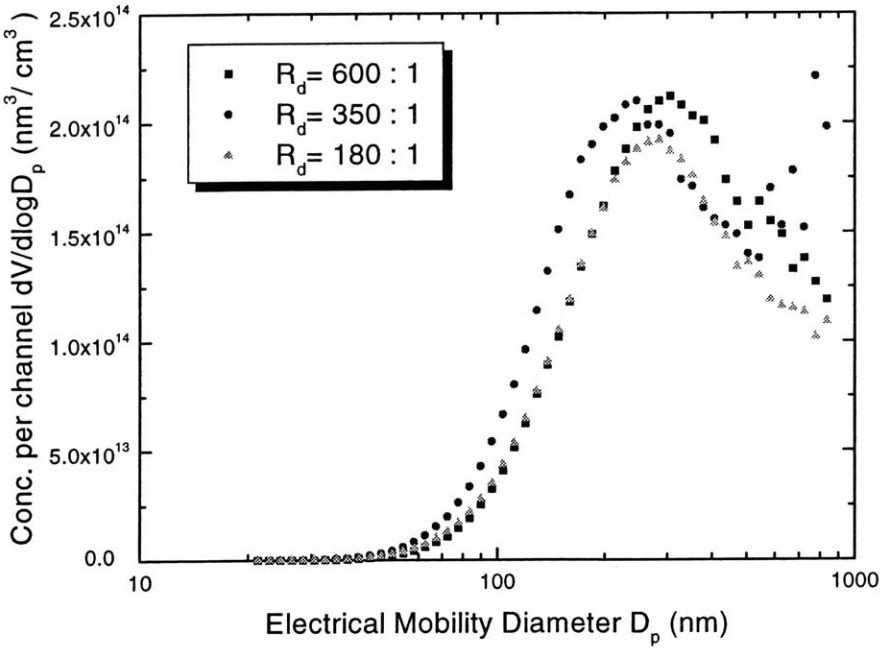

Figure 5.8 SMPS volume concentration per channel versus electrical mobility diameter for different dilution ratios (R_d).

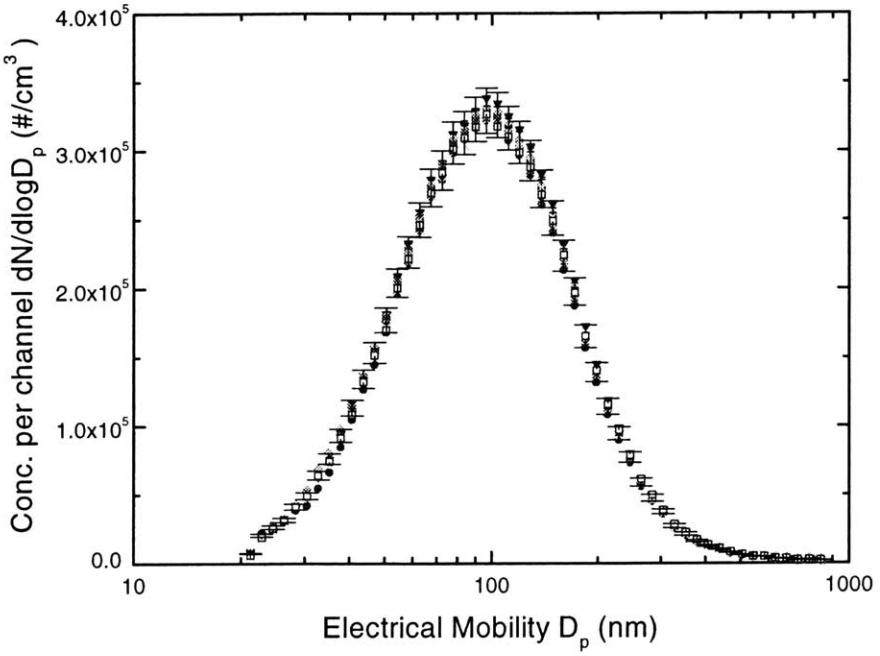

Figure 5.9 SMPS number concentration versus electrical mobility diameter for 30 scans with the base fuel (D-377). The error bars represent a 95% confidence interval.

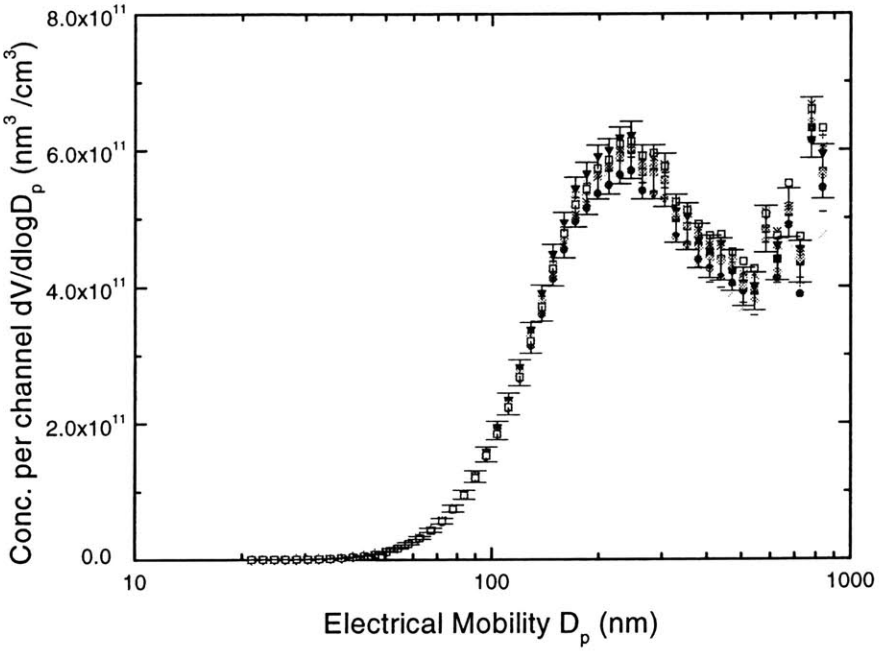

Figure 5.10 SMPS volume concentration versus electrical mobility diameter for 30 scans with the base fuel (D-377). The error bars represent a 95% confidence interval.

CHAPTER 6

IMPACT OF ENGINE OPERATING PARAMETERS

6.1 INTAKE TEMPERATURE

The impact on emissions was investigated at three different air intake temperatures, 30, 70, and 100° C, while running on the base fuel (D-377). During normal engine operation, the intake air temperature averaged 32° C with an ambient air temperature of 25° C. Intake air temperatures of 70° C and 100° C were achieved by utilizing the pre-heater located in the intake runner. As the air's density decreased (with an increase in air temperature) the engine's volumetric efficiency decreased. The decrease resulted in an increase in the fuel-air equivalence ratio, a decrease in imep, and shorter the ignition delay period. The SOI timing for the three different temperatures was held fixed at 6° BTDC (Figures 6.1). As the intake temperature was increased from 30° C to 70° C and 100° C, the mass airflow decreased by 10% and 15%, respectively over the normal baseline conditions (M_{air} = 9.2 g/s). Normalized engine torque also decreased by 8% and 10% from the imep value of 5.6 bar. The increase in temperature also changed the rate of heat release (ROHR), shown in Figure 6.2. An intake temperature of 100° C caused the start of combustion (SOC) to occur 1.5° CA earlier in the cycle, reducing the maximum premixed burn energy release rate by nearly 30%.

The PM number and volume distributions are also impacted by the temperature changes. The number of particles increases and is accompanied by a shift to larger particle diameters as the temperature increases. The particle's electrical mobility diameter (D_p) versus number concentration per channel (#/cm^3) is given in Figure 6.3. The SMPS assumes a spherical shaped particle with diameter D_p and outputs a volume fraction measurement based on the number of particles at a given diameter. Figure 6.4 represents the electrical mobility diameter versus volume concentration per channel (nm^3/cm^3). The increase in the number of particles in the distribution and shift to larger particle diameters, resulted in a dramatic increase in the volume of particles emitted for

increasing temperatures. Figure 6.5 represents the SMPS integrated number and volume of particles over the 21 – 865 nm size range. The results are normalized with respect to the base intake temperature of 30° C. In addition, the oxides of nitrogen, expressed in the emission index (EI) are also represented along with the relative SMPS totals. The error bars show a 95% confidence interval for the SMPS results. Note that the total number of particles increased by 50% and the total volume fraction increased by a factor of 4.5. The increased air temperature also resulted in a 25% increase in EI_{NO_x} emissions. Absolute integrated SMPS results can also be found in Table 6.1.

6.2 INDICATED MEAN EFFECTIVE PRESSURE

Engine emission measurements were taken for three indicated mean effect pressures, 5.5, 5.6, and 5.7 bar. The standard base fuel (D-377) was utilized with a fixed 6° BTDC SOI timing and 30° C air intake temperature. Injector needle lift traces, Figure 6.7, indicated a later end of injection (EOI) as the load, and fueling, increase. The combustion phasing, indicated by the rate of heat release analysis, show the SOC and premixed burn magnitudes to be approximately equal, for all three load conditions (Figure 6.6).

The SMPS number results, Figure 6.8, indicate an increase in the number of particles across all particle diameters, 21 – 865 nm, with increasing load. The particle volume concentration also increases with load, as a result of the number increase, Figure 6.9. The largest contribution to the volume concentration arises from particles with diameters greater than 200 nm. The integrated SMPS number and volume concentrations indicate a 20% increase in the total number concentration of particles and over a 60% increase in the total volume fraction with a 4% change in imep (Figure 6.10). The integrated total number concentration increases and is accompanied by an increase in the total volume concentration of particulates. The location of the peak number and volume does not change with load, only an increase in the number throughout the size range is observed (Table 6.2). EI_{NOx} emissions were reduced as the engine load increased. This effect could be attributed to the later EOI therefore with later end of combustion where

the burned gas temperatures produce lower rates of NO formation for the additional injected fuel.

6.3 START OF INJECTION TIMING

Changes in SOI timing was held fixed at 6° BTDC, corresponding to the MBT timing for the base fuel (D-377) and Diglyme additives at an imep of 5.6 bar. The impact of injection timing on emissions was explored by advancing and retarding the fixed SOI timing by 4° CA from the MBT timing. Advancing the timing from the optimized to 10° BTDC, resulted in a 17% increase in the premixed burn maximum heat release, located 2° BTDC, and an increase of 1° CA in ID. The rapid release of energy resulted in higher peak in-cylinder pressures (Figure 6.12). When the timing was retarded to a SOI timing of 2° BTDC, the magnitude of the premixed burn was reduced by 5% and was located 4.5° CA later in the cycle, Figure 6.11.

SMPS results indicated a shift in the number distribution as the injection timing was varied. The advanced, 10° BTDC, timing increased the number of particles and shifted the distribution to slightly larger particle diameters. The number increase paired with a shift to larger PM, also increased the volume fraction of particles (Figures 6.13 and 6.14). Integrated SMPS number and volume of particles increased by 10% and nearly 50% for the advanced timing case. A 10% change in the total volume concentration for the retarded timing case was also observed (Figure 6.15 and Table 6.3). The advanced timing experienced an increase of 55% in EI_{NOx} levels, a result of the higher in-cylinder pressures and burned gas temperatures near top-dead-center.

6.4 IGNITION DELAY

The ignition delay (ID), defined as the period of time between SOI and SOC, was modified using two cetane additives, 2-ethylhexyl nitrate (2-EHN) and di-tert-butyl peroxide (DTBP). Both cetane improvers were added, 10,000 ppmv, to the base fuel (D-377) increasing the cetane number from 42 to approximately 58. At the engine operating

conditions of 2400 RPM and 5.6 bar imep, the ID changed from 4.5° CA to 2.5° CA (Figure 6.17). The shorter delay resulted in a 10% lower energy release during the premixed combustion burn, Figure 6.16.

Results from the SMPS distribution data indicated a modest change in the number of particles emitted at diameters near 100 nm, refer to Figures 6.18. The volume distribution indicated an increase in the volume fraction of particles emitted over 200 nm in diameter (Figure 6.19). Integrated SMPS results suggested that the addition of a cetane improver has little effect on the total number of particles (less than 5%), but might slightly increase the total volume fraction (approximately 12%), Table 6.4 and Figure 6.20. The oxides of nitrogen also slightly increased as a result of the reduction in ID, changing the rate of pressure rise (Figure 6.20). A reduction in pressures reduces the temperature of the unburned gas temperature before combustion. Therefore, a higher peak pressure results in an increase in NO formation.

Intake Temperature	Total No. ($\#/cm^3$)	Peak No. ($\#/cm^3$)	Peak No. D_p (nm)	Total Vol. (nm^3/cm^3)	Peak Vol. (nm^3/cm^3)	Peak Vol. D_p (nm)
30 °C	2.04E+05	1.03E+04	97	4.59E+11	1.88E+10	246
70°C	2.86E+05	1.40E+04	104	1.22E+12	5.36E+10	305
100 °C	3.26E+05	1.58E+04	129	2.05E+12	9.60E+10	437

Table 6.1 Absolute SMPS number and volume concentration totals, peak magnitudes, and peak magnitude diameters, for different intake charge temperatures. Note: as the temperature increases, volumetric efficiency decreases, resulting in an increase in fuel/air equivalence ratio and a decrease in imep with fixed fuel metering.

imep (bar)	Total No. ($\#/cm^3$)	Peak No. ($\#/cm^3$)	Peak No. D_p (nm)	Total Vol. (nm^3/cm^3)	Peak Vol. (nm^3/cm^3)	Peak Vol. D_p (nm)
5.5	1.86E+05	9.30E+03	97	3.77E+11	1.57E+10	246
5.6	2.04E+05	1.03E+04	97	4.59E+11	1.88E+10	246
5.7	2.27E+05	1.13E+04	97	5.59E+11	2.31E+10	246

Table 6.2 Absolute SMPS number and volume concentration totals, peak magnitudes, and peak magnitude diameters, for different indicated mean effective pressures. Standard base fuel (D-377).

SOI (°BTDC)	Total No. ($\#/cm^3$)	Peak No. ($\#/cm^3$)	Peak No. D_p (nm)	Total Vol. (nm^3/cm^3)	Peak Vol. (nm^3/cm^3)	Peak Vol. D_p (nm)
10	2.38E+05	1.19E+04	104	6.93E+11	2.73E+10	246
6	2.04E+05	1.03E+04	97	4.59E+11	1.88E+10	246
2	2.23E+05	1.11E+04	97	4.16E+11	1.81E+10	229

Table 6.3 Absolute SMPS number and volume concentration totals, peak magnitudes, and peak magnitude diameters, for changes in injection timing. Base fuel (D-377) with injection timing advanced/retarded around MBT timing (6 °BTDC).

Ignition Delay (°CA)	Total No. ($\#/cm^3$)	Peak No. ($\#/cm^3$)	Peak No. D_p (nm)	Total Vol. (nm^3/cm^3)	Peak Vol. (nm^3/cm^3)	Peak Vol. D_p (nm)
4.5 (Base)	2.04E+05	1.03E+04	97	4.59E+11	1.88E+10	246
2.5 (2-EHN)	2.03E+05	9.91E+03	97	5.14E+11	2.12E+10	246
2.5 (DTBP)	1.90E+05	9.23E+03	97	4.55E+11	1.81E+10	246

Table 6.4 Absolute SMPS number and volume concentration totals, peak magnitudes, and peak magnitude diameters, for different ignition delays (°CA). Standard base fuel (D-377) and cetane enhanced base fuels with additives, 2-ethylhexyl nitrate (2-EHN) and di-tert-butyl peroxide (DTBP).

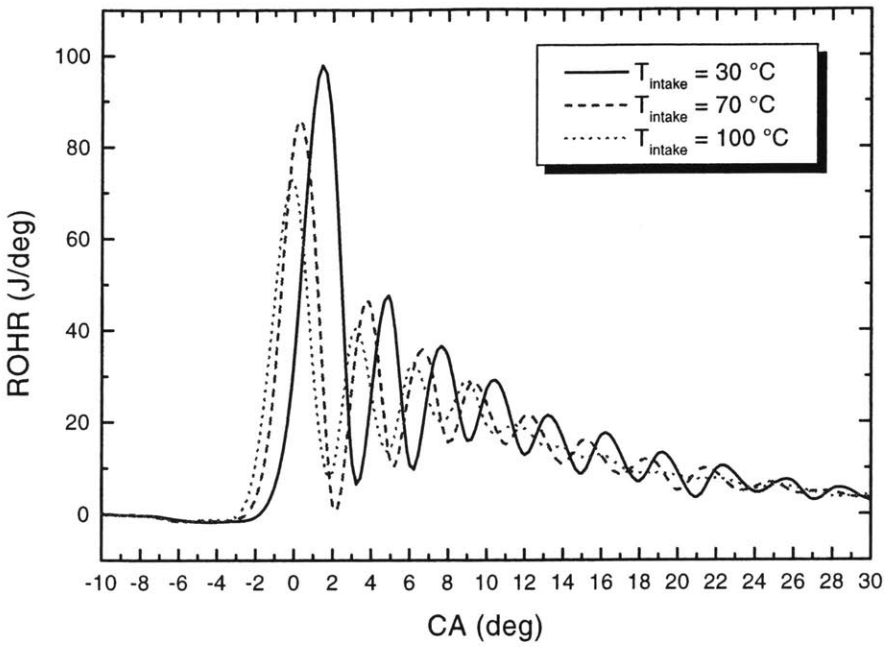

Figure 6.1 Rate of heat release for different intake charge temperatures. Note: as the temperature increases, volumetric efficiency decreases, resulting in an increase in fuel/air equivalence ratio and a decrease in imep with fixed fuel metering and fixed SOI (6 °BTDC).

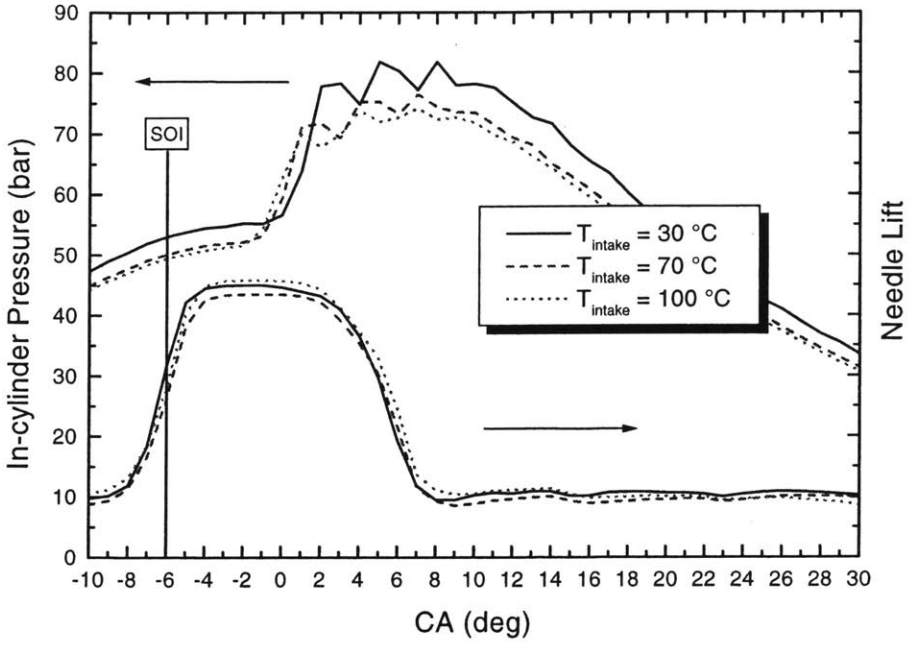

Figure 6.2 In-cylinder pressure and injector needle lift for different intake charge temperatures. Note: as the temperature increases, volumetric efficiency decreases, resulting in an increase in fuel/air equivalence ratio and a decrease in imep with fixed fuel metering and fixed SOI (6 °BTDC).

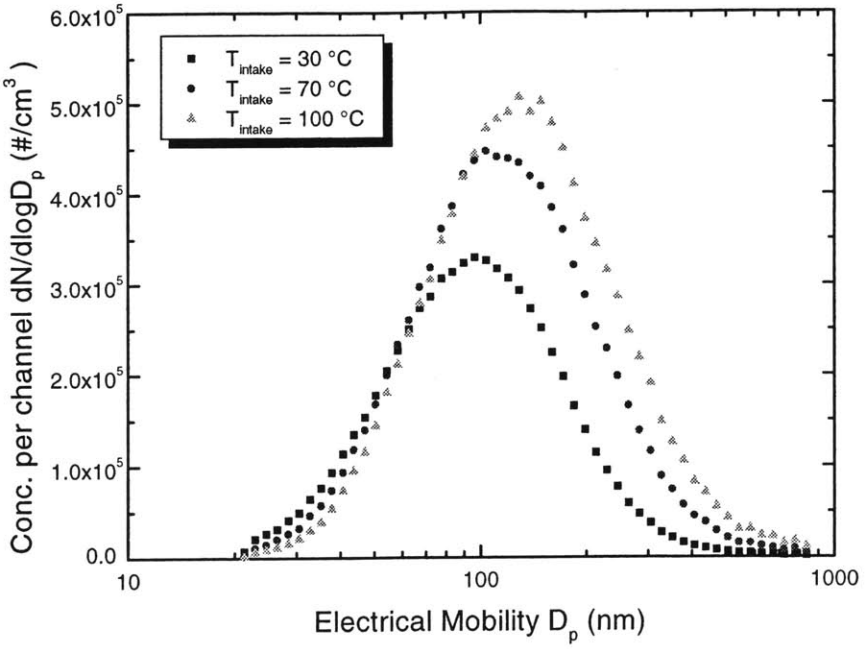

Figure 6.3 SMPS volume concentration versus mobility diameter for different intake charge temperatures. Note: as the temperature increases, volumetric efficiency decreases, resulting in an increase in fuel/air equivalence ratio and a decrease in imep with fixed fuel metering.

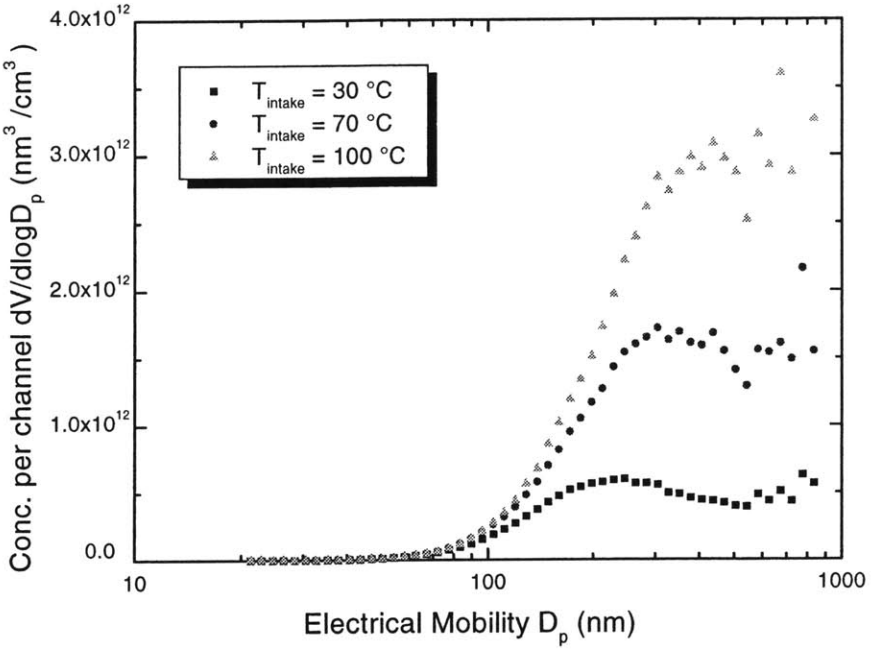

Figure 6.4 SMPS volume concentration versus mobility diameter for different intake charge temperatures. Note: as the temperature increases, volumetric efficiency decreases, resulting in an increase in fuel/air equivalence ratio and a decrease in imep with fixed fuel metering.

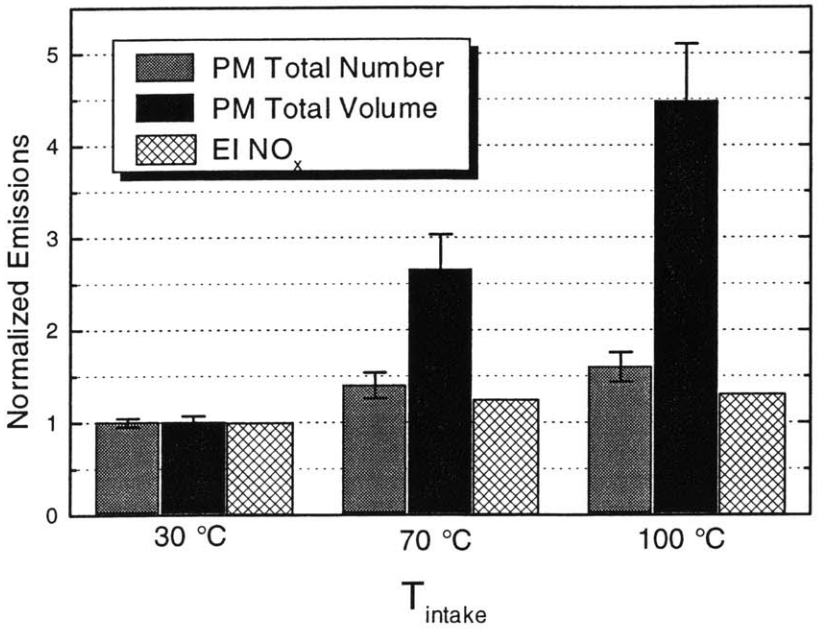

Figure 6.5 Relative SMPS total concentrations and NO_x measurements for different intake charge temperatures. Note: as the temperature increases, volumetric efficiency decreases, resulting in an increase in fuel/air equivalence ratio and a decrease in imep with fixed fuel metering.

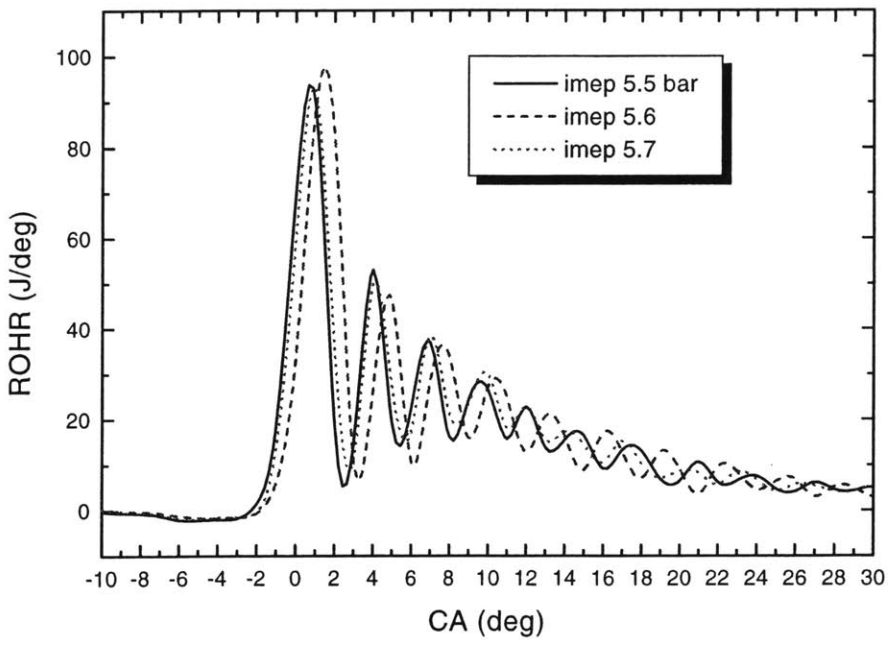

Figure 6.6 Rate of heat release for different indicated mean effective pressures. Fixed SOI 6 °BTDC with standard base fuel (D-377).

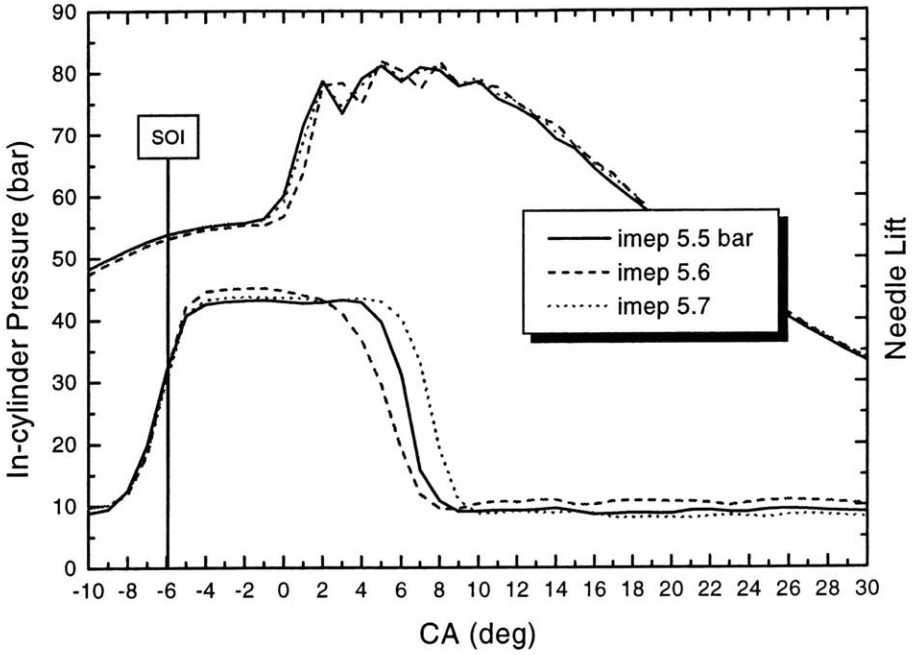

Figure 6.7 In-cylinder pressure and injector needle lift for different indicated mean effective pressures. Fixed SOI 6 °BTDC with standard base fuel (D-377).

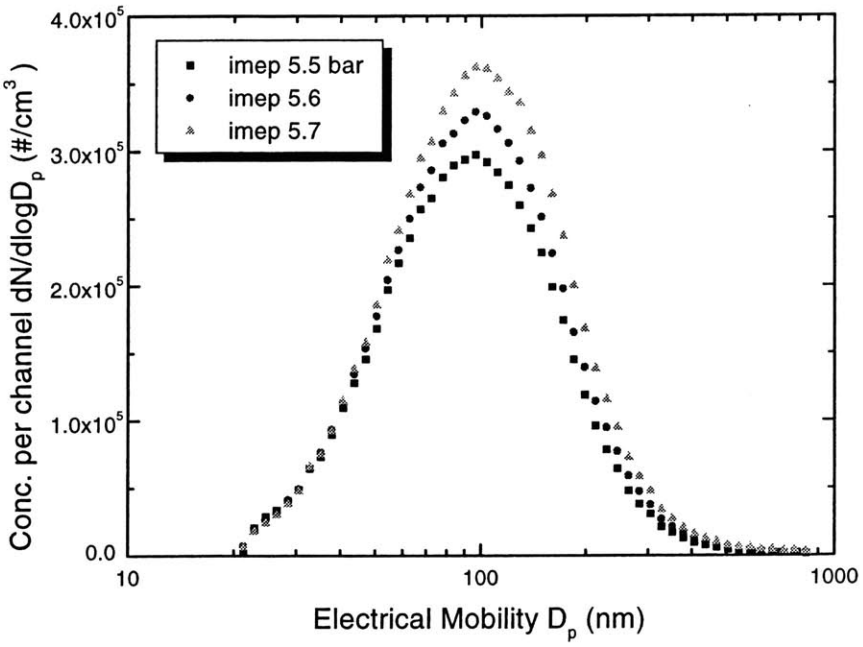

Figure 6.8 SMPS number concentration versus mobility diameter for different indicated mean effective pressures. Standard base fuel (D-377).

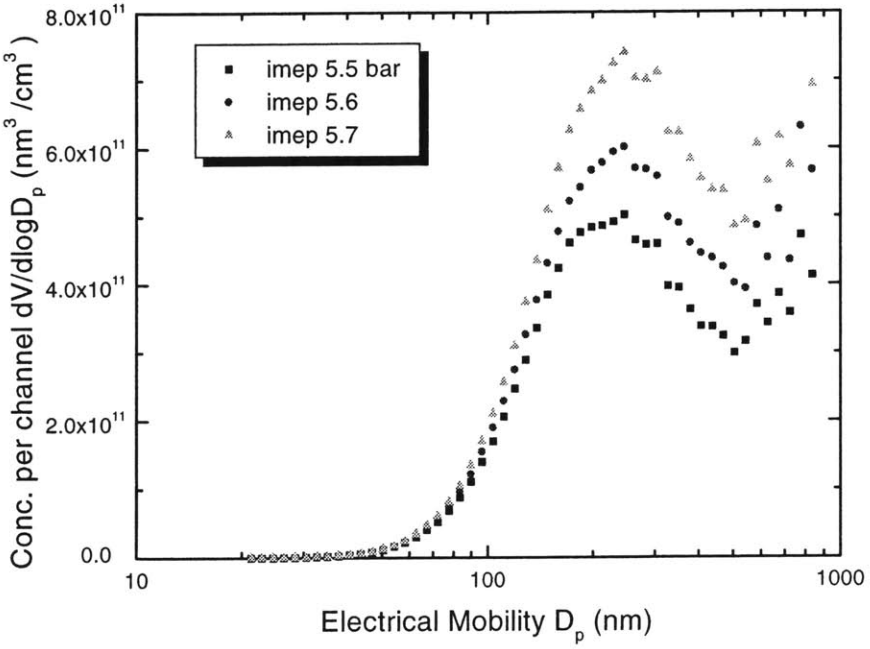

Figure 6.9 SMPS volume concentration versus mobility diameter for different indicated mean effective pressures. Standard base fuel (D-377).

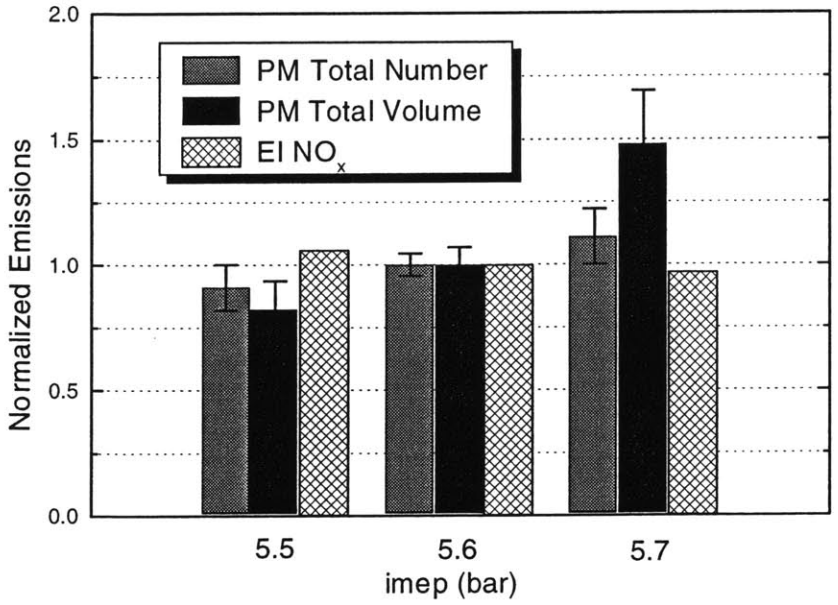

Figure 6.10 Relative SMPS total concentrations and NO_x measurements for different indicated mean effective pressures. Standard base fuel (D-377).

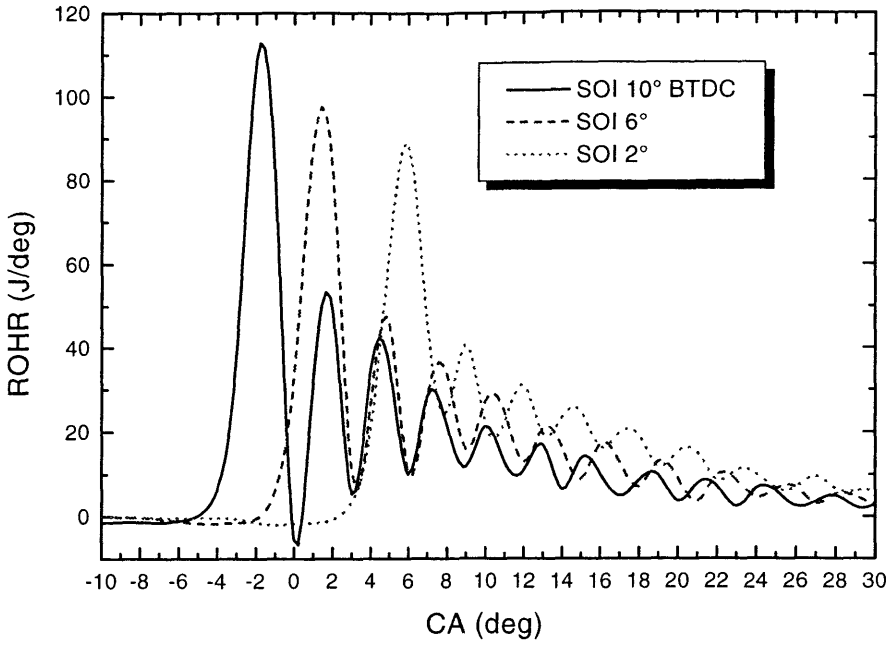

Figure 6.11 Rate of heat release for changes in injection timing. Base fuel (D-377) with injection timing advanced/retarded around MBT timing (6 °BTDC).

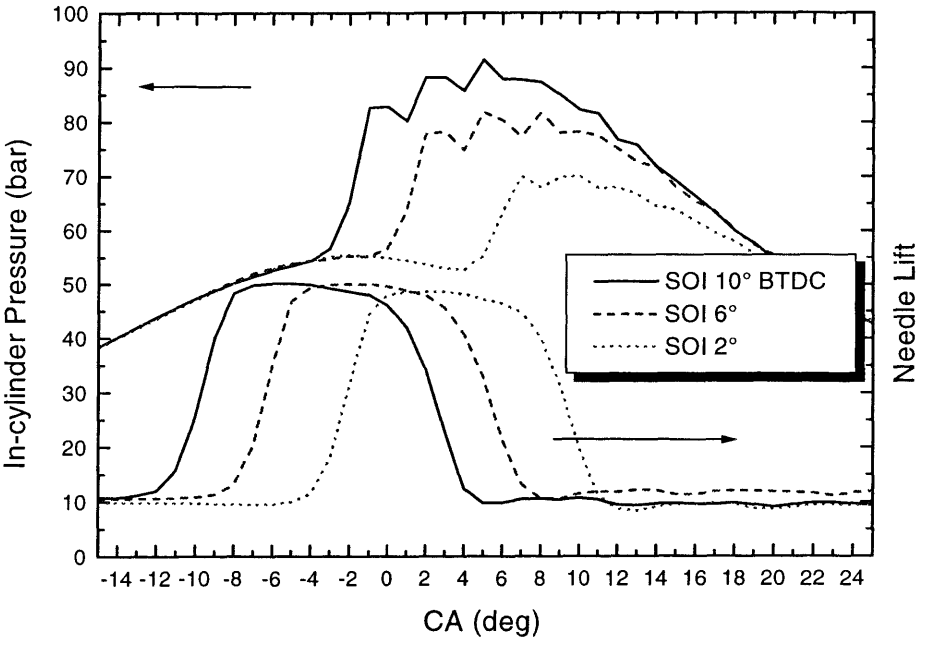

Figure 6.12 In-cylinder pressure and injector needle lift for changes in injection timing. Base fuel (D-377) with injection timing advanced/retarded around MBT timing (6 °BTDC).

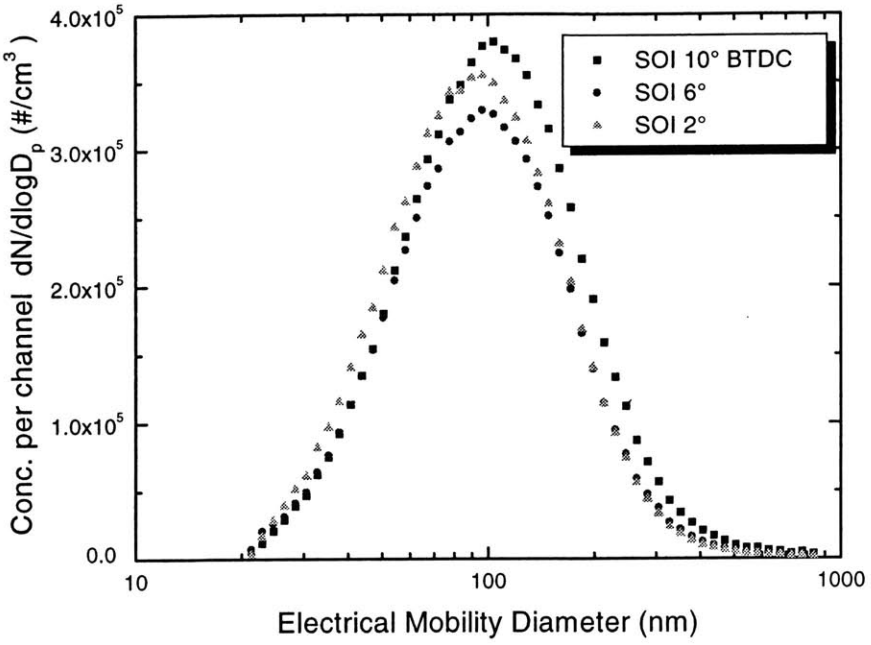

Figure 6.13 SMPS number concentration versus mobility diameter for changes in injection timing. Base fuel (D-377) with injection timing advanced/retarded around MBT timing (6 °BTDC).

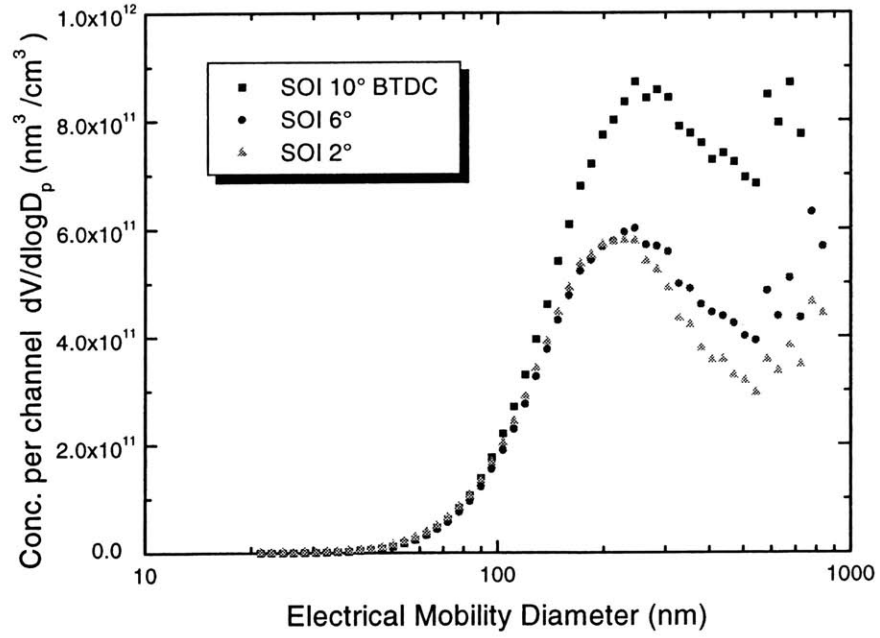

Figure 6.14 SMPS volume concentration versus mobility diameter for changes in injection timing. Base fuel (D-377) with injection timing advanced/retarded around MBT timing (6 °BTDC).

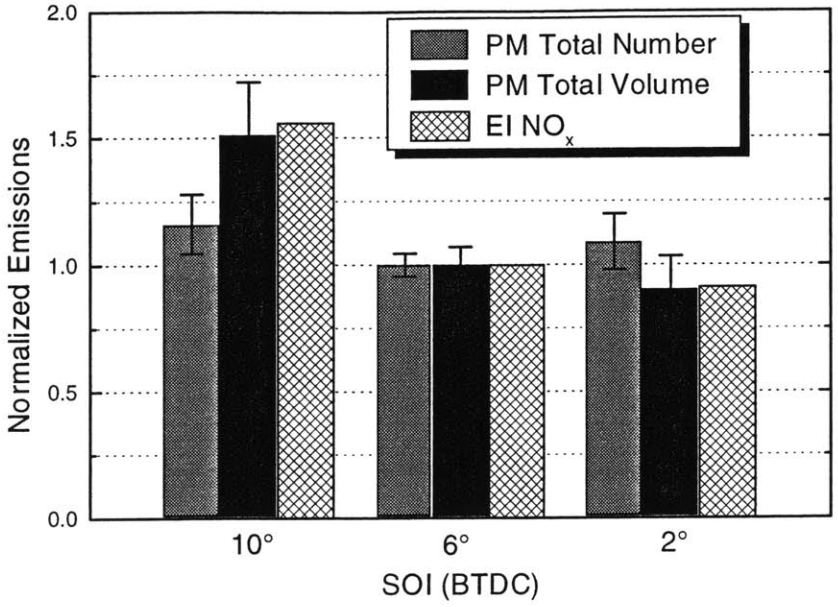

Figure 6.15 Relative SMPS total concentrations and NO_x measurements for changes in injection timing. Base fuel (D-377) with injection timing advanced/retarded around MBT timing (6 °BTDC).

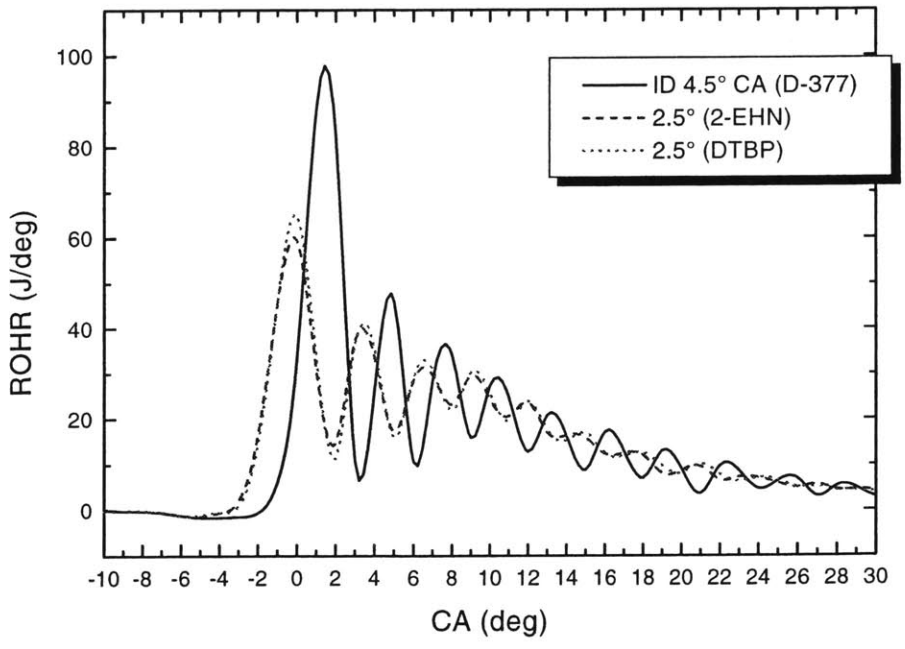

Figure 6.16 Rate of heat release for changes in ignition delay (°CA). Fixed SOI 6 °BTDC with standard base fuel (D-377) and cetane enhanced base fuels containing additives, 2-ethylhexyl nitrate (2-EHN) and di-tert-butyl peroxide (DTBP).

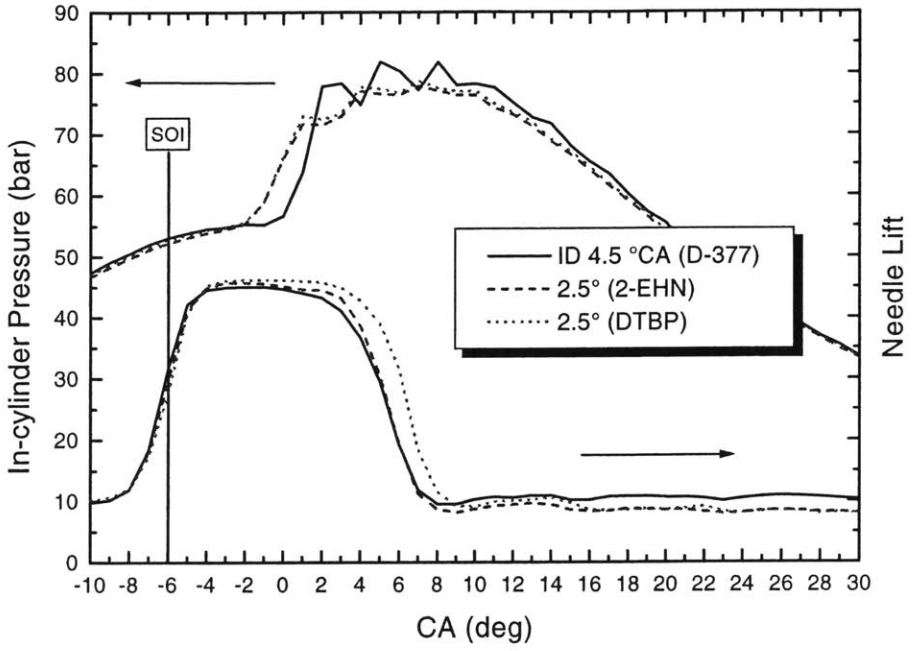

Figure 6.17 In-cylinder pressure and injector needle lift for changes in ignition delay (°CA). Fixed SOI 6 °BTDC with standard base fuel (D-377) and cetane enhanced base fuels containing additives, 2-ethylhexyl nitrate (2-EHN) and di-tert-butyl peroxide (DTBP).

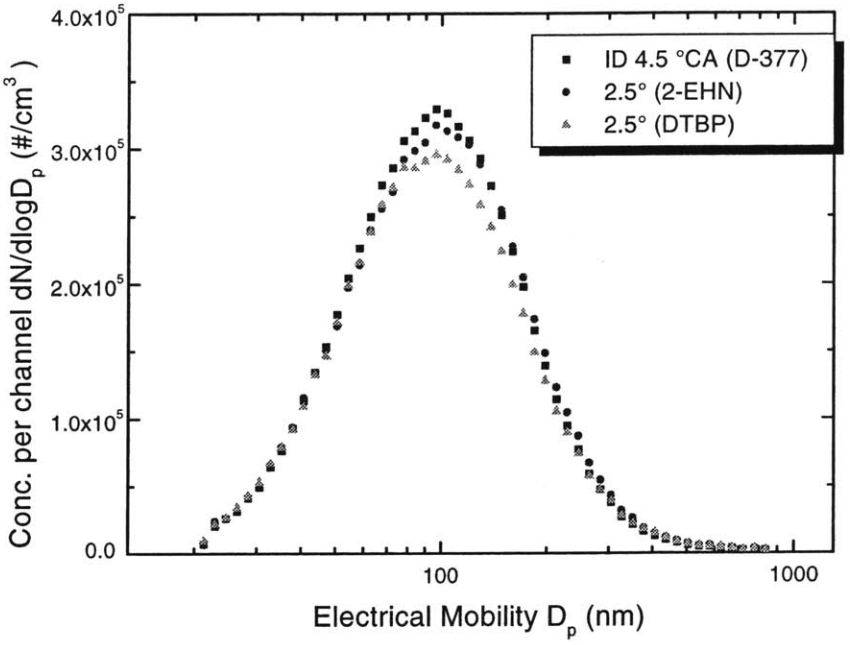

Figure 6.18 SMPS number concentration versus mobility diameter with changes in ignition delay (°CA). Standard base fuel (D-377) and cetane enhanced base fuels with cetane additives, 2-ethylhexyl nitrate (2-EHN) and di-tert-butyl peroxide (DTBP).

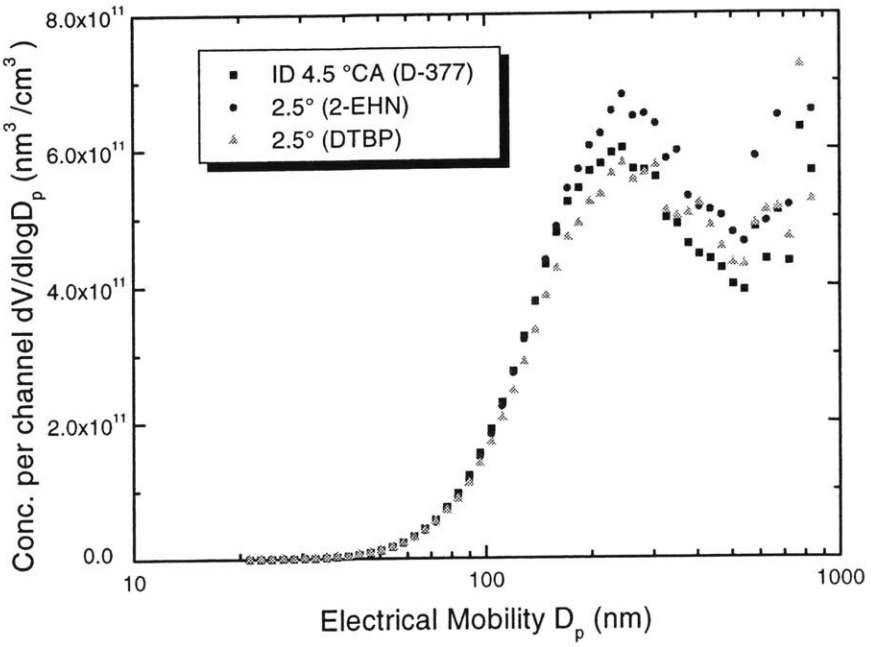

Figure 6.19 SMPS volume concentration versus mobility diameter with changes in ignition delay (°CA). Standard base fuel (D-377) and cetane enhanced base fuels with cetane additives, 2-ethylhexyl nitrate (2-EHN) and di-tert-butyl peroxide (DTBP).

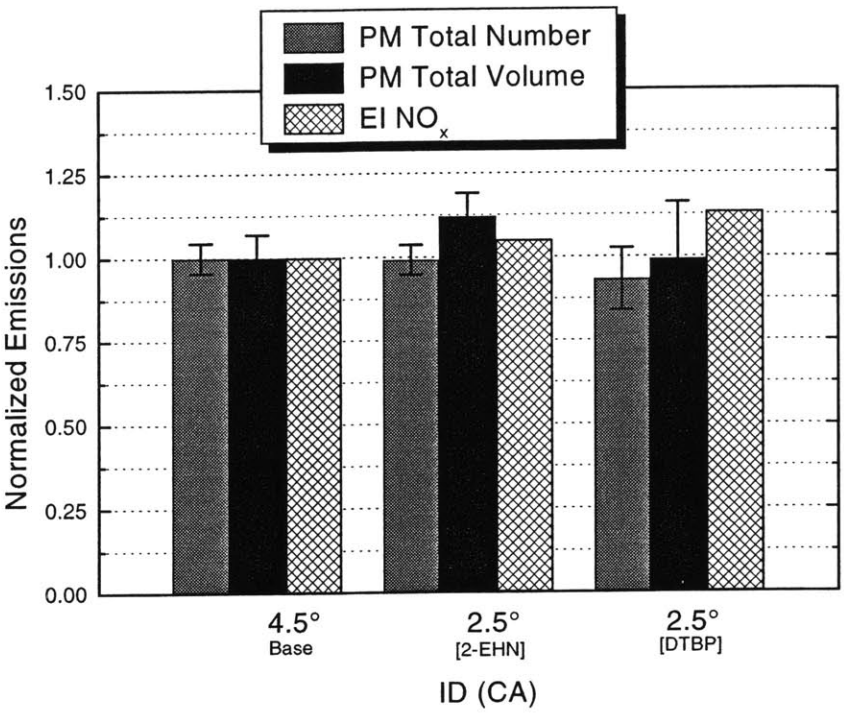

Figure 6.20 Relative SMPS total concentrations and NO_x measurements for different ignition delays (°CA). Standard base fuel (D-377) and cetane enhanced base fuels with additives, 2-ethylhexyl nitrate (2-EHN) and di-tert-butyl peroxide (DTBP).

CHAPTER 7

IMPACT OF OXYGENATES

7.1 OXYGENATE PROPORTIONALITY

The oxygenate, Diglyme, was added 10%, 20%, and 30% by volume, to the low-sulfur base fuel (D-377). The three oxygenated fuels denoted as DG10, DG20, and DG30, contained 4, 8, and 12 percent of oxygen by weight. These blended fuels, had cetane numbers in the mid-fifties, requiring the addition of the cetane improver, 2-EHN, to the base fuel to match the ignition delay. The ID matched base fuel with a cetane number rating of 58, denoted as D-377+, and the fuels containing Diglyme were evaluated at an equivalent 6° BTDC SOI timing, ROHR, and 5.6 bar imep normalized torque value (Figures 7.1 and 7.2). The oxygenates experienced slight differences in the premixed burn magnitude and EOI due to the differences in volatility, energy density, and density (Table 7.8).

SMPS results indicated changes in the number concentration distribution with increasing weight percent oxygen added to the fuel, Figure 7.3. The effect on the volume concentration can be noted in Figure 7.4. Integrated SMPS measurements indicate a modest 5% increase in the number of particles emitted as the weight percent of oxygen increases. Figure 7.5 shows the PM and NO_x emissions normalized with respect to the cetane improved base fuel (D-377+). As the weight percent of oxygen increased, the total volume PM concentration decreases. The trend in Figure 7.5 follows that of Figure 1.2, with a logarithmic reduction with increasing weight percent oxygen in the fuel. Absolute totals for number and volume concentrations, peak diameter locations, and peak magnitudes can be found in Table 7.1. NO_x emission appeared to increase less than 10% for the fuels containing oxygen.

7.2 OXYGENATE VOLATILITY

The Glyme family of poly-ethers was utilized to determine the impact an oxygen containing compound's volatility had on the reduction of PM. Three different oxygenates, Monoglyme, Diglyme, and Tetraglyme, boiling points 85° C, 162° C, and 276° C, respectively, were blended with the base fuel until each of the mixtures contained 8 percent of oxygen by weight. The blended test fuels were all subjected to the same engine load conditions, SOI timing, and equivalent ROHR. Variations in volatility, energy density, and density, fuel to fuel causes changes in the premixed burn magnitude and EOI timing (Table 7.8 and Figures 7.6 and 7.7). The high volatility oxygenated, MG21, experienced the greatest premixed burn heat release, and the lowest volatility oxygenated, TG19, had the lowest premixed burn heat release.

SMPS results for both number and volume concentrations versus particle diameter can be found in Figures 7.8 and 7.9. Integrated results in Figure 7.10 and Table 7.2 indicate a modest change in the total number of particles emitted as the volatility of the oxygenate is decreased. The total volume fraction also remains constant at 35% as the volatility decreases. The highest volatility fuel experienced a 20% reduction in EI_{NOx}, fuels with the less volatile oxygenates showed a slight increase (less than 10%).

7.3 OXYGENATE STRUCTURE

Different functional groups were tested in order to determine their impact on the effectiveness of the oxygenates on reducing emissions. An ether, acetate, and ester were tested at amounts yielding 8 wt-% oxygen when blended with the base fuel. Diglyme, propylene glycol monomethyl ether acetate, and diethyl maleate all have similar physical properties; however, each compound has a different chemical structure. It was necessary to add 5,000 ppm of 2-EHN to the ester and acetate fuels in order to achieve comparable ROHR that of the ether and cetane improved base fuel, Figure 7.11. Again, variations in properties were responsible for the changes in premixed burn magnitude and EOI (Table 7.8 and Figure 7.12).

SMPS results for both number and volume concentrations versus particle diameter can be found in Figures 7.13 and 7.14. Integrated SMPS results in Figure 7.15 and Table 7.3 indicate a modest change (less than 10%) in the total number of particles emitted with different oxygen containing functional groups. Changes in the total volume fraction of particles suggests that structure does influence the reduction in PM, Figure 7.15 and Table 7.3. The ether compound, Diglyme, reduced the total volume concentration of PM by 37%, where as the maleate and acetate compounds were less effective, only reducing PM levels by approximately 12%.

7.4 HYDROCARBONS WITHOUT OXYGEN

In order to isolate the impact of oxygen from other properties effected by splash blending chemicals, three compounds without oxygen were tested to determine their influence on emissions. Normal decane (alkane) was evaluated along with diethylene triamine (amine) and 1-bromopropane (alkyl halide). Again, SOI timing, ROHR, and torque were held constant. All of the fuel required the addition of 2-EHN to match the heat release of the other fuels in the test matrix, Figures 7.16 and 7.17

SMPS results for both number and volume concentrations versus particle diameter can be found in Figures 7.18 and 7.19. Integrated results in Figure 7.20 and Table 7.4 indicate a modest changes in the total number of particles emitted, with the exception of the alkyl halide compound, 1-bromopropane. The total volume concentrations decrease 25% with the alkane (ND20+) when compared to cetane improved base fuel. The amine (DT17+) and alkyl halide (BP10+) compounds both experienced a 15% and 85% increase in the volume fraction of PM. The oxides of nitrogen decreased slightly (less than 10%) for the alkane and alkyl halide, but increased (10%) for the nitrogen containing fuel, DT17+.

7.5 DIFFERENT BASE FUEL

A fuel from the Fischer-Tropsch (FT) process was compared to the cetane improved low-sulfur base fuel (D-377+). The emission levels from the low-sulfur and FT derived fuel were compared with and without the presents of molecular oxygen. The tests with oxygenates were blended with Diglyme to contain 8 wt-% oxygen. However, the FT process yielded a fuel with an extremely high cetane rating, 85, resulting in a ROHR that could not be matched by adding 2-EHN. As a result, the SOI timing and torque were held constant, but the SOC, EOI, and premixed burn location and magnitude, were not matched for each fuel tested, Figures 7.21 and 7.22.

SMPS results for both number and volume concentrations versus particle diameter can be found in Figures 7.23 and 7.24. Fuel from the FT process had an increase in the number of particles emitted and a shift to smaller particle diameters. Integrated results in Figure 7.25 and Table 7.5 indicate a 20% increase in the total number of particles emitted. However, fuels from the FT had a significant reduction, 40%, in the total volume fraction of particles emitted. Little change was noted with the addition of 8 wt-% oxygen to the FT fuels. In addition to reducing PM levels, the FT experienced a reduction in EI_{NOx} levels by 60%.

7.6 MATCHED FUEL/AIR EQUIVALENCE RATIOS

All the previous results have been careful matched for torque (5.6 bar imep). However, the addition of oxygenates to diesel fuel changes the stoichiometric air-fuel ratio. Fuels containing oxygenates operate leaner ($\phi = 0.48$) than the base fuel ($\phi = 0.50$) at the same load condition. Engine tests were conducted at matched fuel/air equivalence ratios and the impact on emissions was recorded. The cetane improved base fuel (D-377+), and Diglyme (DG20), and propylene glycol monomethyl ether acetate (PG19+). Both test fuels contained 8 wt-% oxygen. The oxygen containing fuels were run at an imep of 5.8 bar to reflect an equivalence ratio of 0.50. The cetane improved base fuel was operated at 5.6 bar and $\phi = 0.50$ (Figures 7.26 and 7.27).

SMPS number and volume concentrations versus particle diameter are shown in Figures 7.28 and 7.29. Integrated SMPS measurements in Figure 7.30 and Table 7.6 indicate the PM and NO_x levels at the matched equivalence ratio. At an equivalence ratio of 0.50, the Diglyme containing fuel with 8 wt-% oxygen has approximately the same emissions as the cetane improved base fuel (D-377+). Whereas the acetate (PG19+) containing 8 wt-% oxygen has a 20% increase in both the total number and volume of PM emissions compared to the cetane base fuel (D-377+).

7.7 LIGHTER LOAD CONDITION

The several fuels in the test matrix were also tested at an imep of 3.7 bar in order to evaluate emission changes at a lower load condition. The SOI timing and engine speed were held constant with previous tests. The SOC, ID, and premixed burn location and magnitude were identical to the corresponding fuels at the 5.6 bar imep operating condition. The reduction in fueling resulted in an earlier EOI and decreased mixing-controlled burn heat release (Table 7.9 and Figures 7.31 and 7.32).

SMPS number and volume concentrations versus particle diameters, Figures 7.33 and 7.34, indicated a shift to smaller particle diameters compared to the imep value of 5.6 bar. The number distribution is centered about 70 nm at the lower load condition rather than 100 nm at an imep of 5.6 bar. Integrated SMPS results in Figure 7.35 and Table 7.6 show normalized emission levels to the base fuel (D-377) and absolute SMPS results of number and volume totals and locations and magnitudes of the peaks. The overall trends in emission levels are similar to the higher load condition, but the reduction in PM levels are reduced. Similar finds were observed in previous studies, reconfirming the importance of the local fuel/air equivalence ratio and benefit of additional oxygen at high equivalence ratios.

wt-% Oxygen [Fuel]	Total No. (#/cm^3)	Peak No. (#/cm^3)	Peak No. D_p (nm)	Total Vol. (nm^3/cm^3)	Peak Vol. (nm^3/cm^3)	Peak Vol. D_p (nm)
0 wt-% [D-377+]	2.03E+05	9.91E+03	97	5.14E+11	2.12E+10	246
4 wt-% [DG10]	2.08E+05	1.05E+04	97	4.02E+11	1.72E+10	229
8 wt-% [DG20]	2.11E+05	1.07E+04	97	3.22E+11	1.46E+10	198
12 wt-% [DG30]	1.99E+05	9.91E+03	90	3.19E+11	1.43E+10	229

Table 7.1 Absolute SMPS number and volume concentration totals, peak magnitudes, and peak magnitude diameters, for increasing wt-% oxygen. Cetane matched base fuel (D-377+) and varying amounts of Diglyme blended with the base fuel.

T_b [Fuel]	Total No. (#/cm^3)	Peak No. (#/cm^3)	Peak No. D_p (nm)	Total Vol. (nm^3/cm^3)	Peak Vol. (nm^3/cm^3)	Peak Vol. D_p (nm)
Base [D-377+]	2.03E+05	9.91E+03	97	5.14E+11	2.12E+10	246
85 °C [MG21]	2.05E+05	1.04E+04	90	3.29E+11	1.45E+10	198
162 °C [DG20]	2.11E+05	1.07E+04	97	3.22E+11	1.46E+10	198
276 °C [TG19]	2.00E+05	1.01E+04	97	3.04E+11	1.34E+10	198

Table 7.2 Absolute SMPS number and volume concentration totals, peak magnitudes, and peak magnitude diameters, for decreasing oxygenate volatility. Cetane matched base fuel (D-377+) and constant 8 wt-% oxygen with different volatility Glyme ethers.

Structure [Fuel]	Total No. (#/cm^3)	Peak No. (#/cm^3)	Peak No. D_p (nm)	Total Vol. (nm^3/cm^3)	Peak Vol. (nm^3/cm^3)	Peak Vol. D_p (nm)
Base [D-377+]	2.03E+05	9.91E+03	97	5.14E+11	2.12E+10	246
Ether [DG20]	2.11E+05	1.07E+04	97	3.22E+11	1.46E+10	198
Acetate [PG19+]	2.09E+05	1.01E+04	97	4.52E+11	1.88E+10	246
Ester [DM17+]	2.02E+05	1.00E+04	97	4.40E+11	1.80E+10	229

Table 7.3 Absolute SMPS number and volume concentration totals, peak magnitudes, and peak magnitude diameters, for changes in oxygenate function group. Cetane matched base fuel (D-377+) and different function group with 8 wt-% oxygen.

Fuel	Total No. (#/cm^3)	Peak No. (#/cm^3)	Peak No. D_p (nm)	Total Vol. (nm^3/cm^3)	Peak Vol. (nm^3/cm^3)	Peak Vol. D_p (nm)
Base [D-377+]	2.03E+05	9.91E+03	97	5.14E+11	2.12E+10	246
Alkane [ND20+]	1.99E+05	9.91E+03	97	3.88E+11	1.63E+10	246
Amine [DT17+]	2.21E+05	1.07E+04	97	5.76E+11	2.40E+10	246
Alkyl Halide [BP10+]	3.15E+05	1.53E+04	104	1.00E+12	4.04E+10	305

Table 7.4 Absolute SMPS number and volume concentration totals, peak magnitudes, and peak magnitude diameters, for matched fuel properties without oxygen. Cetane matched base fuel (D-377+) and non-oxygen containing hydrocarbons.

Fuel	Total No. (#/cm^3)	Peak No. (#/cm^3)	Peak No. D_p (nm)	Total Vol. (nm^3/cm^3)	Peak Vol. (nm^3/cm^3)	Peak Vol. D_p (nm)
Base [D-377+]	2.03E+05	9.91E+03	97	5.14E+11	2.12E+10	246
Base 8 wt-% [DG20]	2.11E+05	1.07E+04	97	3.22E+11	1.46E+10	198
Fischer Tropsch [FT]	2.38E+05	1.28E+04	90	3.29E+11	1.53E+10	172
FT 8 wt-% [FTDG19]	2.48E+05	1.34E+04	97	3.26E+11	1.52E+10	172

Table 7.5 Absolute SMPS number and volume concentration totals, peak magnitudes, and peak magnitude diameters, for different base fuels neat and containing the oxygenate Diglyme. Cetane enhanced base fuel (D-377+), base fuel with 8wt-% oxygen (DG20), Fischer Tropsch fuel neat (FT), Fischer Tropsch fuel with 8 wt-% oxygen (FTDG19).

Fuel [imep]	Total No. (#/cm^3)	Peak No. (#/cm^3)	Peak No. D_p (nm)	Total Vol. (nm^3/cm^3)	Peak Vol. (nm^3/cm^3)	Peak Vol. D_p (nm)
D-377+ [5.6 bar]	2.03E+05	9.91E+03	97	5.14E+11	2.12E+10	246
DG20 [5.8 bar]	2.16E+05	1.07E+04	97	5.16E+11	2.10E+10	246
PG19+ [5.8 bar]	2.59E+05	1.31E+04	105	6.68E+11	2.81E+10	246

Figure 7.6 Absolute SMPS number and volume concentration totals, peak magnitudes, and peak magnitude diameters, for matched fuel/air equivalence ratios (ϕ = 0.5). Cetane equivalent base fuel (D-377+) and oxygenated fuel with 8 wt-% oxygen (DG20).

Fuel [imep 3.7 bar]	Total No. ($\#/cm^3$)	Peak No. ($\#/cm^3$)	Peak No. D_p (nm)	Total Vol. (nm^3/cm^3)	Peak Vol. (nm^3/cm^3)	Peak Vol. D_p (nm)
D-377	7.30E+04	4.20E+03	78	8.30E+10	2.87E+09	184
D-377+	7.44E+04	4.28E+03	78	1.00E+11	3.32E+09	205
ND20+	6.31E+04	3.25E+03	63	7.88E+10	3.02E+09	198
MG21	6.41E+04	3.68E+03	78	6.63E+10	2.50E+09	172
DG20+	7.04E+04	3.99E+03	78	7.77E+10	2.86E+09	172
FT	8.11E+04	4.35E+03	63	6.32E+10	2.49E+09	149

Table 7.7 Absolute SMPS number and volume concentration totals, peak magnitudes, and peak magnitude diameters, for various test fuels at an imep of 3.7 bar.

Fuel Abbrevation	Description**	M_{fuel} (g/s)	M_{air} (g/s)	Equiv Ratio	ID (CA)	SOC (CA)	Injection Duration (CA)	EOI (CA)	Premixed Burn Peak Location (CA)	Peak Rate (J/deg)	Premixed Fraction	Mixing-Controlled Fraction
D-377	Base fuel	0.315	9.2	0.50	4.5	-1.5	11.5	5.5	1.5	95	43%	57%
D-377+	Cetane matched w/2-EHN	0.315	9.2	0.50	2.5	-3.5	11.5	5.5	0.0	60	33%	67%
ND20+	Alkane	0.313	9.2	0.50	2.5	-3.5	11.0	5.0	0.0	52	28%	72%
MG21	8 wt-% (Monoglyme)	0.334	9.2	0.48	3.5	-2.5	13.0	7.0	0.3	82	37%	63%
DG10	4 wt-% (Diglyme)	0.326	9.2	0.49	3.5	-2.5	12.5	6.5	0.5	78	35%	65%
DG20	8 wt-% (Diglyme)	0.337	9.2	0.48	3.0	-3.0	12.0	6.0	0.0	70	32%	68%
DG30	12wt-% (Diglyme)	0.349	9.2	0.48	3.0	-3.0	13.5	7.5	0.0	68	31%	69%
TG19	8 wt-% (Tetraglyme)	0.342	9.2	0.49	2.5	-3.5	12.0	6.0	-0.3	62	32%	68%
PG19+	8 wt-% (Acetate)	0.337	9.2	0.48	3.0	-3.0	12.5	6.5	0.0	60	26%	74%
DM17+	8 wt-% (Maleate)	0.336	9.2	0.48	2.5	-3.5	13.5	7.5	0.0	78	40%	60%
DG20	5.8 bar, 8 wt-% (Equivalence matched)	0.348	9.2	0.50	2.5	-3.5	12.5	6.5	-0.3	70	34%	66%
PG19+	5.8 bar, 8 wt-% (Equivalence matched)	0.349	9.2	0.50	2.0	-4.0	12.0	6.0	-1.0	72	35%	65%
FT	Fischer Tropsch	0.310	9.2	0.50	1.3	-4.8	11.0	5.0	-1.0	41	24%	76%
FTDG19	8 wt-% (Diglyme w/FT)	0.332	9.2	0.49	1.0	-5.0	11.5	5.5	-2.0	32	15%	85%
DT17+	Amine	0.326	9.2	0.50	2.5	-3.5	13.5	7.5	0.5	65	40%	60%
BP10+	Alkyl Halide	0.324	9.2	0.46	2.5	-3.5	11.0	5.0	0.0	54	29%	71%
D-377	70 °C Intake	0.315	8.3	0.50	3.5	-2.5	11.5	5.5	0.3	85	35%	65%
D-377	100 °C Intake	0.315	7.8	0.50	3.0	-3.0	11.5	5.5	0.0	72	34%	66%
D-377	10° SOI (BTDC)	0.315	9.2	0.50	5.5	-4.5	12.5	2.5	-2.0	112	42%	58%
D-377	2° SOI (BTDC)	0.315	9.2	0.50	4.5	2.5	11.0	9.0	6.0	90	46%	54%
D-377	5.5 bar imep	0.309	9.2	0.49	4.5	-1.5	11.5	5.5	1.5	90	39%	61%
D-377	5.7 bar imep	0.321	9.2	0.51	4.5	-1.5	11.5	5.5	1.5	100	42%	58%
D-377#	Cetane matched w/DTBP	0.315	9.2	0.50	2.5	-3.5	11.5	7.0	0.0	64	34%	66%
***Tests at 5.6 bar imep, 6° SOI (BTDC), 2400 RPM, T_{intake} 30 °C unless noted otherwise*												

Table 7.8 Fueling and ROHR data at an imep of 5.6 bar.

Fuel Abbrevation	Description**	M_{fuel} (g/s)	M_{air} (g/s)	Fuel/Air Equivalence Ratio	ID (CA)	SOC (CA)	Injection Duration (CA)	EOI (CA)	Premixed Burn Peak Location (CA)	Peak Rate (J/deg)	Premixed Fraction	Mixing-Controlled Fraction
D-377	Base fuel	0.190	9.4	0.30	5.0	-1.0	7.0	1.0	1.5	86	47%	53%
D-377+	Cetane matched w/2-EHN	0.190	9.4	0.30	3.0	-3.0	7.0	1.0	0.0	50	33%	67%
ND20+	Alkane	0.189	9.4	0.30	3.0	-3.0	7.5	1.5	0.0	52	34%	66%
MG21	8 wt-% (Monoglyme)	0.202	9.4	0.28	4.5	-1.5	8.2	2.2	1.0	75	41%	59%
DG20	8 wt-% (Diglyme)	0.204	9.4	0.29	3.5	-2.5	8.0	2.0	0.5	70	46%	54%
FT	Fischer Tropsch	0.187	9.4	0.30	1.8	-4.3	7.0	1.0	-1.8	32	17%	83%
***Tests at 3.7 bar imep, 6° SOI (BTDC), 2400 RPM, T_{intake} 30 °C unless noted otherwise*												

Table 7.9 Fueling and ROHR data at an imep of 3.7 bar.

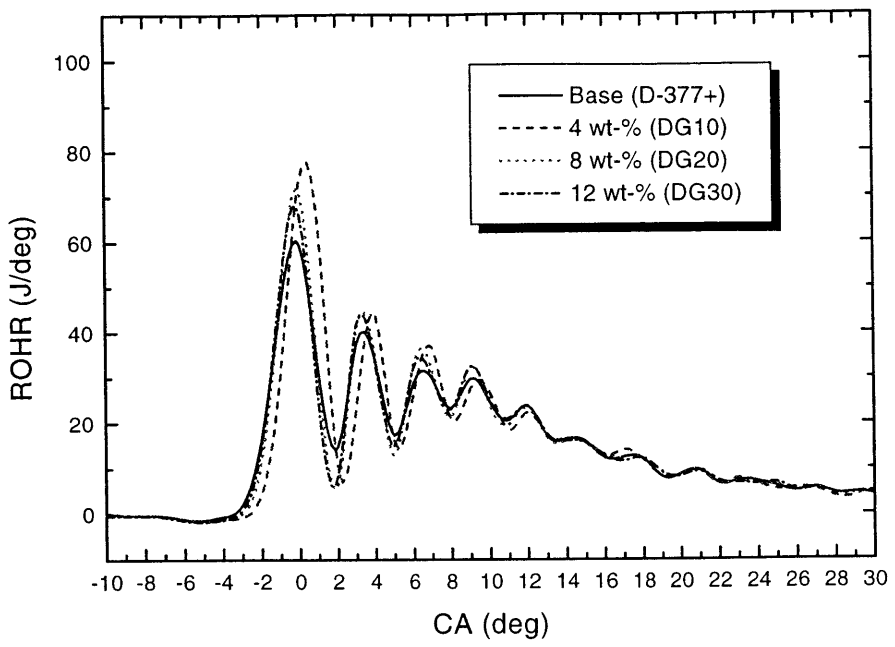

Figure 7.1 Rate of heat release for increasing wt-% oxygen. Fixed SOI 6 °BTDC with cetane matched base fuel (D-377+) and varying amounts of Diglyme blended with the base fuel.

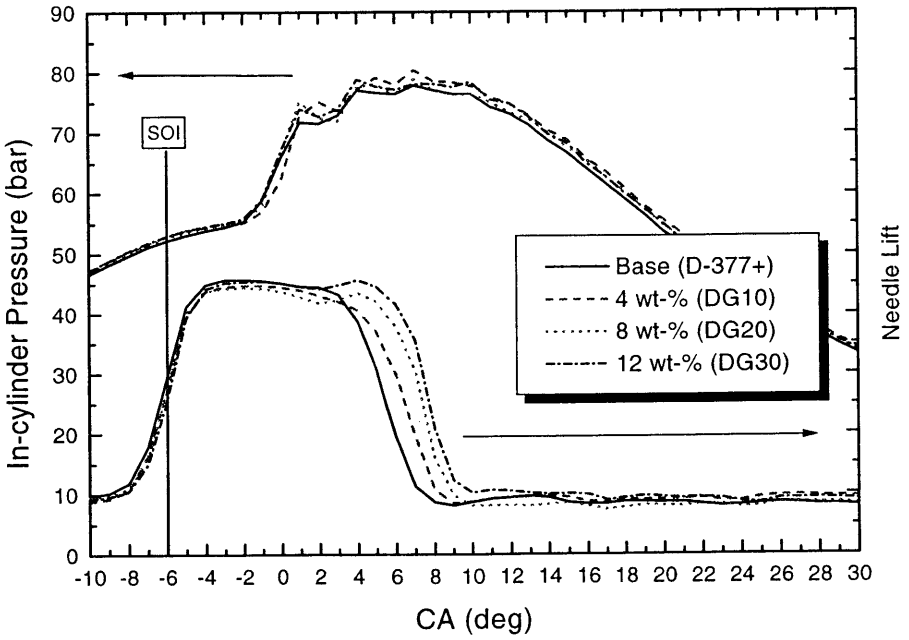

Figure 7.2 In-cylinder pressure and injector needle lift for increasing wt-% oxygen. Fixed SOI 6 °BTDC with cetane matched base fuel (D-377+) and varying amounts of Diglyme blended with the base fuel.

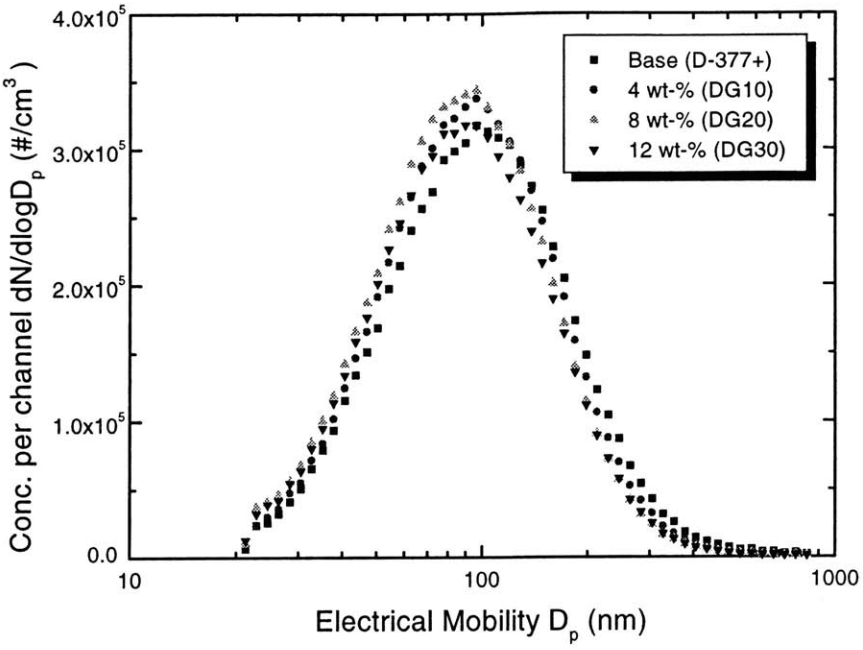

Figure 7.3 SMPS number concentration versus mobility diameter for increasing wt-% oxygen. Cetane matched base fuel (D-377+) and varying amounts of Diglyme blended with the base fuel.

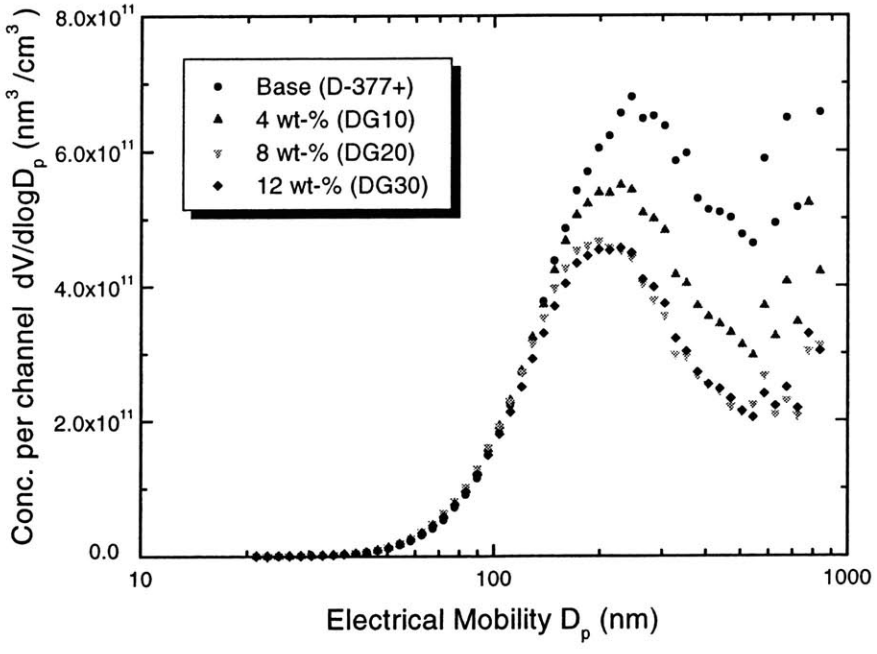

Figure 7.4 SMPS volume concentration versus mobility diameter for increasing wt-% oxygen. Cetane matched base fuel (D-377+) and varying amounts of Diglyme blended with the base fuel.

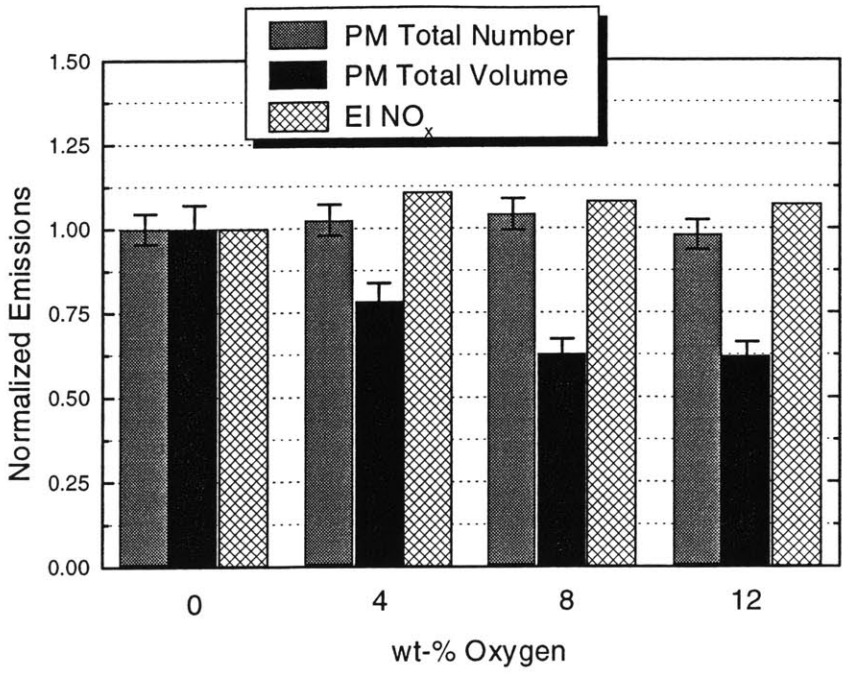

Figure 7.5 Relative SMPS total concentrations and NO_x for increasing wt-% oxygen. Cetane matched base fuel (D-377+) and varying amounts of Diglyme blended with the base fuel.

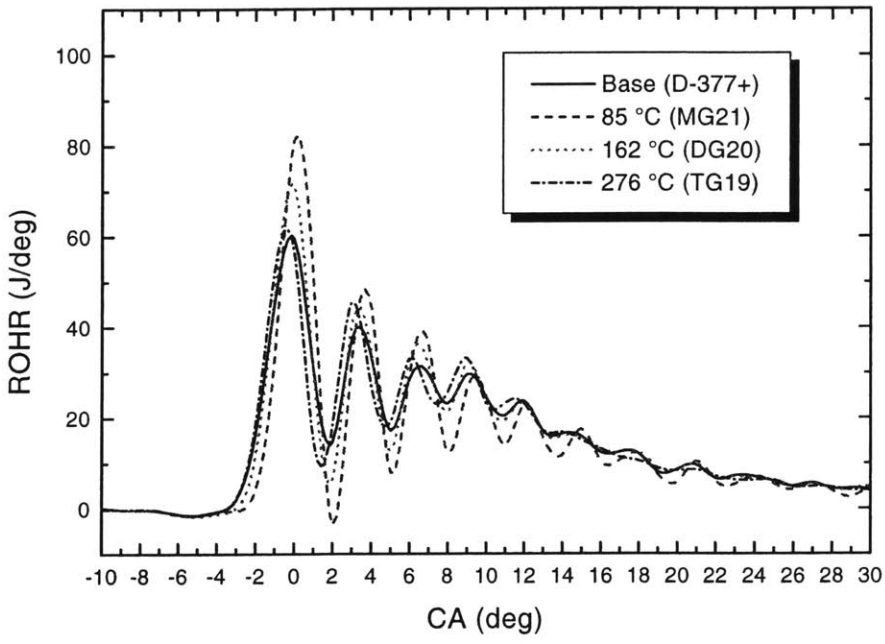

Figure 7.6 Rate of heat release for decreasing oxygenate volatility. Fixed SOI 6 °BTDC with cetane matched base fuel (D-377+) and constant 8 wt-% oxygen with different volatility Glyme ethers.

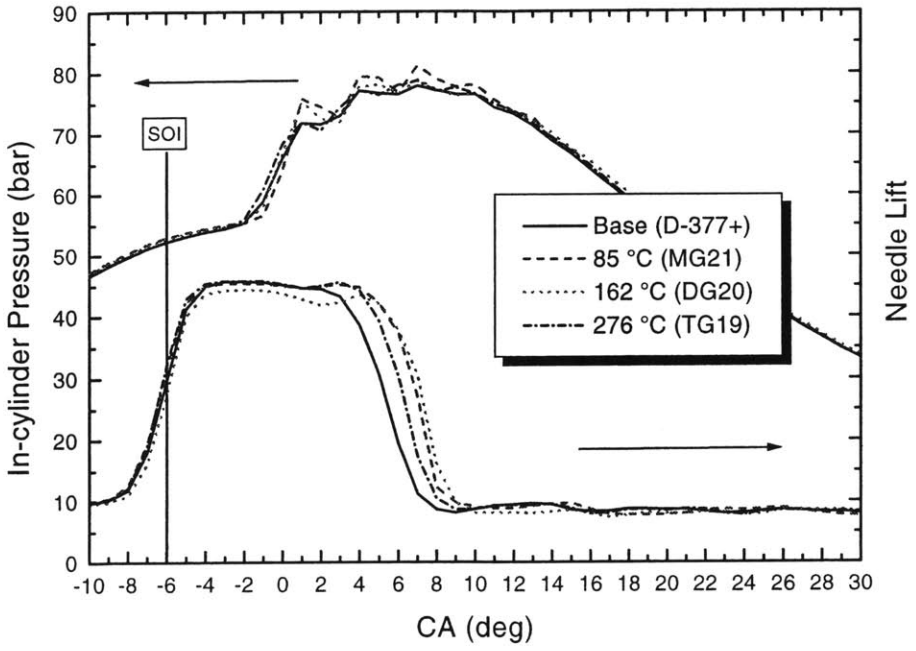

Figure 7.7 In-cylinder pressure and injector needle lift for decreasing oxygenate volatility. Fixed SOI 6 °BTDC with cetane matched base fuel (D-377+) and constant 8 wt-% oxygen with different volatility Glyme ethers.

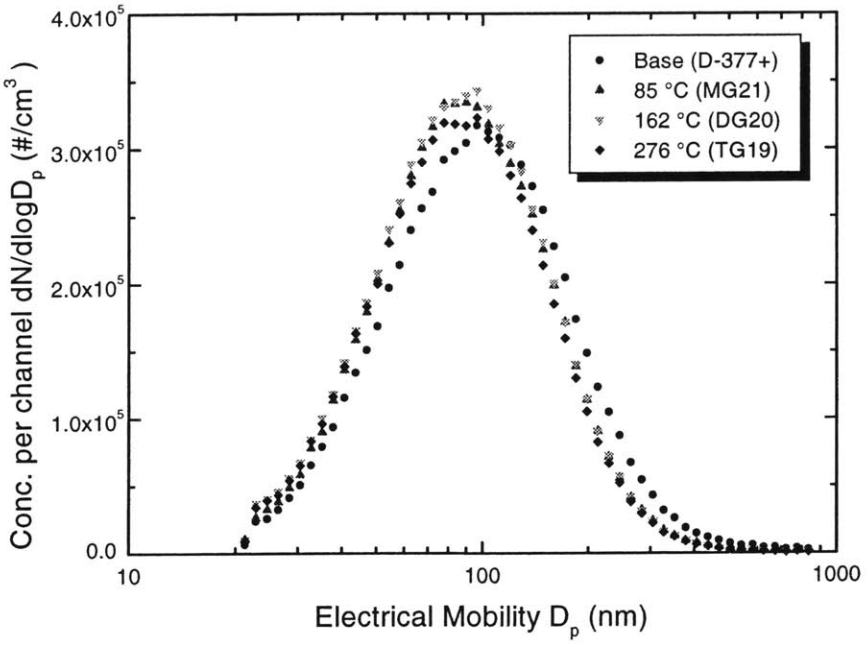

Figure 7.8 SMPS number concentration versus mobility diameter for decreasing oxygenate volatility. Cetane matched base fuel (D-377+) and constant 8 wt-% oxygen with different volatility Glyme ethers.

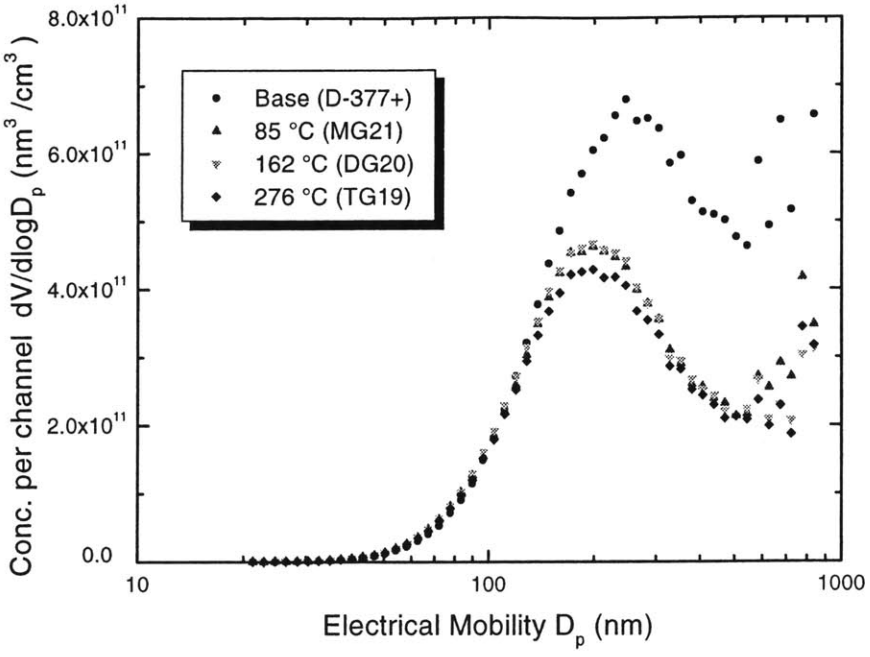

Figure 7.9 SMPS volume concentration versus mobility diameter for decreasing oxygenate volatility. Cetane matched base fuel (D-377+) and constant 8 wt-% oxygen with different volatility Glyme ethers.

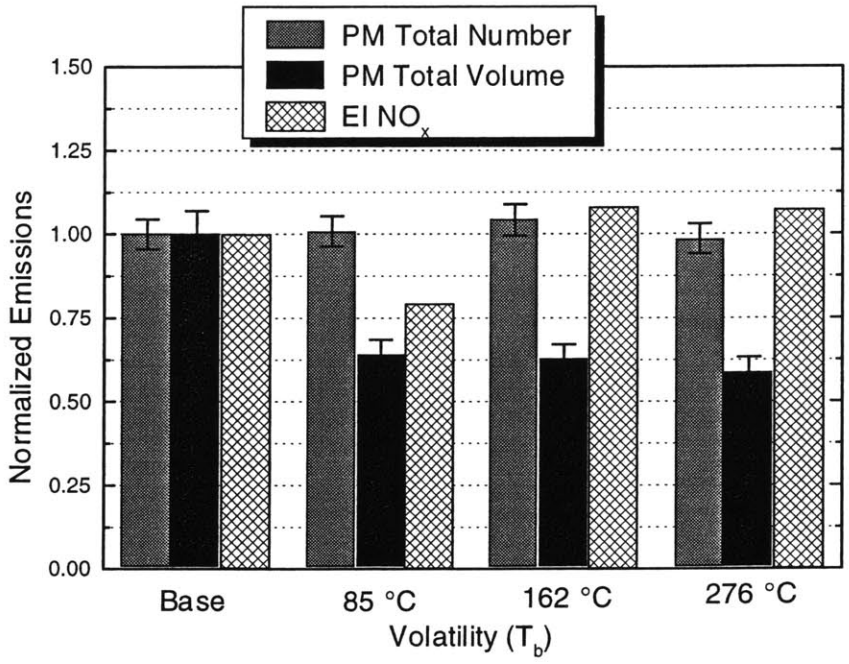

Figure 7.10 Relative SMPS totals concentrations and NO_x measurements for decreasing oxygenate volatility. Cetane matched base fuel (D-377+) and constant 8 wt-% oxygen with different volatility Glyme ethers.

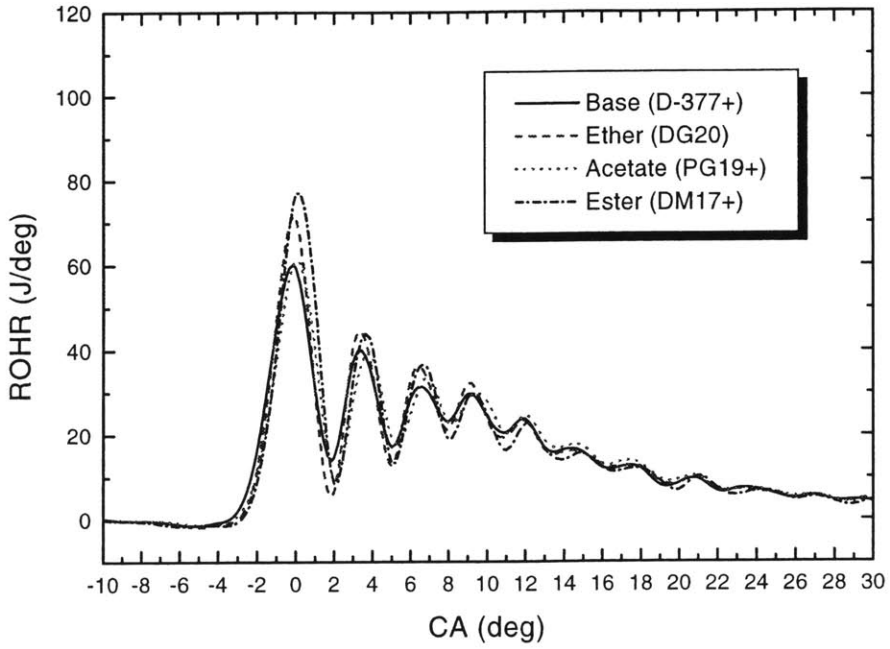

Figure 7.11 Rate of heat release for changes in oxygenate function group. Fixed SOI 6 °BTDC with cetane matched base fuel (D-377+) and different function group with 8 wt-% oxygen.

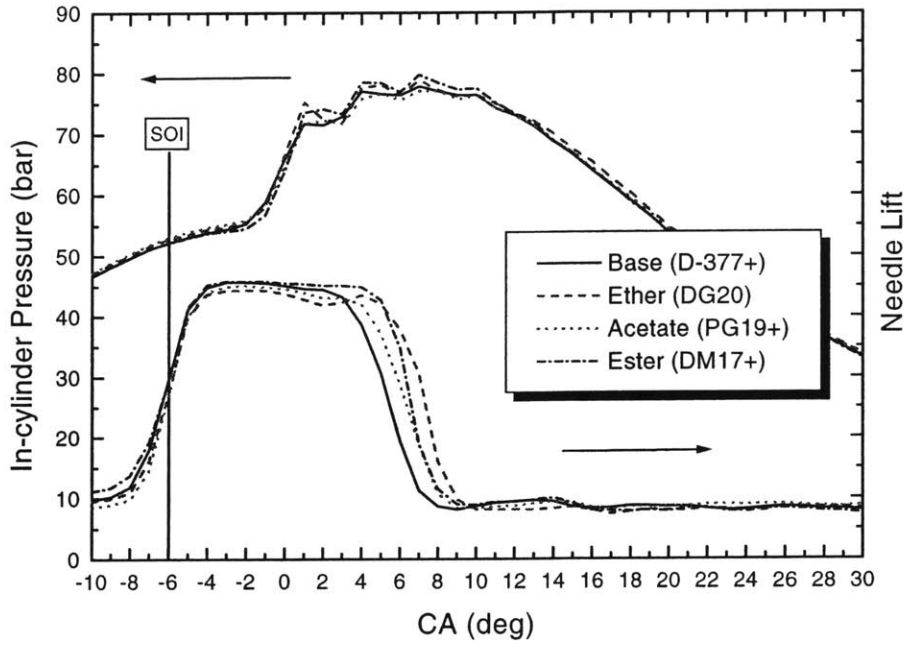

Figure 7.12 In-cylinder pressure and injector needle lift for changes in oxygenate function group. Fixed SOI 6 °BTDC with cetane matched base fuel (D-377+) and different function group with 8 wt-% oxygen.

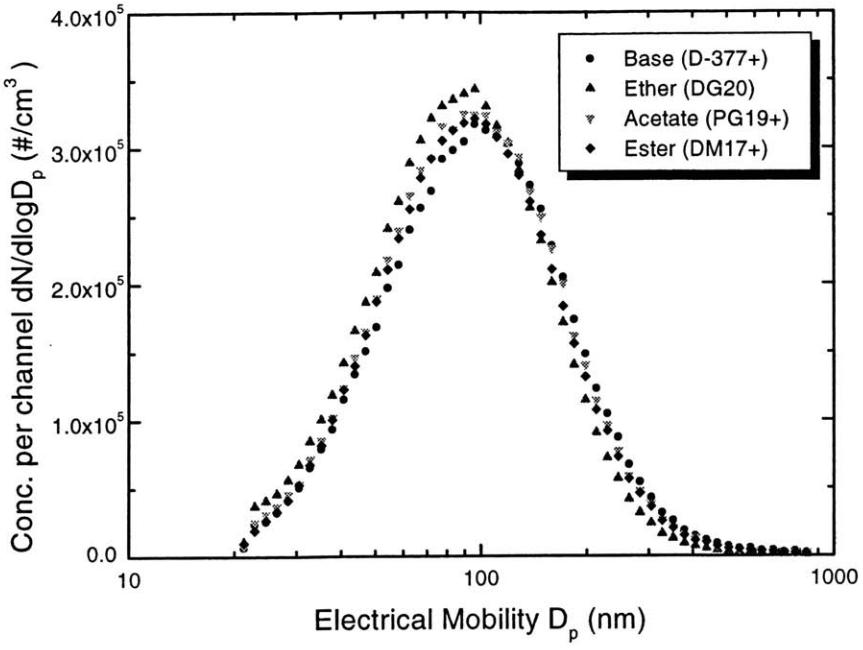

Figure 7.13 SMPS number concentration versus mobility diameter for changes in oxygenate function group. Cetane matched base fuel (D-377+) and different function group with 8 wt-% oxygen.

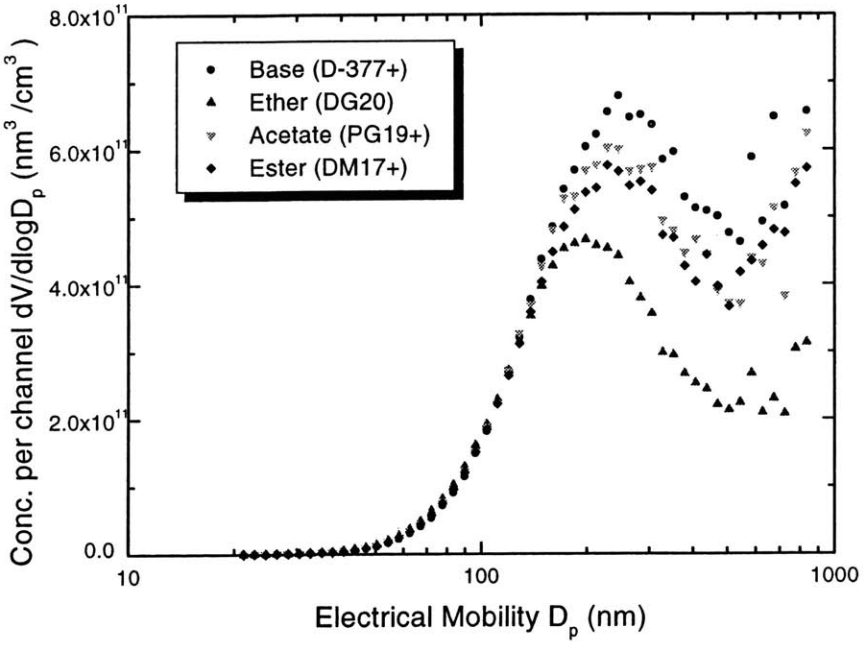

Figure 7.14 SMPS volume concentration versus mobility diameter for changes in oxygenate function group. Cetane matched base fuel (D-377+) and different function group with 8 wt-% oxygen.

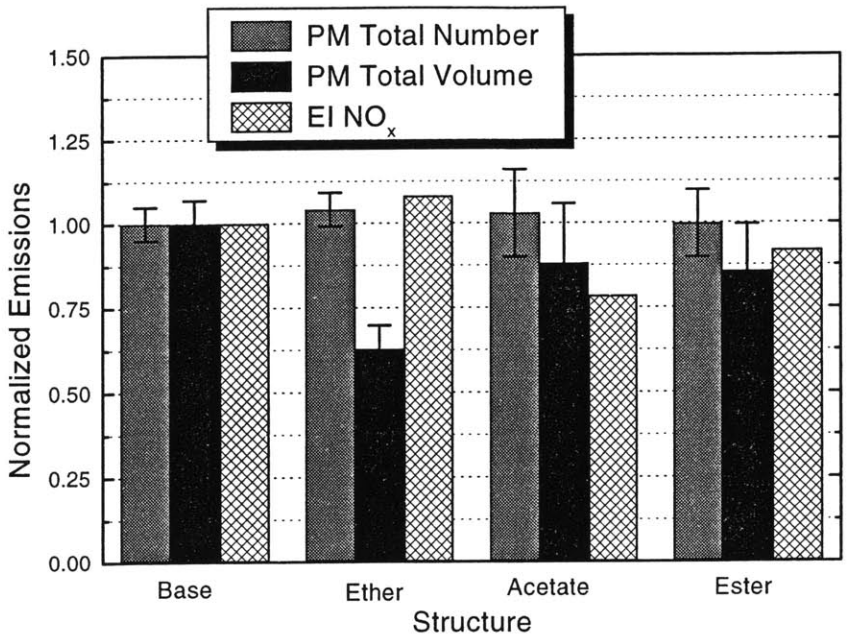

Figure 7.15 Relative SMPS total concentrations and NO_x measurements for changes in oxygenate function group. Cetane matched base fuel (D-377+) and different function group with 8 wt-% oxygen.

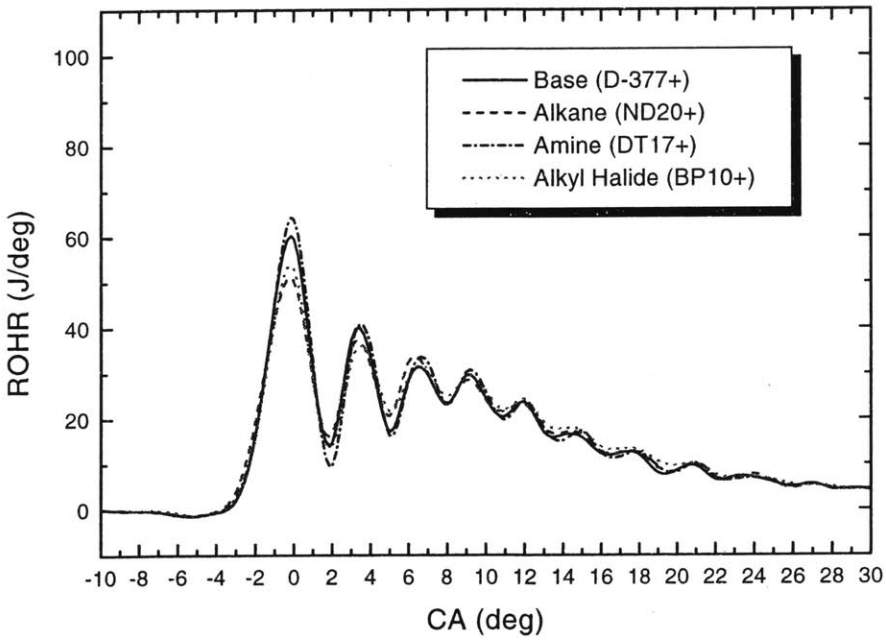

Figure 7.16 Rate of heat release for matched fuel properties without oxygen. Fixed SOI 6 °BTDC with cetane matched base fuel (D-377+) and non-oxygen containing hydrocarbons.

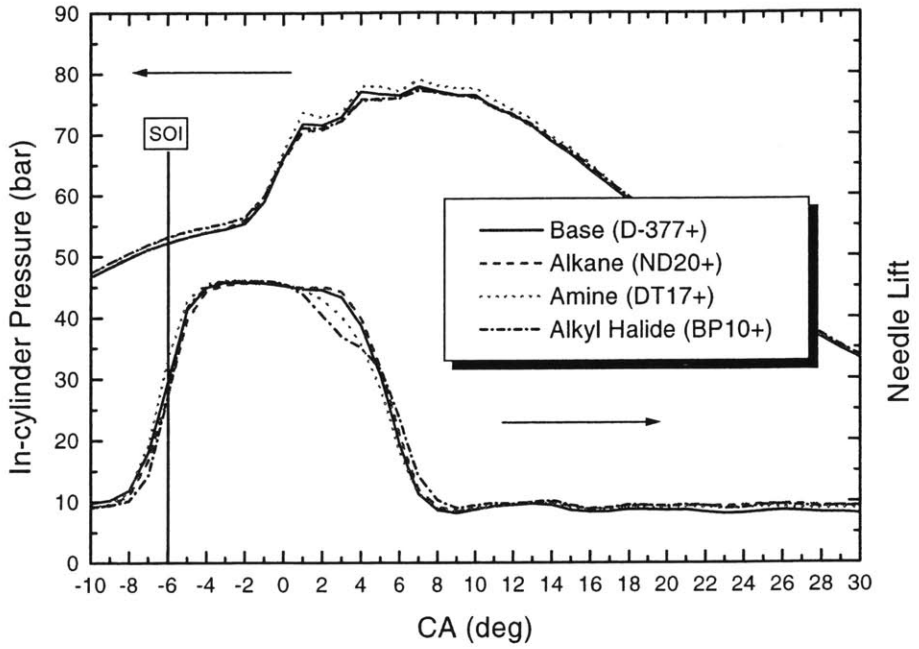

Figure 7.17 In-cylinder pressure and injector needle lift for matched fuel properties without oxygen. Fixed SOI 6 °BTDC with cetane matched base fuel (D-377+) and non-oxygen containing hydrocarbons.

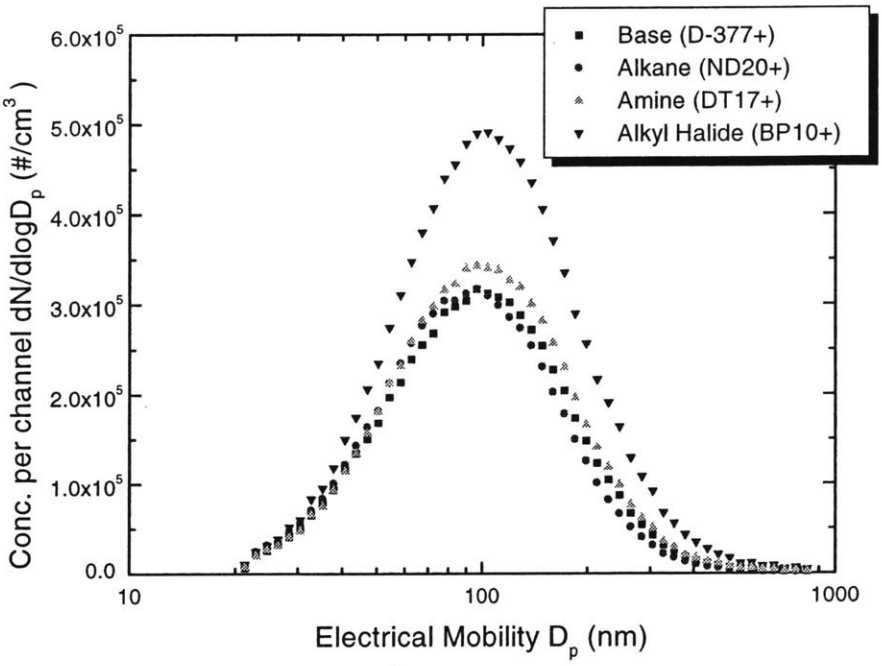

Figure 7.18 SMPS number concentration versus mobility diameter for matched fuel properties without oxygen. Cetane matched base fuel (D-377+) and non-oxygen containing hydrocarbons.

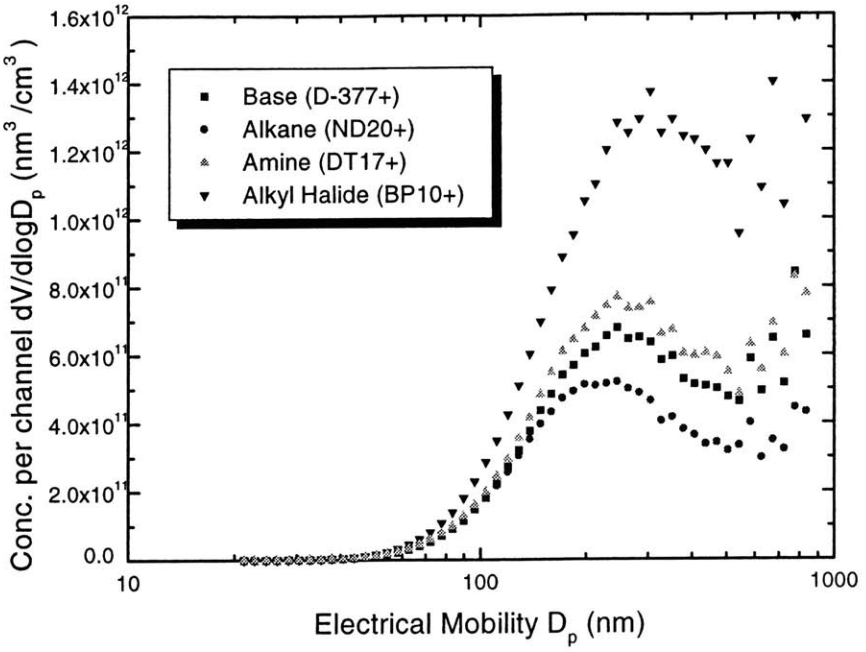

Figure 7.19 SMPS volume concentration versus mobility diameter for matched fuel properties without oxygen. Cetane matched base fuel (D-377+) and non-oxygen containing hydrocarbons.

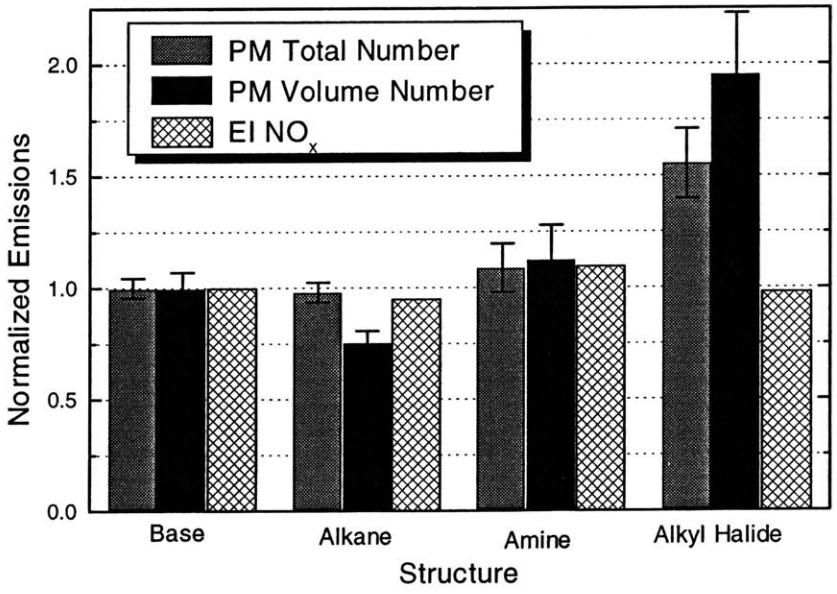

Figure 7.20 Relative SMPS total concentrations and NO_x measurements for matched fuel properties without oxygen. Cetane matched base fuel (D-377+) and non-oxygen containing hydrocarbons.

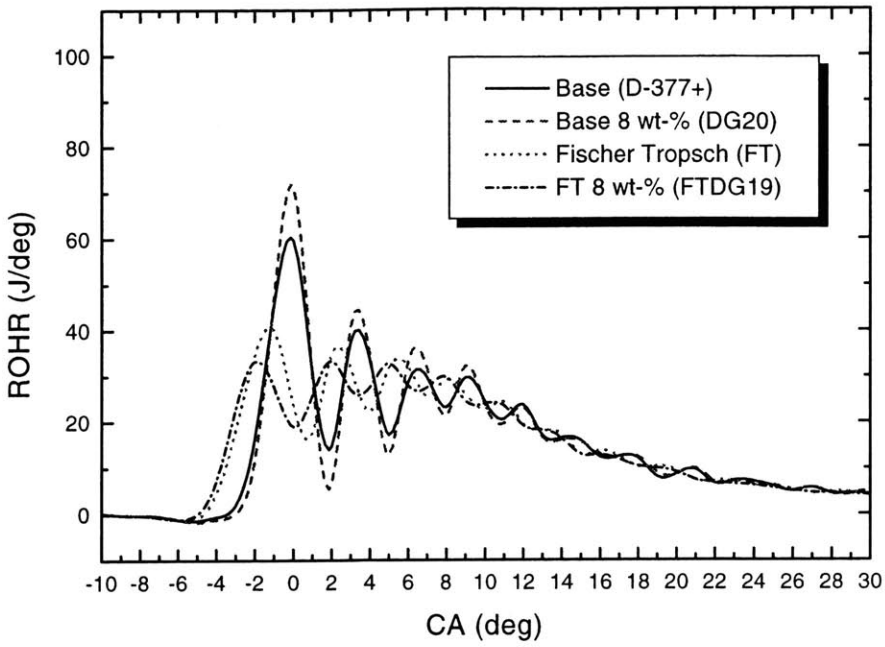

Figure 7.21 Rate of heat release for different base fuels neat and containing the oxygenate Diglyme. Fixed 6 °BTDC with cetane enhanced base fuel (D-377+), base fuel with 8wt-% oxygen (DG20), Fischer Tropsch fuel neat (FT), Fischer-Tropsch fuel with 8 wt-% oxygen (FTDG19).

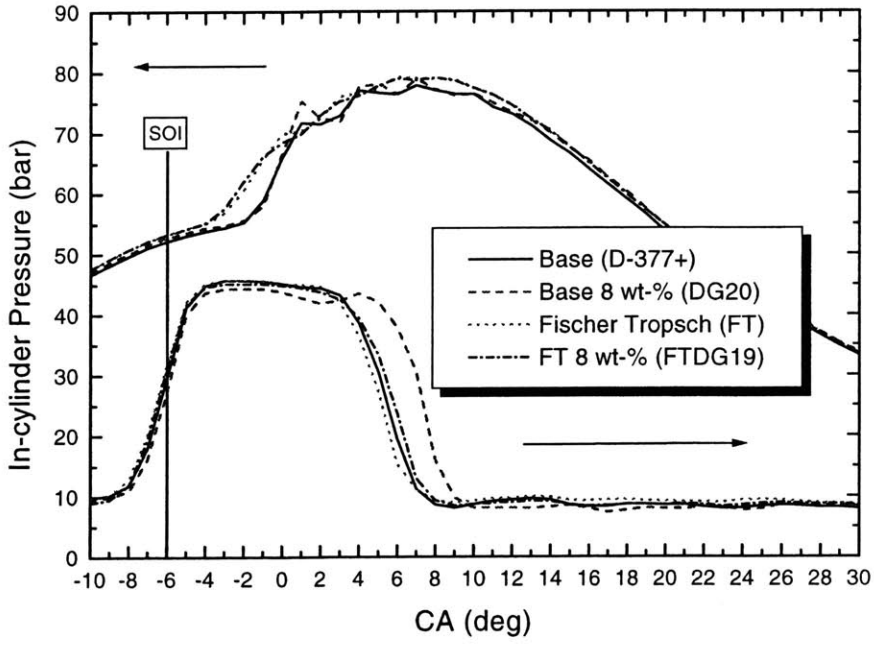

Figure 7.22 In-cylinder pressure and injector needle lift for different base fuels neat and containing the oxygenate Diglyme. Fixed 6 °BTDC with cetane enhanced base fuel (D-377+), base fuel with 8wt-% oxygen (DG20), Fischer Tropsch fuel neat (FT), Fischer Tropsch fuel with 8 wt-% oxygen (FTDG19).

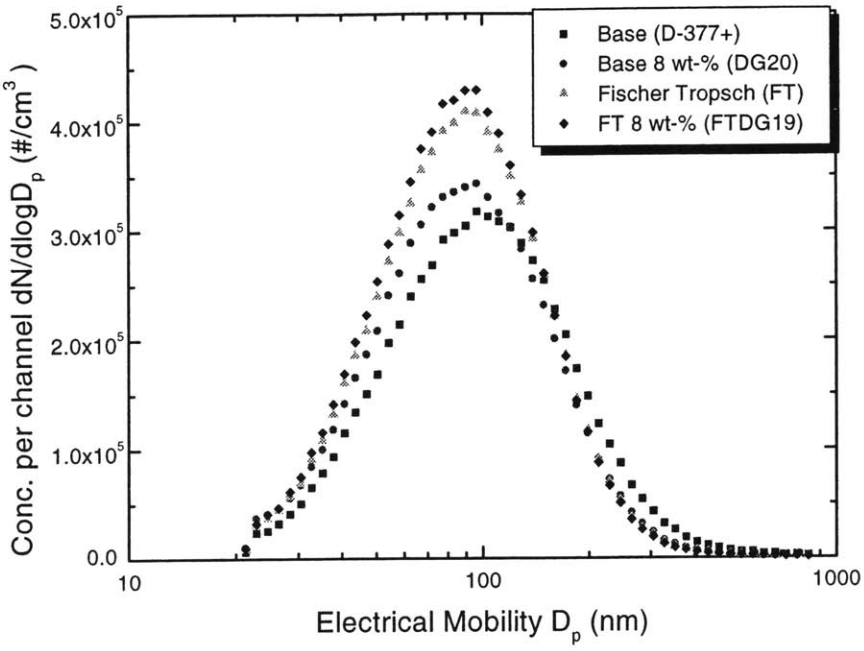

Figure 7.23 SMPS number concentration versus mobility diameter for different base fuels neat and containing the oxygenate Diglyme. Cetane enhanced base fuel (D-377+), base fuel with 8wt-% oxygen (DG20), Fischer Tropsch fuel neat (FT), Fischer-Tropsch fuel with 8 wt-% oxygen (FTDG19).

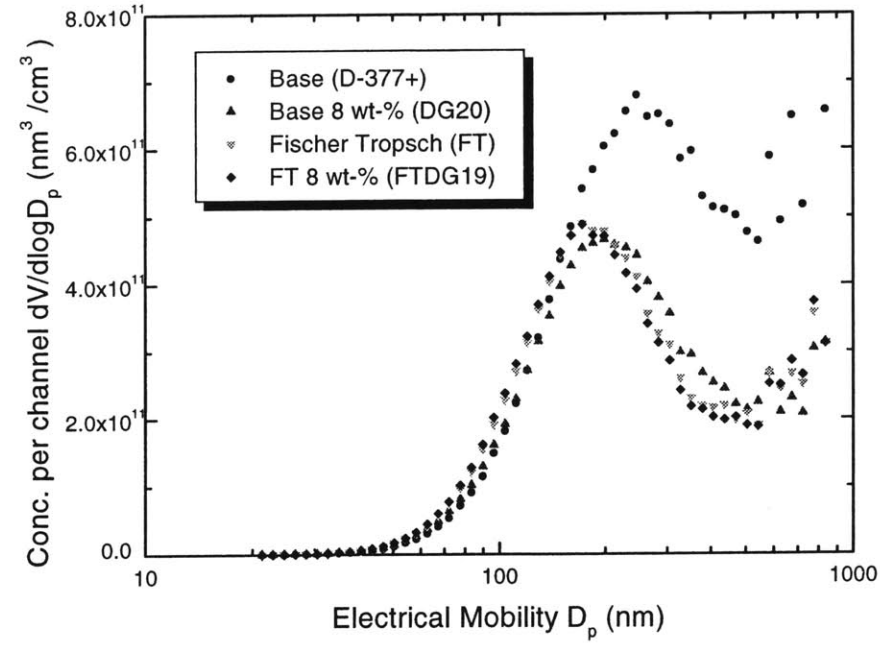

Figure 7.24 SMPS volume concentration versus mobility diameter for different base fuels neat and containing the oxygenate Diglyme. Cetane enhanced base fuel (D-377+), base fuel with 8wt-% oxygen (DG20), Fischer-Tropsch fuel neat (FT), Fischer Tropsch fuel with 8 wt-% oxygen (FTDG19).

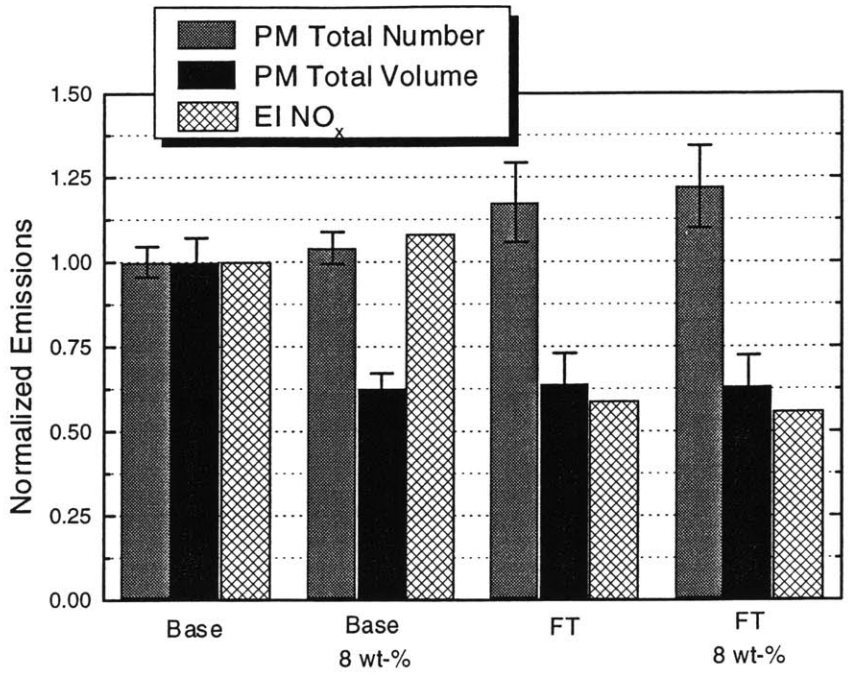

Figure 7.25 Relative SMPS total concentrations and NO_x measurements for different base fuels neat and containing the oxygenate Diglyme. Cetane enhanced base fuel (D-377+), base fuel with 8wt-% oxygen (DG20), Fischer-Tropsch fuel neat (FT), Fischer Tropsch fuel with 8 wt-% oxygen (FTDG19).

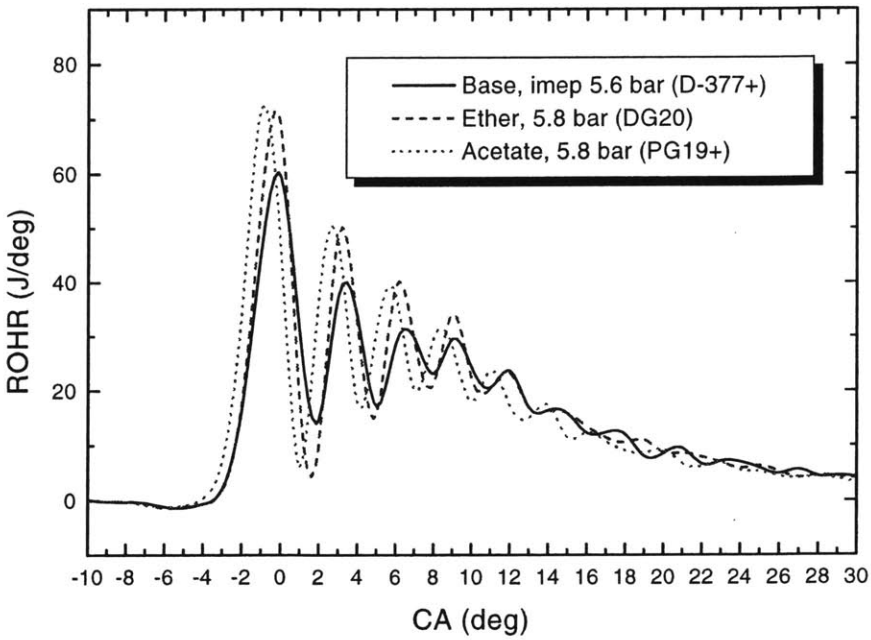

Figure 7.26 Rate of heat release for matched fuel/air equivalence ratios (ϕ = 0.5). Fixed SOI 6 °BTDC with cetane equivalent base fuel (D-377+) and oxygenated fuel with 8 wt-% oxygen (DG20).

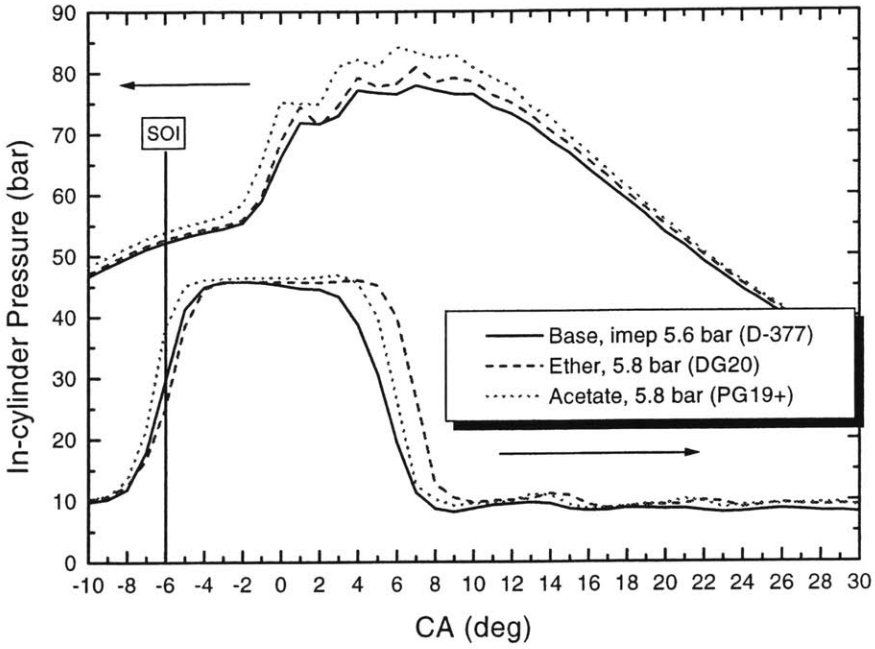

Figure 7.27 In-cylinder pressure and injector needle lift for matched fuel/air equivalence ratios (ϕ = 0.5). Fixed SOI 6 °BTDC with cetane equivalent base fuel (D-377+) and oxygenated fuel with 8 wt-% oxygen (DG20).

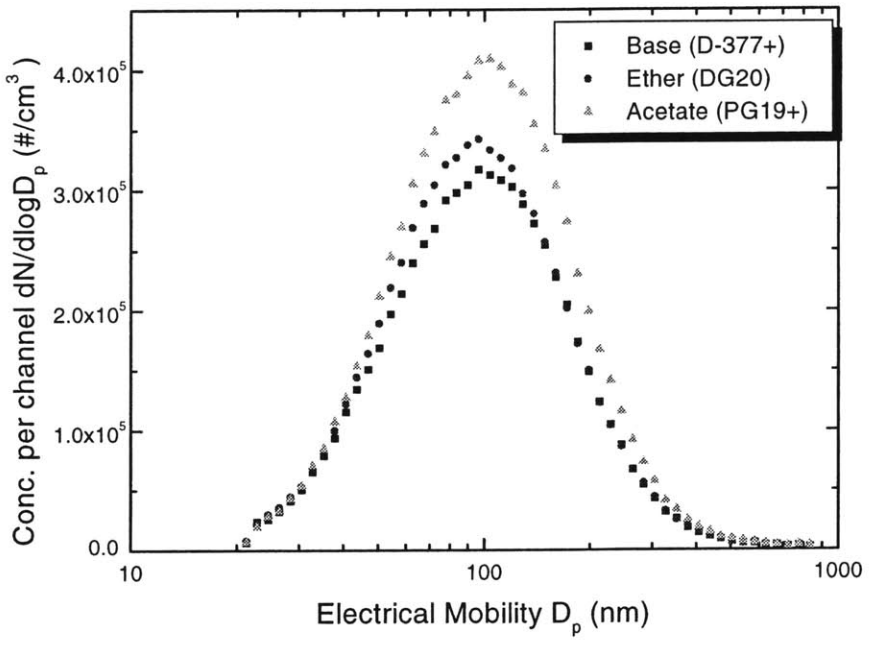

Figure 7.28 SMPS number concentration versus mobility diameter for matched fuel/air equivalence ratios (ϕ = 0.5). Cetane equivalent base fuel (D-377+) and oxygenated fuel with 8 wt-% oxygen (DG20).

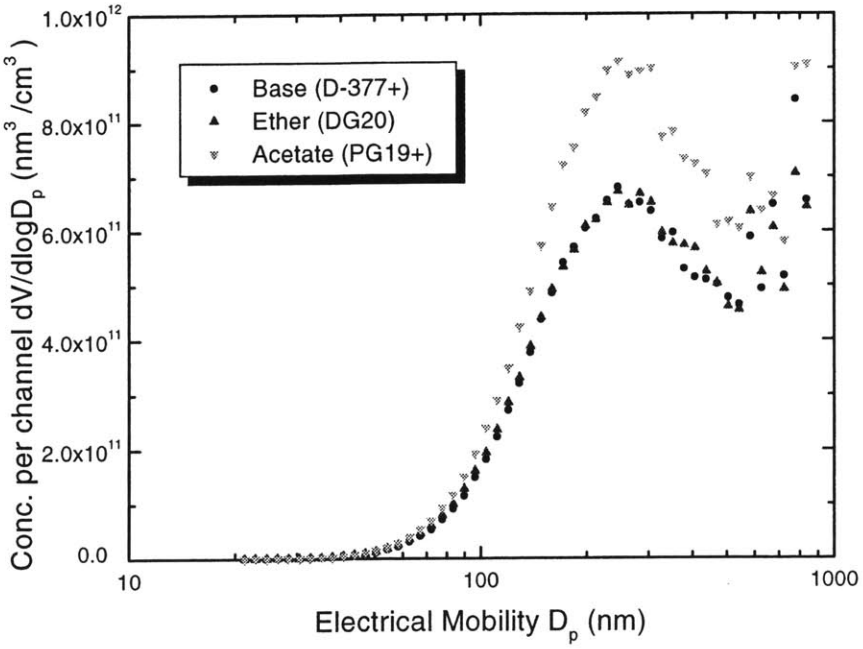

Figure 7.29 SMPS volume concentration versus mobility diameter for matched fuel/air equivalence ratios (ϕ = 0.5). Cetane equivalent base fuel (D-377+) and oxygenated fuel with 8 wt-% oxygen (DG20).

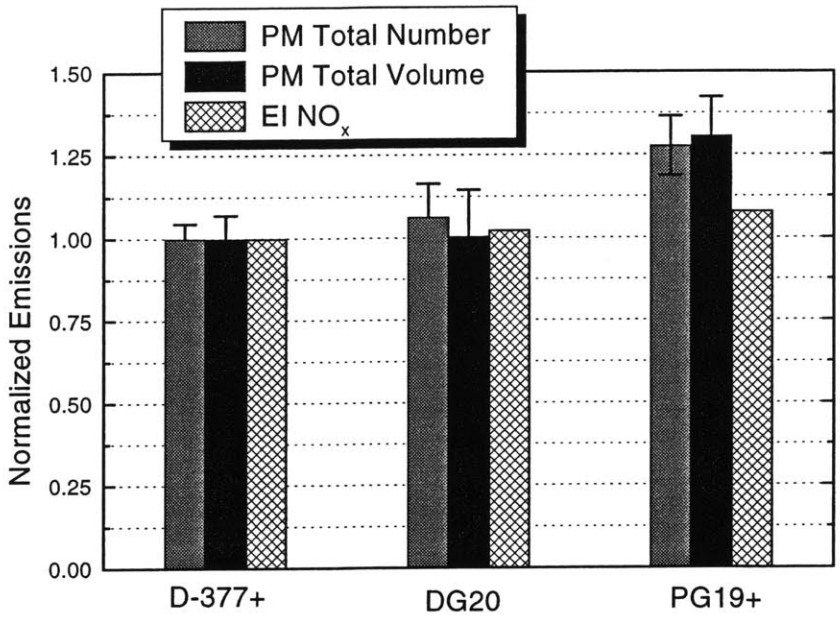

Figure 7.30 Relative SMPS total concentrations and NO_x measurements for matched fuel/air equivalence ratios (ϕ = 0.5). Cetane equivalent base fuel (D-377+) and oxygenated fuel with 8 wt-% oxygen (DG20).

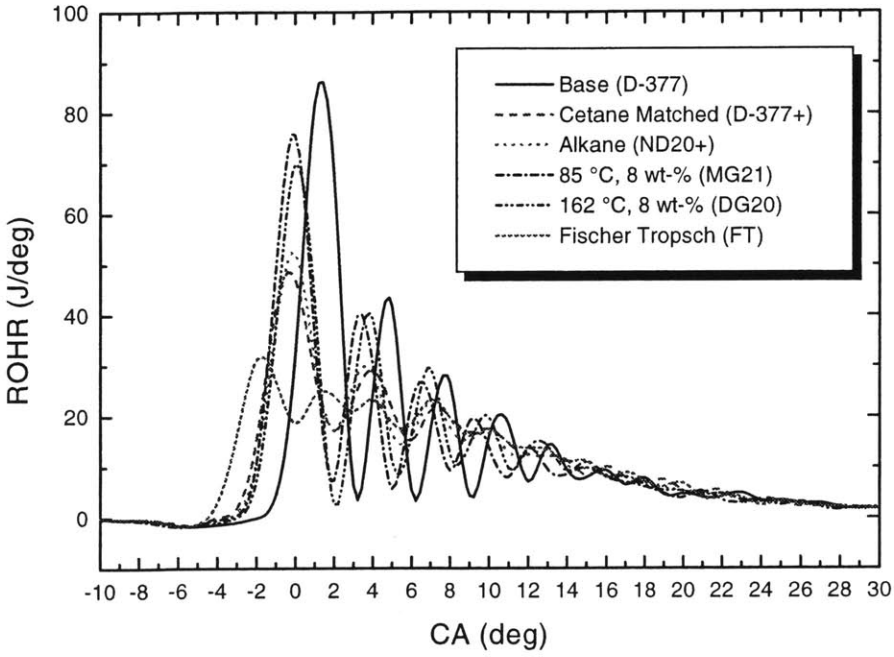

Figure 7.31 Rate of heat release for various test fuels at an imep of 3.7 bar. Fixed SOI 6° BTDC and 2400 rpm.

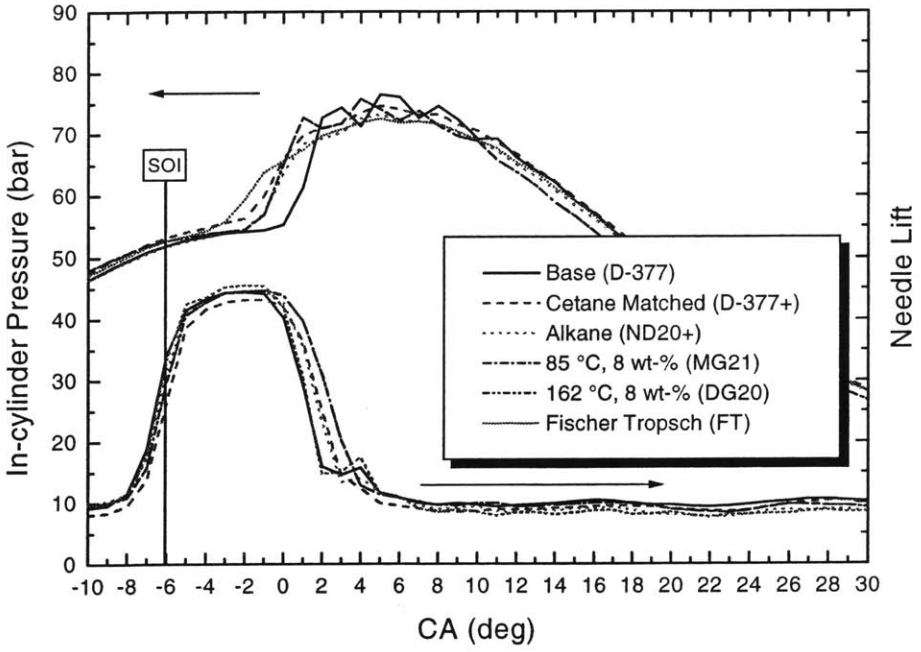

Figure 7.32 In-cylinder pressure and injector needle lift for various test fuels at an imep of 3.7 bar. Fixed SOI 6° BTDC and 2400 rpm.

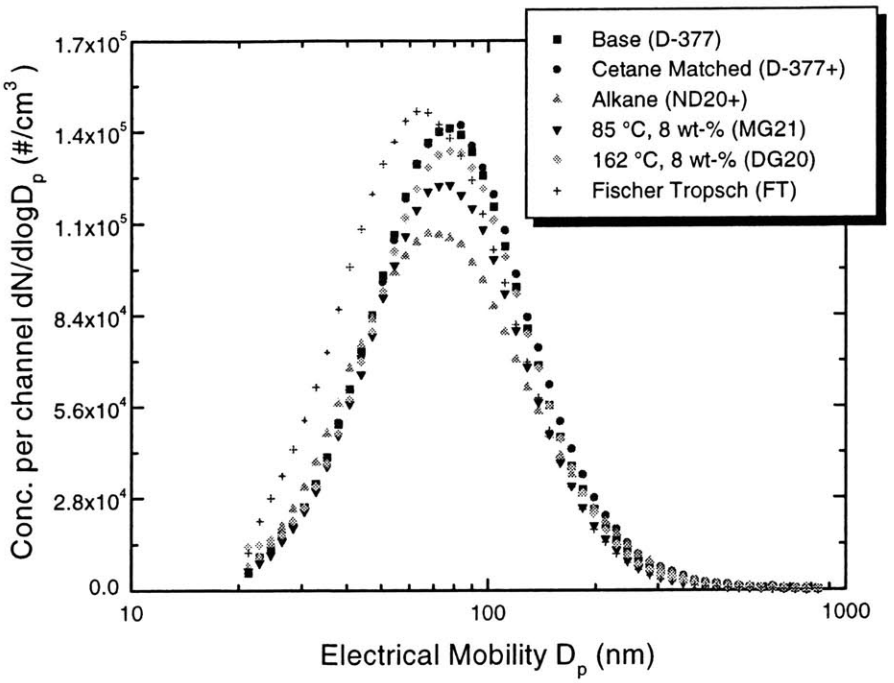

Figure 7.33 SMPS number concentration versus mobility diameter for various test fuels at an imep of 3.7 bar.

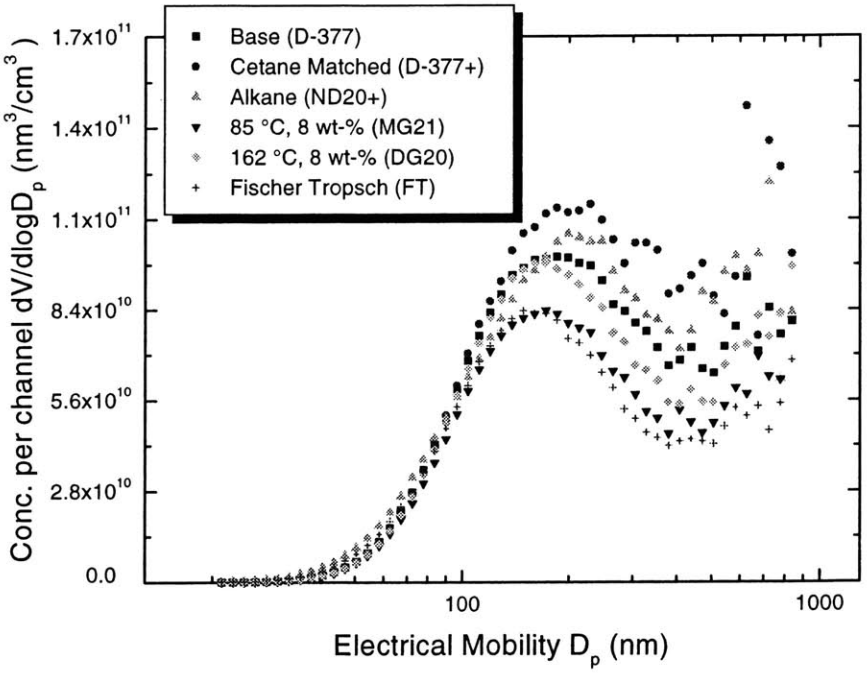

Figure 7.34 SMPS volume concentration versus mobility diameter for various test fuels at an imep of 3.7 bar.

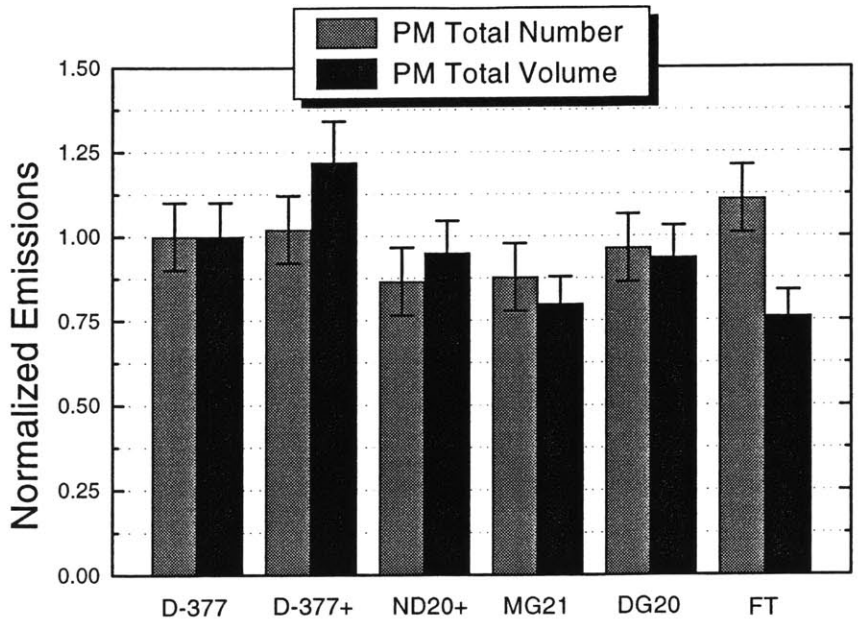

Figure 7.35 Relative SMPS total concentrations for various test fuels at an imep of 3.7 bar.

CHAPTER 8

DISCUSSION OF EMISSIONS

8.1 NO_X AND HYDROCARBON EMISSIONS

The effects of fuel changes on the oxides of nitrogen and hydrocarbons (HC) emissions were evaluated at the following test conditions, 2400 RPM, 5.6 bar imep, and 6° BTDC SOI. NO_x levels, expressed in the emission index (EI_{NOx}), for the 14 test fuels and different engine test conditions, are given in Figure 8.1. A NO_x increase of 55% was observed as the injection timing was advanced 4° to 10° BTDC. The second largest increased was noted for the 100° C air intake temperature, resulting in a 25% increase.

Unburned hydrocarbon (HC) measurements at an imep of 5.6 bar were recorded for the base fuel (D-377), cetane improved base fuel (D-377+), alkane (ND20+), and low volatility oxygenated fuel containing 8 wt-% oxygen (TG19). The results are given in Figure 8.2 with the error bars representing a 95% confidence interval. All of the fuels tested had approximately equivalent hydrocarbon levels, ranging between 1350 – 1450 $ppmC_1$.

8.2 COMPARISON OF FILTER AND SMPS MEASUREMENTS

Gravimetric filter measurements for several fuels in the experimental test matrix were taken at an imep of 5.6 bar. The PM emissions were expressed in indicated specific particles (isPart) versus weight percent oxygen, Figure 8.3. Filter measurements showed an isPart level of 0.55 g/kW-h with the cetane matched base fuel (D-377+) and approximately 0.45 g/kW-h with standard base fuel (D-377). A reduction in PM emissions was noted with the fuel containing n-decane (ND20+) and the fuel from the Fischer-Tropsch process (FT). Likewise, as the weight percent of oxygen was increased, a logarithmic reduction in the mass of PM was noted. Filter test addressing the volatility

of an oxygenated was not detectable, lying within the scatter of the filter measurements due to the current filter measuring system. However, approximate-quantitative agreement was observed between the relative comparison of the SMPS total volume concentrations data for the fuel matrix, and filter measurements, Figure 8.4.

8.3 Converting SMPS Size Distribution to a Mass Emission

There is good agreement between the relative trends in the filters and the SMPS total volume concentration. Therefore, it would be advantageous to convert the SMPS result into an isPart emission measurement. Two methods were attempted in an effort to converting the SMPS measurement into a mass. The first method utilizes the total volume concentration and assumes a constant PM density over the entire particle size range. The density of diesel PM is though to be between 1.0 and 2.0 g/cm^3 [35]. A constant density of 1.2 g/cm^3 was chosen over the entire size range (See Appendix for calculation). Utilizing the total number concentration yielded results nearly an order of magnitude higher than the standard filter measurements.

A second method assumes a lognormal number distribution of particulates. This technique, used by Maricq at Ford [35], utilized parameters such as geometric mean size, standard deviation, and total number concentration. This method provided semi-quantitative agreement, resulting in 50 – 100% error when comparing the filters and SMPS measurement. The second technique is based on the assumption that diesel PM should follow a lognormal distribution (See Appendix for details). However, there are no fundamental reasons for diesel PM being lognormal [36, 37]. A comparison of these two conversion methods to standard filters can be found in Figure 8.5

Exact agreement between the SMPS and filters is not expected. The SMPS scanning range of 21 to 835 nm is a narrow range in terms of the mass fraction of particulates. One would expect the SMPS results to be lower than that of the filters, not an over estimation as shown Figure 8.5. The discrepancies between these two PM measurement techniques will be examined in the following sections.

8.4 SAMPLING CONSIDERATIONS

The intended use of the SMPS is for aerosols of a known geometric shape, preferable, spherical [36]. However, diesel PM is not spherical in shape, but rather composed of many 30 nm spherules agglomerated into highly chained aggregates (Figure 8.6). These aggregates are heterogeneous particulates created from individual spherules and held together by van der Waals force or surface tension. The individual components vary from one another in size, shape, and chemical composition and are not easily broken from the aggregates. They consist of complex chains, self-similar in nature, with resembling geometric shapes at different levels of magnification. The fractal morphology can be characterized in terms of a fractal dimension ranging from 1.3 to 1.5 on a Richardson plot [36, 37].

The spherical model approximation is used throughout the SMPS system, from the initial Boltzmann charge distribution of the incoming aerosol to the final volume concentration. The actual diameter is based on the electrical induced motion of a particle to transverse a flow field. The diameter is based on the particle's behavior and is not a physical property. The calculated diameter is equivalent to the diameter of a sphere with the same electrical mobility. One of the main disadvantages of the differential mobility analyzer, DMA, is the occurrence of different particulates sizes with different number of electrostatic charges classified at a single diameter [36]. A charge correction algorithm in the software was used. However, the correction factor is based upon a spherical shape assumption.

The condensation particle counter (CPC) is another possible source of error. Larger particles passing through the optical counter can undergo coincidence errors. It is possible for the CPC to mistake multi-particles for a single particle. High statistical uncertainties exist for diameters greater than 600 nm. Additionally, possible transport losses exist at the low flow rates through the classifier and even lower rates through the CPC. Transport losses such as Brownian diffusion and inertial deposition, and other such as thermophoretic and electrostatic effects can impact the SMPS measurement. Theses

losses were reduced by keeping all lines as short as possible, utilizing stainless steel tubing, and monitoring the temperatures at the sampling points in the dilution tunnel.

There are limitations regarding the filter measurements as well, face velocities and filter loading can also influence the measurements. As with the SMPS system, transport losses can also impact the particulates. Care was taken to use stainless steel tubing and monitoring the temperature on either side of the filter holder.

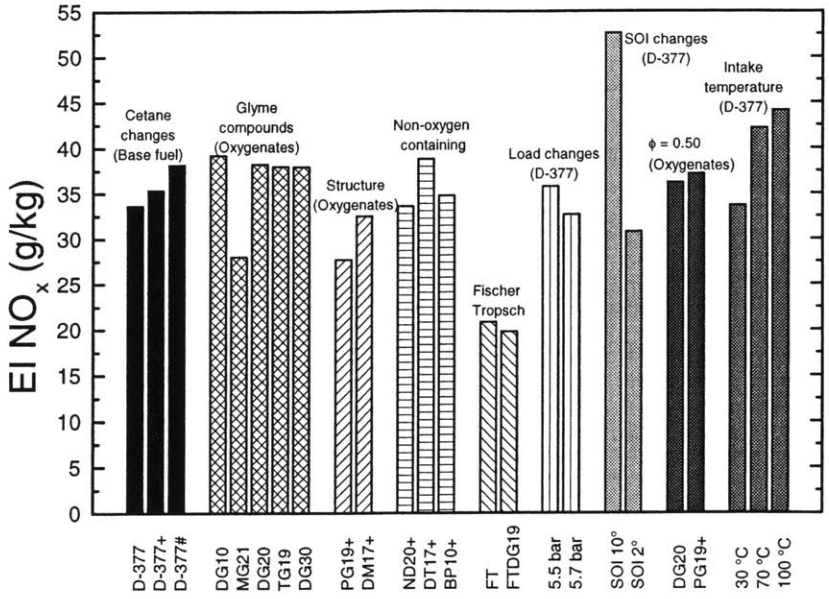

Figure 8.1 Oxides of nitrogen for various test fuels and engine operation conditions.

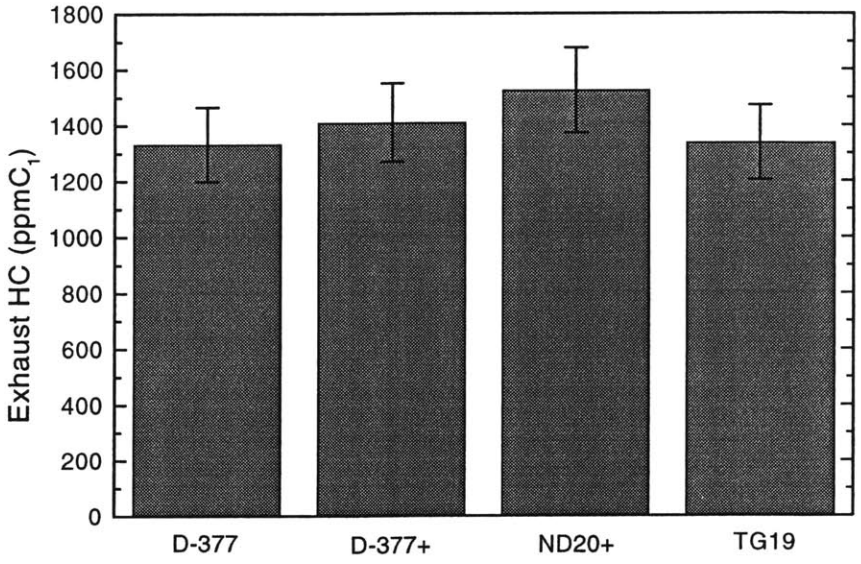

Figure 8.2 Exhaust HC measured with a FID for the base fuel (D-377), cetane enhanced base fuel (D-377+), non-oxygen containing fuel (ND20+), and a low volatility oxygenate containing 8 wt-% oxygen (TG19).

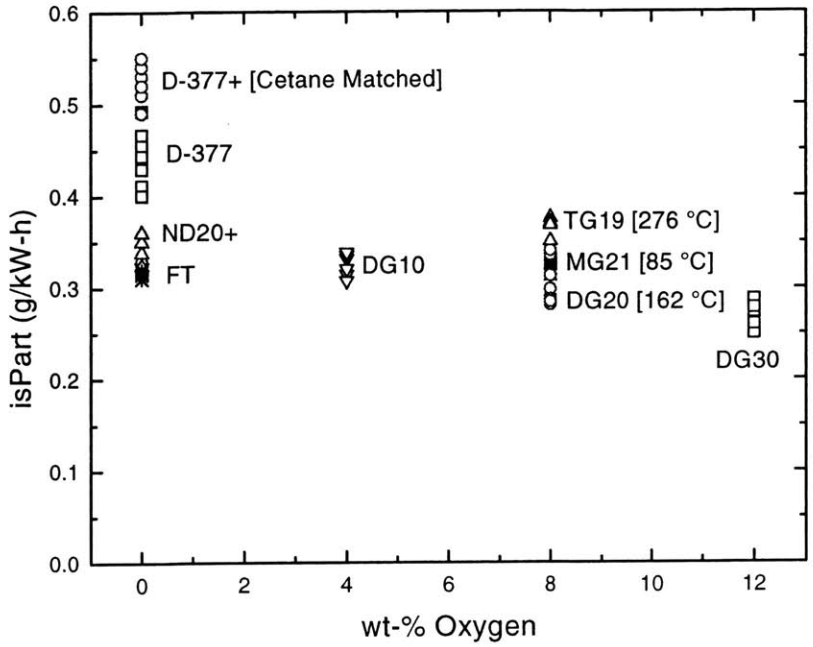

Figure 8.3 Filter measurements (isPart) versus wt-% oxygen content for various fuels in the test matrix.

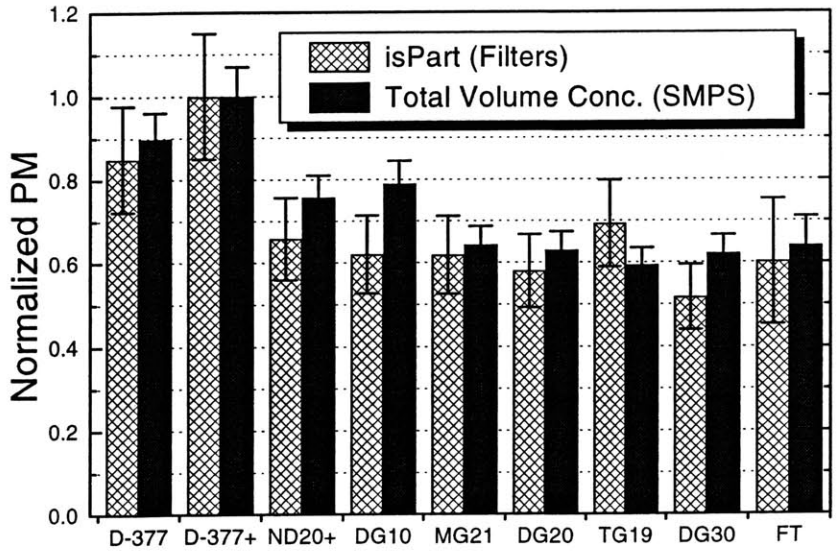

Figure 8.4 Relative comparison of filter measurements (isPart) and SMPS total volume concentration measurements for various fuels in the test matrix.

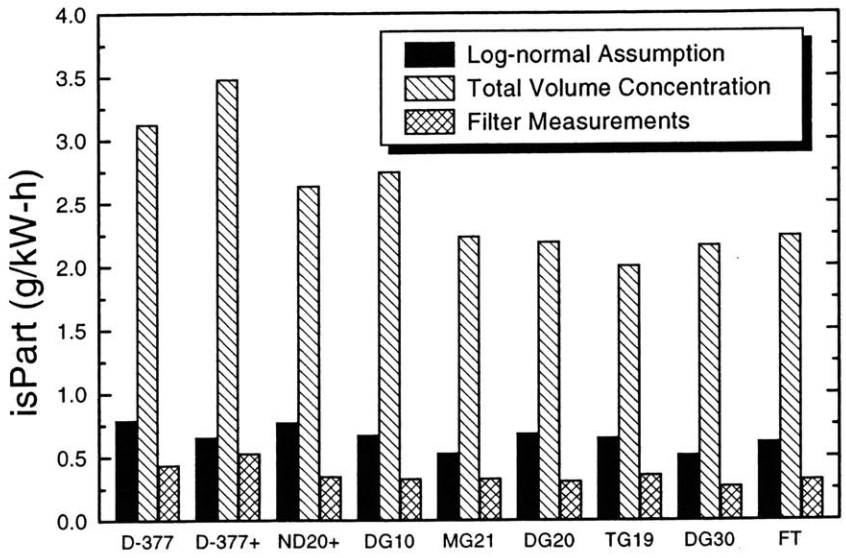

Figure 8.5 Indicated specific particulate measurements for standard filter measurements and SMPS log-normal and total volume conversion methods.

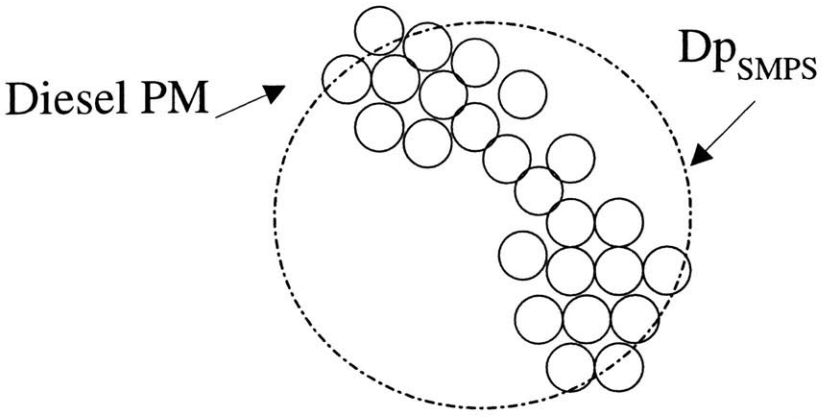

Figure 8.6 Sketch of possible SMPS diameter measurement for diesel PM.

CHAPTER 9

PHYSICAL AND CHEMICAL CHARACTERIZATION

9.1 OVERVIEW

Several of the test fuel's PM was analyzed for morphological and chemical changes. Diesel PM structure was evaluated utilizing transmission electron microscopy (TEM) and chemical analysis was preformed to determine the soluble organic fraction (SOF) to the insoluble organic fraction (ISOF). The analysis was preformed in an effort to better interpret SMPS measurements, identify any changes in the combustion process, and explore parameters that impact the health hazard of diesel exhaust; such as PM size (inhalation) and surface area (absorbed organic compounds).

9.2 PHOTOMICROGRAPHS

Soot particles emitted from a diesel engine are usually observed as chain-like aggregates (secondary particles) composed of tens to hundreds of primary spherical particles. The aggregates, not eliminated by in-cylinder oxidation, are observed to contain planar crystallites comprising of several PAH layers that are oriented concentrically. The primary particle of diesel soot contains an inner core and outer shell, each with a distinct structure. The inner core is 10 nm in diameter and located at the center of the primary particle. The core is composed of several fine particles, 3 to 4 nm in diameter, each containing tens of carbon atoms. The fine particles are characterized by a closed-shell nucleus with a diameter on the order of 1 nm located at the center of the inner core. The formation of the inner core ceases after the coagulation of several fine particles. The nucleus is then covered by an outer shell composed of carbon micro-crystallites with periodic orientations, graphitic in structure. The crystallites are planar and oriented perpendicular to the radius of the primary particle. A recent study by Toyota

[38] indicated that the outer shell is grown by surface reaction and condensation of small chemical species in sequence.

Preliminary analysis was conducted on the two test fuels, one containing 8 wt-% oxygen (DG20), the other the base fuel (D-377), in order to determine possible differences in morphology. The soot particles were collected on PTFE filters during the mass measurements and then allowed to soak in an ethanol bath for 30 minutes. The ethanol and suspended PM were then sonicated to separated into individual aggregates and deposited on a "holey" 3 mm carbon film (Ladd model 40750). The ethanol was given ample time to evaporate, leaving the soot particles for observation in a Jeol 2000 FX Transmission Scanning Microscope (TEM) 200 kV microscope. A narrow beam of electrons is focused on the sample, creating an image on a fluorescent screen from the undeflected (transmitted) electrons passing through the sample. Electrons that undergo deflection (elastic and inelastic scattering) are separated, providing an image [53].

Results from the transmission electron microscopy can be seen in Figures 9.1 and 9.2. The PM microphotograph derived from the base fuel (D-377) in Figure 9.1, contains both graphitic and amorphous carbon structures. The fuel containing the oxygenate Diglyme (DG20), depicts an amorphous carbon structure (Figure 9.2). The aggregates in both microphotographs are composed of carbon spherules on the order of 30–40 nm in diameter. These preliminary pictures do not indicate dramatic changes in the particlulates' morphology with the addition of molecular oxygen blended in the fuel.

9.3 CHEMICAL ANALYSIS

Diesel emissions are derived from fuel and lubricating oil in vapor and particle phases. Diesel PM is composed of carbonaceous spherical particles, approximately 30 nm in diameter, agglomerated into highly chained aggregates. Typically 10% to 40% of diesel PM's mass is soluble organic chemicals. The soluble organic fraction (SOF) comes from the high boiling point fuel components, the T90 fraction, and the lubrication oil. Newer technology diesel engines experience a decrease in the SOF, due to better oil consumption. Aside from health concerns from the absorbed compounds, HC also

impact the PM weight and size distribution. The condensation and absorption of HC on the particulates increases the liquid film layer, thus increasing the surface tension, allowing the aggregate to acquire more spherules and grow in both size and mass. Both engine operation and fuel properties influence the SOF. For instance, Tanaka *et al* [40] observed a shift to smaller particle diameters and a decrease in the SOF as the fuel's cetane rating was increased. The increase in cetane number reduces over-mixing of fuel and air, reducing HC emissions. Similar findings have been noted using an oxidation catalyst to reduce the SOF content, shifting diesel particles to smaller diameters. An increase in the poly-aromatic content increases the SOF and raises the PM emissions at all particle diameters. In general, a larger percentage of the SOF has been identified with the larger diameter particles and increases with decreasing engine torque [36].

Previous studies conducted with the oxygenate, Diglyme, experienced a reduction in the total amount of carbonous soot, but the relative SOF remained equal to that of the base diesel fuel [9]. The SOF primarily consists of alkanes with 18 or more carbon atoms. The higher boiling point fraction of the fuel adheres to soot particles as they pass through the filter, adding to the total mass of particulates, whereas the lower boiling point components pass through the filter as gaseous HC [39], see Figure 9.3.

Four samples were sent out for analysis of the soluble organic fraction (SOF) versus the insoluble organic fraction (ISOF). Southwest Research Institute (SWRI) preformed the analysis on the following samples; the low-sulfur base fuel (D-377), the cetane improved base fuel (D-377+), 8 wt-% oxygen in the fuel containing the oxygenate Diglyme (DG20), and the Fischer-Tropsch derived diesel fuel (FT). Removal of the organic solubles from the 47mm Pallflex filters was accomplished using a Soxhlet extraction system. The extraction solvent was a mixture of 30% toluene (C_7H_8) and 70% ethanol (C_2H_6O) by volume. The extraction procedure removed the organic fraction from the insoluble fraction collected on 47 mm PTFE filters. The filters are weighed prior to the extraction and again after the extraction. The difference in the weight is attributed to the soluble organic of organic extractables in diesel particulates by filter weight difference. The extraction was run long enough to complete a minimum of 40 cycles (one cycle is the lapsed time when the solvent begins to siphon into the flask and the

Soxhlet reservoir, 25 ml, empties, fills, and begins to siphon again). Following extraction, the filters are removed from the Soxhlet apparatus, and allowed to dry for approximately five hours. The filters are then put back in their respective petri dishes, placed in the weighing chamber, and allowed to equilibrate for 1 hour. The final weight is determined after the equilibration period.

PM composition is shown Figure 9.4. The highest percentage (50 - 60 % by mass) of SOF was noted in the Fischer-Tropsch (FT) derived fuel. The FT derived fuel has a T90 temperature of 340 °C, 50 °C higher than that of the ultra-low sulfur base fuel. The SOF has been shown to increase with a rise in T90 temperatures [51]. The cetane improved base fuel (D-377+) and oxygenated fuel (DG20) contained roughly equivalent (30%) SOF fractions. Previous studies confirm these finding, noting that the ratio between the SOF and ISOF does not differ for oxygenated or standard reference diesel fuels [3,5]. The lowest SOF was observed with the standard low-sulfur (approximately 20%). An increase in cetane number reduces the over-mixing of fuel with air before the start of combustion, reducing HC emission and SOF. It is unclear why an increase in cetane number increases the SOF for the low-sulfur base fuel test case.

In addition to standard SOF/ISOF analysis, more specific chemical characterization was attempted by extracting the volatile organic compounds from the filters with two different solvents. The PTFE filters were extracted in methanol (CH_4O) and dichloromethane (CH_2Cl_2) for a period of 30 hours and then injecting into a Hewlett-Packard (HP) 5890 Series II Plus Gas Chromatograph (GC). The HP 50 series column was initial set to a temperature of 50 °C with a 8 °C per minute temperature increase until a final temperature of 310 °C (held for 10 minutes) was achieved, resulting in a total run duration of 44 minutes. The separated components then passed through a HP 5972 Mass Spectrometer (MS) to determine the mass-to-charge (m/e) of ionized molecules for species identification. However, the results from the chromatography indicated poor separation of the extracted chemical components. The total ion concentration (TIC) spectrum did not clearly show an abundance peak (other than the signatures from the solvents) above the background scatter. Therefore, the results were not included in the thesis, but an attempt was made as part of the research effort.

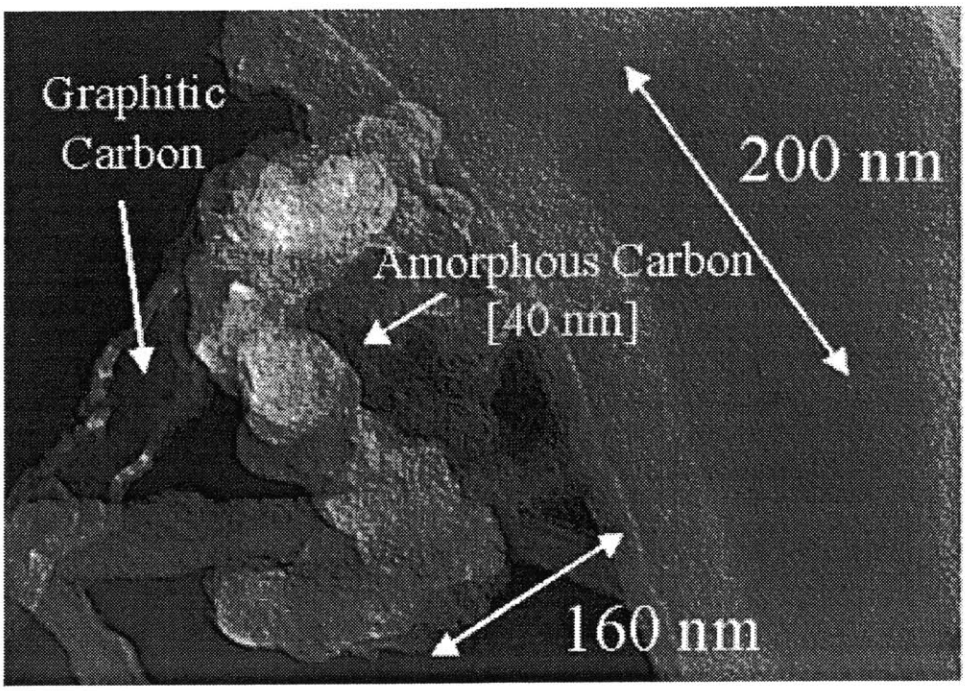

Figure 9.1 TEM photomicrograph of PM from the low-sulfur base fuel (D-377).

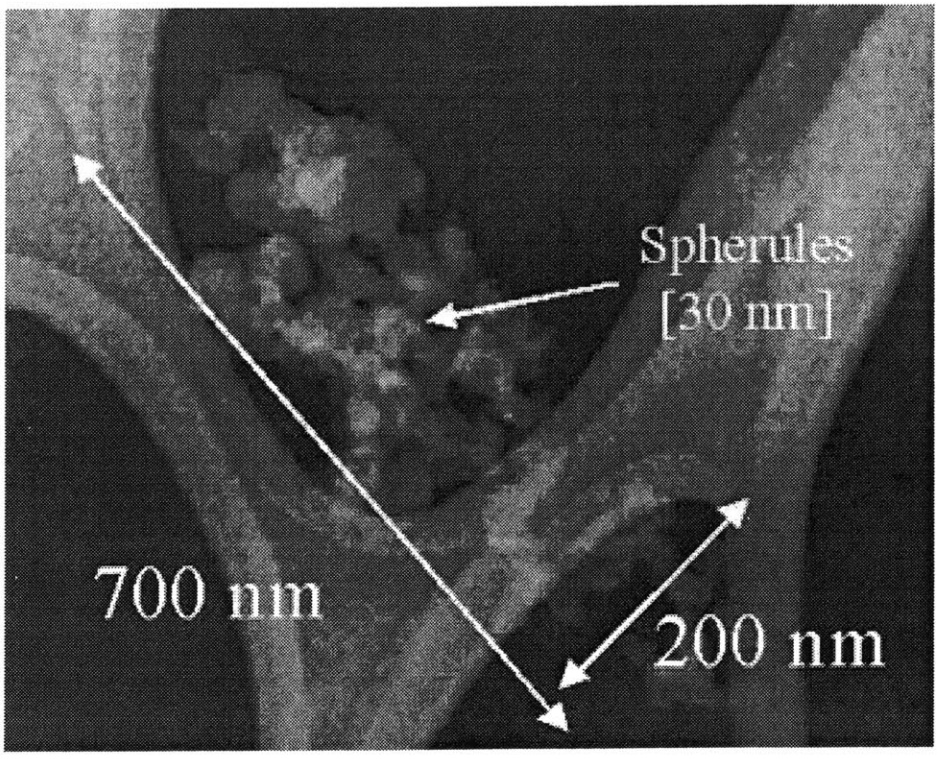

Figure 9.2 TEM photomicrograph of PM from an oxygenated fuel containing 8 wt-% oxygen (DG20).

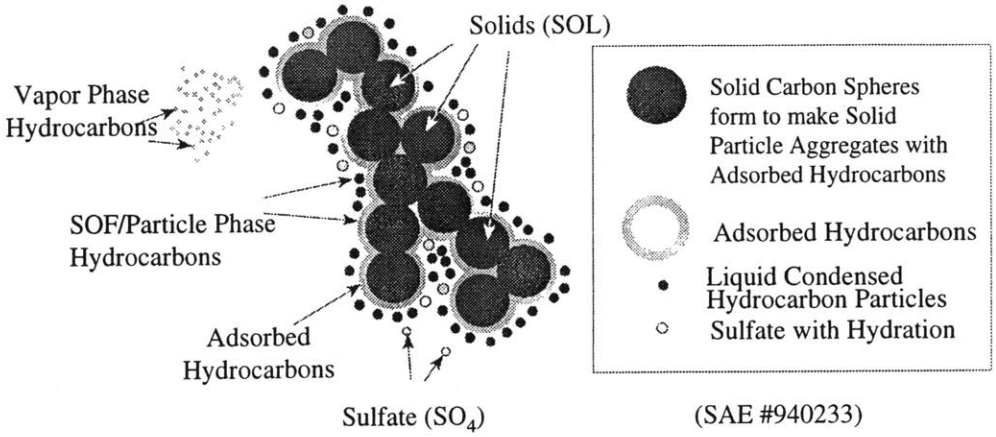

Figure 9.3 Schematic of diesel particulates and vapor phase compounds.

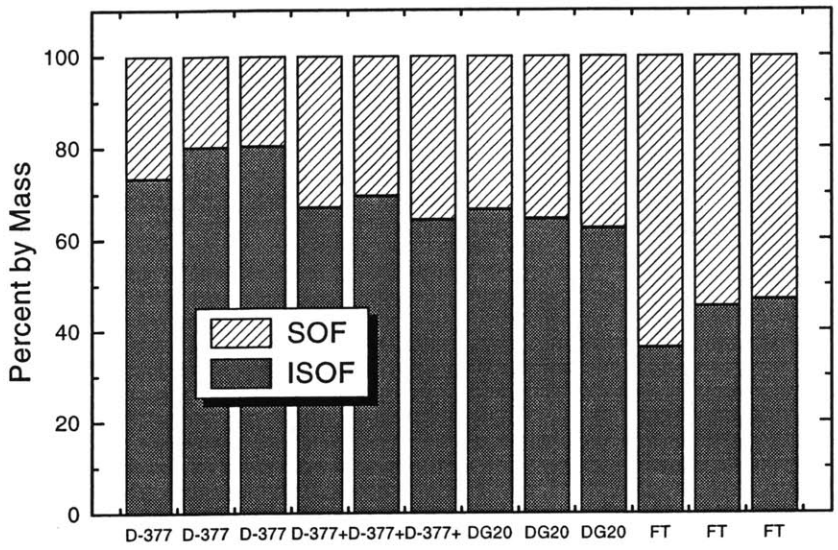

Figure 9.4 Percent by mass of soluble organic fraction (SOF) versus insoluble organic fraction for base fuel (D-377), cetane improved base fuel (D-377+), oxygenated containing 8 wt-% (DG20), and Fischer-Tropsch (FT).

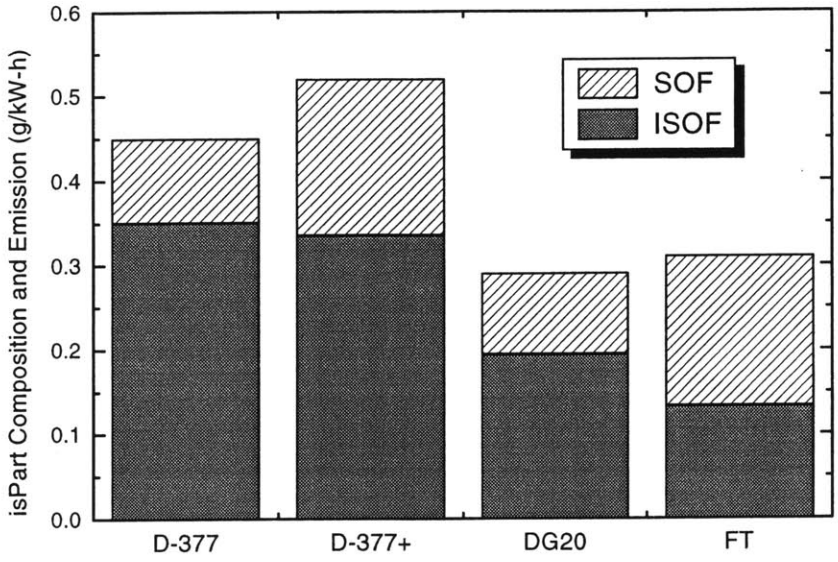

Figure 9.5 Indicated specific particulates (isPart) composition and emissions for base fuel (D-377), cetane improved base fuel (D-377+), oxygenated containing 8 wt-% (DG20), and Fischer-Tropsch (FT).

CHAPTER 10

SUMMARY AND CONCLUSIONS

10.1 ENGINE OPERATION

Before evaluating the impact of oxygenated fuels on emissions, several experiments were conducted to determine the sensitivity of emission levels to engine operating parameters such as intake air temperature, load, start of injection timing, and ignition delay. The intake air temperature was varied from 30° C to 70° C and 100° C. This increase in air temperature had the greatest impact on emissions, increasing the SMPS integrated number concentration by as much as 50% and SMPS integrated volume by a factor of 4.5. The elevated air temperatures also increased NO_x emissions by 25%. The increase in PM is due to the reduction in volumetric efficiency, resulting in an increase in the fuel/air equivalence ratio. The change in intake temperature also impacts the thermal NO formation rate. However, the reported air temperatures of 70 °C and 100 °C are measured at intake port and are not the temperatures during the start of compression. Heat transfer changes the charge temperature in the cylinder during the intake process, to the 40° C or 70° C increase in inlet air temperature may not be preserved inside the engine cylinder.

The sensitivity to engine loads was also investigated. PM levels were found to increase as the imep was increased. Figure 10.1 shows the normalized integrated SMPS number and volume PM concentrations versus normalized imep, indicating the importance of holding a constant imep value throughout the engine tests. A 2 % change in imep was shown to increase the SMPS integrated volume concentration by approximately 50 %.

The start of injection timing was also noted to impact emissions by changing the rate of heat release. By advancing the timing from MBT (6° BTDC) to 10° BTDC, the SMPS integrated volume of particles increased by nearly 50 % and shifted the number

distribution to larger particle diameters. A retarded SOI timing of 2° BTDC resulted in approximately equivalent emission levels as the MBT condition.

The importance of matching combustion phasing was observed by holding a fixed MBT injection timing of 6° BTDC and varying the ignition delay by adding cetane improvers. As the ID was shortened from 4.5° CA to 2.5° CA, the peak magnitude of the premixed burn heat release was reduced by 30 %, and the SMPS integrated volume concentration of particles increased by approximately 12 %. As a result, a cetane improver was used to approximately match the combustion phasing of all fuels in the matrix, eliminating differences in emissions due to changes in ID.

10.2 OXYGENATED FUELS

A matrix of fuels was created to address how emissions scale with: 1) increasing weight percent oxygen in the blended fuel mixture, 2) oxygenate volatility, 3) oxygenate structure, 4) a similar non-oxygen containing hydrocarbon. Secondary questions such as the impact of different base fuels and load conditions on the effectiveness of oxygenates, were also investigated.

As the amount of the oxygenated Diglyme was increased in the base fuel, the increase in weight percent oxygen resulted in a logarithmic reduction of particulate matter on a volume and mass basis. The SMPS total number of particles emitted did not change compared to the cetane improved base fuel. In addition, an increase of approximately 10 % was noted in NO_x emissions.

The volatility of the oxygenate used did not impact PM mass or size distributions. Three fuels from the Glyme family of chemicals, containing 8 wt-% oxygen, were observed to have similar SMPS size distributions and filter measurements. Previous studied have observed similar results, concluding that there was no effect of boiling point for either the Glyme family or maleate family of chemical compounds [27].

The structure of the oxygenate blended with the base fuel does appear to impact the effect oxygenates have on emission. The Glymes family of chemicals have been observed to be less effective than the maleates family in reducing PM [27], while other

studies indicate no differences in PM levels with different structured oxygenates [4,5]. Experiments conducted during this research, did observe differences in PM emission with changes in the oxygenates' structure. The oxygenate Diglyme (DG20), a member of the Glyme family, reduced PM emission to lower levels than those achieved with the same weight percent oxygen using either diethyl maleate (DM17+) or propylene glycol monomethyl ether acetate (PG19+).

Non-oxygen containing hydrocarbons were matched for cetane number, volatility, and aromatic content. The addition of n-decane (alkane) decreased PM engine emissions by 25%. The use of n-decane (ND20+) decreased the fuel's overall aromatic content and increased the H/C ratio. An increase in the H atom concentration lead to increased soot pyrolysis rates, reducing soot formation [41]. The addition of a halogen containing compound, 1-bromopropane, dramatically increased PM emission levels by approximately a factor of 2. The addition of a halogen group to fuels has been shown to decreases soot pyrolysis rates, increasing soot production [41]. The addition of an amine was observed to slightly increase the oxides of nitrogen emissions, due to the nitrogen containing hydrocarbon fuel.

The fuel produced from the Fischer-Tropsch process had the greatest impact on the particle size distribution. The number of particles emitted increased by 20% with a shift to smaller diameter particles, resulting in a 40% reduction in the volume fraction of particulates. The Fischer-Tropsch fuel containing 8 wt-% oxygen did not produce a measured difference in emission levels compared to the Fischer-Tropsch fuel tested in neat form.

At the same load condition, oxygenated fuels operate at leaner equivalence ratio than that of the ultra-low sulfur base fuel. Rather than matching load conditions, a fuel/air equivalence ratio of 0.5 was used for all engine tests. At the same equivalence ratios, the oxygenated fuels experience an increase (with PG19+) or approximately equal (with DG20) PM levels compared to the cetane improved base fuel (D-377+).

At a lighter load condition, the effectiveness of adding additional molecular oxygen was reduced. At an imep of 3.7 bar, the SMPS number distribution shifted to smaller particle diameters, approximately 70 nm, from a diameter of 100 nm at 5.6 bar

imep. The SMPS integrated number concentration decreased by 50% and the volume concentration was reduced by an order of magnitude. The relative trends experienced by the fuels at the low load condition are similar to the higher load. However, the reduction in PM is greater with the oxygenates at the higher load condition; the larger relative additional of oxygen plays a greater role in reducing PM.

10.3 CONCLUSIONS

- Engine experiments must be carefully structured in order to understand the fundamental impact fuel modifications have on engine particulate emissions. The emission level sensitivity to the engine's intake air temperature, normalized torque, ignition delay, and start of injection timing was investigated. The largest impact of these variables on emissions was the increase in air intake temperature. All fuels in the matrix were matched for combustion phasing using cetane improver.

- As the weight percent of oxygen in the fuels increases the reduction in particulate matter appears to be logarithmic, in agreement with previous studies.

- Three members of the Glyme family of polyethers, with substantially different boiling points, were blended with the base fuel to containing 8 wt-%. The oxygenate's volatility did not appear to impact PM emissions.

- The chemical structure of the oxygenate did impact the relative reduction in PM. Ether containing function groups were more effective in reducing PM emissions than either the acetate or maleate family compound tested, with a blended 8 wt-% oxygen content.

- Three non-oxygen containing compounds with similar impacts on fuel properties (aromatic content, cetane, number, and volatility) as the oxygen containing Diglyme

compound. N-decane (alkane) had the greatest reduction in PM compared to the improved base fuel (D-377+). The fuel's H/C ratio is an important parameter in assessing the sooting tendency.

- A fuel derived from the Fischer-Tropsch process was substituted in place of the ultra-low sulfur fuel. In neat form, the FT fuel resulted in a 20 % increase in the number of particles and 40% reduction in the volume of particles. However, the blending of oxygenates with the FT fuel had a negligible impact on particulate emissions compared to the FT fuel in neat form.

- When matching engine experiments for fuel/air equivalence, rather than for load (imep), oxygenates had approximately equivalent or slightly higher PM emissions.

- At a lighter load condition (imep of 3.7 bar), the total number concentration of particulates was reduced by 50% and the volume fraction was reduced by an order of magnitude. Compared to an imep of 5.6 bar, the impact of additional fuel oxygen on PM emissions was reduced.

- Quantitative agreement between the filter and SMPS-measurement based relative volume fraction was achieved. However, conversion of the SMPS volume fraction into an absolute mass estimate, comparable to the filter based particulate mass was unsuccessful. A better understanding of the electrical mobility diameter measured by the SMPS system and the particulate structure, as a function of diameter is required.

- Preliminary physical and chemical analysis does not indicate any significant morphological or compositional changes for the PM formed from the oxygenated fuels, relative to the base diesel fuels.

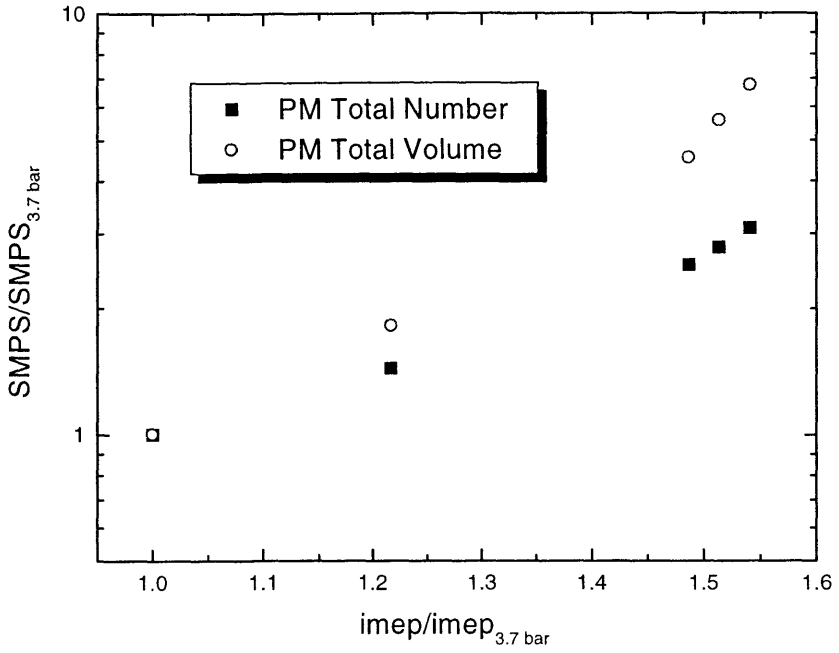

Figure 10.1 Normalized SMPS total number and volume versus normalized torque. Tests conducted with the standard base fuel (D-377) and normalized with respect to conditions at an imep of 3.7 bar.

REFERENCES

1. Office of Transportation and Air Quality, USEPA [web page] March 2000; http://www.epa.gov/oms/ [Accessed 10 April 2000].
2. Akasaka, Y. and Sakurai, Y. "Effects of Oxygenated Fuel and Cetane Improver on Exhaust Emission form Heavy-Duty DI Diesel Engines," *SAE Paper* 942023 (1994).
3. Liotta, F. and Montalvo, D. "The Effect of Oxygneated Fuels on Emissions from a Modern Heavy-Duty Diesel Engine," *SAE Paper* 932734 (1993).
4. Miyamoto, N., Ogawa, H., Arima, T., and Miyakawa, K. "Improvement of Diesel Combustion and Emission with Addition of Various Oxygenated Agents to Diesel Fuels," *SAE Paper* 962115 (1996).
5. Tsurutani, K., Takei, Y., Fujimoto, Y., Matsudaira, J. and Kumamoto, M. "The Effects of Fuel Properties and Oxygenates on Diesel Exhaust Emissions," *SAE Paper* 952349 (1995).
6. Spreen, K. B., Ullman, T. L., and Mason, R. L. "Effects of cetane number, aromatics, and oxygenates on emissions from a 1994 heavy-duty diesel engine with exhaust catalyst," *SAE Paper* 950250 (1995).
7. Bertoli, C., Del Giacomo, N., and Beatrice, C. "Diesel combustion improvements by the use of oxygenated synthetic fuels," *SAE Paper* 972972 (1997).
8. Stoner, M. and Litzinger, T. "Effects of structure and boiling point of oxygenated blending compounds in reducing diesel emissions," *SAE Paper* 1999-01-1475 (1999).
9. Tamanouchi, M., Akimoto, T., Aihara, S., and Morihisa, H. "Effects of DGM and oxidation catalyst on diesel exhaust emissions," *SAE Paper* 1999-01-1137 (1999).
10. Donahue, R. and Foster, D. "Effects of oxygen enhancement on the emissions from a DI diesel via manipulation of fuels and combustion chamber gas composition," *SAE Paper* 2000-01-0512 (2000).

11. Cartellieri, W. "Worldwide trend of heavy duty truck diesel engine technologies to meet future stringent exhaust emission legislation," AVL keynote lecture held at JSME conference 1998.

12. Heywood, J.B. Internal combustion Engine Fundamentals, McGraw-Hill, Inc., New York, 1988.

13. Donaldson, K., Li, X. Y., and MacNee, W. "Ultrafine (Nanometre) particle mediated lung injury," Journal of Aerosol Science, Vol 29, No. 5/6, 1998.

14. Health Effects Institute "Diesel Exhaust: A Critical Analysis of Emissions, Exposure, and Health Effect," April 1995.

15. Lee, R., Pedley, J., and Hobbs, C. "Fuel Quality Impact on Heavy Duty Diesel Emissions: - A Literature Review," *SAE Paper* 982649 (1998).

16. Flynn, P. F., Durrett, R. P., Hunter, G. L., zur Loye, A. O., Akinyemi, O. C., Dec, J. E., and Westbrook, C. K. "Diesel combustion: An integrated view combining laser diagnostics, chemical kinetics, and empirical validation," *SAE Paper* 1999-01-0509 (1999).

17. Frenklach, M. and Wang, H. "Detailed modeling of soot particle nucleation and growth," T*wenty-Third Symposium (International) on Combustion*, The Combustion Institute, Pittsburgh, PA, 1991.

18. Glassman, I. Combustion, 3rd edition, Academic Press, New York, 1997.

19. Nakakita, K., Takasu, S., Ban, H., Ogawa, T., Naruse, H., Tsukasaki, Y., and Yeh, L.I. "Effect of Hydrocarbon Molecular Structure on Diesel Exhaust Emissions Part 2: Effect of Branched and Ring Structures of Paraffins on Benzene and Soot Formation," *SAE Paper* 982495 (1998).

20. Owen, K. and Coley, T. Automotive Fuels Handbook, Society of Automotive Engineers, Warrendale, PA, 1990.

21. Peyton, K.B. Fuel Field Manual: Sources and Solutions to Performance Problems, McGraw-Hill, New York, 1997.

22. Booth, M., Marriot, J.M., and Rivers, K.J. "Diesel fuel quality in an environmentally-conscious world," *IMechE* 1993.

23. Winsor, R.E. "Effect of fuel modification on Detroit diesel engine exhaust emissions," *IMechE* 1993.

24. Ullman, T.L., Spreen, K.B., and Mason, R.L. "Effects of Cetane Number, Cetane Improver, Aromatics, and Oxygenates on 1994 Heavy-Duty Diesel Engine Emissions," *SAE Paper* 941020 (1994).

25. Tamanouchi, M., Morihisa, H., Yamada, S., Iida, J., Sasaki, T., and Sue, H. "Effects of fuel properties on exhaust emissions for diesel engines with and without oxidation catalyst and high pressure injection," *SAE Paper* 970758 (1997).

26. Miyamoto, N., Ogawa, H., Nurun, N., Obata, K., and Arima, T. "Smokeless, low NOx, high thermal efficiency, and low noise diesel combustion with oxygenated agents as main fuel," *SAE Paper* 980506 (1998).

27. Bosch GmbH, R. Diesel Fuel Injection, SAE Publication 1994.

28. Shihadeh, A. L. "Rural Electrification from Local Resources: Biomass Pyrolysis Oil Combustion in a Direct Injection Diesel Engine," Ph.D. Thesis, M.I.T., 1998.

29. Cheung, H. M. "A Practical Burn Rate Analysis for Use in Engine Development and Design," S.M. Thesis, M.I.T., 1993.

30. EPA Test Procedure TP 713D "Sample Collection, Continuous Hydrocarbon Analysis and Particulate Collection of the Light Duty Diesel Tests," Garter, D., 1994.

31. "Model 3071A Electrostatic Classifier" Instruction Manual, TSI Incorporated 1997.

32. EPA Test Procedure TP 714C "Diesel Particulate Filter Handling and Weighing," Hormes, L., 1994.

33. Lüders, H., Krüger, M., Stommel, P., and Lüeurs, B. "The role of sampling conditions in particle size distribution measurements," *SAE Paper* 981374 (1998).

34. Maricq, M., Chase, R.; Podsiadlik, D., and Vogt, R. "Vehicle exhaust particle size distributions: A comparison of tailpipe and dilution tunnel measurements," *SAE Paper* 1999-01-1461 (1999).

35. Maricq, M., Podsiadlik D., and Chase, R. "An examination of the size resolved and transient nature of motor vehicle particle emissions," Ford Publication, 1999.

36. Willeke, K. and Baron, P.A. Aerosol Measurement Principles Techniques and Aplications, Van Nostrand Reinhold, New York, 1993.

37. Hinds, W.C. Aerosol technology : properties, behavior, and measurement of airborne particles, 2nd edition, J. Wiley, New York, 1999.

38. Ishigureo, T., Takatori, Y., and Akihama, K. "Microstructure of Diesel Soot Particles Probed by Electron Microscopy: Fist Observation of Inner Core and Outer Shell," Combustion and Flame 108231-234 (1997).

39. Hori, S. and Narusawa, K. "Fuel Composition Effects on SOF and PAH Exhaust Emissions from DI Diesel Engines," *SAE Paper* 980507 (1998).

40. Tanaka, S. and Shimizu, T. "A study of composition and size distribution of particulate matter from DI diesel engine," *SAE Paper* 1999-01-3487 (1999).

41. Uchida, M. and Akasaka, Y. "A comparison of emissions from clean diesel fuels," *SAE Paper* 1999-01-1121 (1999).

42. Marr, W.W., Sekar, R.R., Cole, R.L., Marciniak, T.J., and Longman, D.E. "Oxygen-enriched diesel engine experiments with a low-grade fuel," *SAE Paper* 932805 (1993).

43. Desai, R.R., Gaynor, E., Watson, H.C., and Rigby, G.R. "Giving standard diesel fuels premium performance using oxygen- enriched air in diesel engines," *SAE Paper* 932806 (1993).

44. Lange, W.W., Schafer, A., Le'Jeune, A., and Naber, D. "The influence of fuel properties on exhaust emissions from advanced Mercedes Benz diesel engines," *SAE Paper* 932685 (1993).

45. Ryan, T.W., Erwin, J., Mason, R.L., and Moulton, D.S. "Relationships between fuel properties and composition and diesel engine combustion performance and emissions," *SAE Paper* 941018 (1994).

46. Johnson, J., Bagley, S., Gratz, L., and Leddy, D. "A review of diesel particulate control technology and emission effects," *SAE Paper* 940233 (1994).

47. Klein, H., Lox, E., Kreuzer, T., Kawanami, M., Thoms R., "Diesel Particulate Emissions of Passenger Cars – New Insight Into Structural Changes During the Process of Exhaust Aftertreatment Using Diesel Oxidation Catalysts," *SAE Paper* 980196 (1998).

48. Diesel Fuel News, *Proceedings of the 2nd Nanoparticle Workshop*, September 21, 1998.

49. Diesel Fuel News, "New Ether Blendstock Might cut cost of 'cleaner' fuel," February 8, 1999.

50. Jaeger, L., Boulouchos, K., and Mohr, M. "Analysis of factors influencing particulate matter emissions of a compression-ignition, direct-injection engine," *SAE Paper* 1999-01-3492 (1999).

51. Johnson, J.H., Bagley, S.T., Gratz, L.D., and Leddy, D.G. "A Review of Diesel Particulate Control Technology and Emissions Effects – 1992 Horning Memorial Award Lecture," *SAE Paper* 940233 (1994).

52. Ogawa, T., Araga, T., Okada, M., and Fujimoto, Y. "Fuel Effects on Particulate Emissions from D.I. Engine – Chemical Analysis and Characterization of Diesel Fuel," *SAE Paper* 952351 (1995).

53. Chescoe, D. and Goodhew, P. J. The Operation of Transmission and Scanning Electron Microscopes, Royal, Royal Microscopical Society Microscopy Handbooks, Oxford University Press, Oxford 1990.

APPENDIX

Heat release analysis for a DI diesel engine. The analysis uses First Law single-zone treatment of the combustion chamber contents assuming perfect gas relations. The SI code was adapted by Shihadeh [28] for diesel combustion, and originally developed by Cheung [29].

$$\frac{dQ_{rel}}{d\theta} = \frac{\gamma}{\gamma - 1} p \frac{dV}{d\theta} + \frac{1}{\gamma - 1} V \frac{dp}{d\theta} + \frac{dQ_{ht}}{d\theta}$$

where: Q_{rel} = energy release by combustion
γ = ratio of specific heats
p = cylinder pressure
V = cylinder volume
Q_{ht} = heat transfer to chamber walls
θ = crank angle

Calculation of the dilution ratio, R_d, in the tunnel during exhaust sampling. All carbon dioxide concentrations are measured on a dry basis, equation corrects for the water vapor removed from the exhaust.

$$R_d = \frac{X_{CO_2,Exhaust}\left(1 - X_{H_2O,Exhaust}\right) - X_{CO_2,Dilution\ Air}\left(\frac{M_{Dilution\ Air}}{M_{Exhaust}}\right)}{X_{CO_2,Dilute\ Exhaust} - X_{CO_2,Dilution\ Air}\left(\frac{M_{Dilution\ Air}}{M_{DiluteExhaust}}\right)} * \left(\frac{M_{Exhaust}}{M_{Dilute\ Exhaust}}\right)$$

where: R_d = dilution ratio mass flow rates of diluted exhaust to undiluted exhaust
$X_{CO2,\ Exhaust}$ = dry molar concentration of carbon dioxide of raw exhaust
$X_{CO2,\ Dilution\ Air}$ = dry molar concentration of carbon dioxide of dilution air
$X_{CO2,\ Dilute\ Exhaust}$ = dry molar concentration of carbon dioxide of raw exhaust
$X_{H2O,\ Exhaust}$ = mole fraction of water in exhaust (calculation based on fuel's hydrogen/carbon ratio)
$M_{Dilution\ Air}$ = molecular weight of dilution air
$M_{Diluted\ Exhaust}$ = molecular weight of dilute exhaust
$M_{Exhaust}$ = molecular weight of exhaust

Estimation of the mass of air, m_{sample}, that passes through the filter during PM sampling. The volume flow rate across the orifice remains constant during choked flow. However, the pressure upstream of the orifice decreases during filter loading. As a result, the following mass flow formula is utilized to correct for the changing air density during sampling.

$$m_{sample} = \frac{P_{ave} \cdot Q_{crit} \cdot MW_{air}}{\tilde{R} \cdot T_{sample}} \cdot t$$

where: m_{sample} = total mass of air sampled through filter
P_{ave} = time averaged pressure upstream of the orifice during the filter measurement
Q_{crit} = orifice choked volume flow rate
R = universal gas constant
MW_{air} = molecular weight of air
T_{sample} = temperature of the air after the filter
t = sampling time

Formula for calculating the indicated (gross) specific particulate emission level using standard filter measurements.

$$isPart = \frac{\left(M_{final} - M_{initial}\right) \cdot \dot{m}_{exhaust}}{m_{sample} \cdot R_d \cdot P_{i,g}}$$

where: isPart = indicated specific particulates emission level
M_{final} = final filter mass
$M_{initial}$ = initial filter mass
$m_{exhaust}$ = mass flow rate of exhaust
m_{sample} = mass of sampled air
R_d = dilution ratio
$P_{i,g}$ = indicated (gross) power

Equation for converting the SMPS total (integrated) PM number concentration into a mass measurement. Developed by Maricq at Ford [35], assuming a lognormal number distribution, utilizes parameters (mean, std, total number) estimated by the TSI SMPS software.

$$Mt = \frac{N \cdot \rho_{PM} \cdot \pi \cdot \mu^3}{6} \cdot \exp\left(\frac{9\sigma^2}{2}\right)$$

where: Mt = mass of PM per volume derived from the SMPS total number concentration [35]
μ = geometric mean size
σ = standard deviation
N = PM total number concentration
ρ_{PM} = PM density

Equation for converting the SMPS total (integrated) PM volume concentration into a mass measurement. Total volume concentration estimated by TSI SMPS software.

$$Mv = V \cdot \rho_{PM}$$

where: Mv = mass of PM per volume based on SMPS total volume concentration
V = PM total volume concentration
ρ_{PM} = PM density

Relating the mass of PM per volume into a indicated specific particulates (isPart) emission level.

$$isPart_{SMPS} = \frac{M \cdot R_d}{P_i} \cdot \frac{\dot{m}_{Exhaust} \cdot \tilde{R} \cdot T_{Exhaust}}{MW_{Exhaust} \cdot P_{Exhaust}}$$

where: $isPart_{SMPS}$ = PM mass emission from SMPS measurements on indicated power basis
M = mass of PM per volume derived from either Mv or Mt
R_d = exhaust dilution ratio
$m_{Exhaust}$ = exhaust mass flow rate
R = universal gas constant
$MW_{Exhaust}$ = molecular weight of exhaust (~MW_{Air})
$P_{Exhaust}$ = pressure at SMPS sampling point
$T_{Exhaust}$ = temperature at SMPS sampling point
P_i = indicated power